FINAL REPORT ON
NASA GRANT NAG 1-1087
"IDENTIFICATION OF AERODYNAMIC MODELS FOR MANEUVERING AIRCRAFT"

KU-FRL-872-5

C. Edward Lan and C. C. Hu

Flight Research Laboratory
The University of Kansas Center for Research, Inc.
Lawrence, Kansas 66045-2969

June 30, 1992

Summary

The method based on Fourier functional analysis and indicial formulation for aerodynamic modeling as proposed by Chin and Lan is extensively examined and improved for the purpose of general applications to realistic airplane configurations. Improvement is made to automate the calculation of model coefficients, and to evaluate more accurately the indicial integral. Test data of large angle-of-attack ranges for two different models, a 70-deg. delta wing and an F-18 model, are used to further verify the applicability of Fourier functional analysis and validate the indicial formulation. The results show that the general expression for harmonic motions throughout a range of k is capable of accurately modeling the nonlinear responses with large phase lag except in the region where an inconsistent hysteresis behavior from one frequency to the other occurs. The results by the indicial formulation indicate that more accurate results can be obtained when the motion starts from a low angle of attack where hysteresis effect is not important.

TABLE OF CONTENTS

LIST OF SYMBOLS

A_j	coefficient of cosine Fourier series
B_j	coefficient of sine Fourier series
C_{ave}	average value of $A_0(k)$ in the indicial formulation
C_j	reference values
C_D	drag coefficient
C_L	lift coefficient.
C_{L_α}	variation of lift coefficient with respect to angle of attack
$C_{L_{\dot{\alpha}}}$	variation of lift coefficient with respect to time rate of angle of attack
C_m	pitching moment coefficient
DS	a given step length
E_{ij}	constants associated with the zero-lag response
F_1	objective function for the first level of the outer optimization loop
F_2	objective function for the second level of the outer optimization loop
G	value of gradient in the gradient method
H_{ij}	constants in amplitude functions
i	imaginary part of a complex number
j	index
k	reduced frequency ($=\omega\ell/V_\infty$)
k_{max}	maximum allowable equivalent reduced frequency
m	index for time interval
M	number of time interval

n	index for reduced frequency. Also index for the coefficients in Padé approximants
N	number of frequencies
PD_j	Padé approximants
P_{ij}	coefficients in Padé approximants
q	pitch rate in rad/sec
$\hat{q}$	nondimensional pitch rate ($=q\ell/V_\infty$)
S	the sum of squared errors
t	time
t'	nondimensional time ($=tV_\infty/\ell$)
V_∞	free stream velocity
α	variation in angle of attack ($=\alpha_0 \cos kt'$)
α_1	$=\alpha_m+\alpha$, total angle of attack
α_o	amplitude of angle-of-attack variation
α_m	mean angle of attack
$\dot{\alpha}$	time rate of change in angle of attack
$\dot{\alpha}_1$	$=\dot{\alpha}$ time rate of change in total angle of attack
ℓ	reference length
τ	dummy time integration variable
θ	$= kt'$
ϕ	phase angle

1. INTRODUCTION

Due to the rapid development of on-board computers, a new air combat tactic, called supermaneuverability, has become more feasible and realistic than before. Fighter designers have recognized the applications of supermaneuverability as one of the major features of next-generation fighters. With the advantage of simplicity, flying up to and beyond post-stall(PST) region has been considered as one way of achieving supermaneuverability(Ref.1). One of the applicable PST maneuverings is a 180-degree change of heading with the additional constraint of returning to the point of departure at the initial speed and altitude (Fig.1). However, the usefulness of PST maneuvering in terms of tactical purpose still is in question. Instead of conducting flight tests, such as X-31 demonstrator, flight simulation is an easier and more flexible way to evaluate the advantage of PST maneuverings.

In flight simulation, aerodynamic forces and moments are needed. According to Tobak and Schiff in Ref.2, the major difficulty in calculating the nonlinear aerodynamic forces and moments acting on a rapidly maneuvering aircraft is that these airloads are, in general, determined not only by the instantaneous motion variables, for example α and $\dot{\alpha}$, but also by all of the prior states of the motion up to the current state. As a result, the currently-used linear and locally-linearized quasi-steady aerodynamic

models incorporated in the look-up tables of wind tunnel test data have become increasingly inadequate for the simulation of a rapid maneuvering flight. Although a simple empirical surface pressure model was proposed lately in Ref 3. to improve the accuracy of nonlinear aerodynamic modeling for a 65-deg. delta wing subjected to large-amplitude high-rate oscillation in roll, it is not applicable to general configurations. Therefore, a more general aerodynamic modeling technique is needed.

In applications of linear potential flow theory, aeroelasticity researchers(Ref.4 and 5) utilized Fourier Transform to relate the aerodynamic responses of a step change in the angle of attack of a wing to those of harmonic oscillatory motions. The transient aerodynamic response corresponding to a step change in the angle of attack, called an "indicial function", has been calculated for several classes of isolated wings(Ref.4-7). Further applications of the indicial function were considered by Tobak and his coworkers by extending the concept of indicial function into the nonlinear aerodynamic regimes(Ref.2 and 8). In addition, the method of separating the time-history data into in-phase and out-phase components has been successfully carried out for the type of response with small-amplitude oscillations(Ref.9). However, the above-mentioned simple model which only includes the fundamental frequency and small-amplitude is not applicable to nonlinear aerodynamic responses involving dynamic stall and

vortex lag.

For this reason, Chin and Lan(Ref.10) proposed a general model based on Fourier analysis to analyze the force and moment data obtained in large amplitude forced oscillation tests at high angles of attack. Test data for a 70-deg. delta wing were used to verify this method of analytically modeling responses of harmonic motions at different reduced frequencies. In addition, harmonic ramp motions for the 70-deg. delta wing also were calculated to verify the indicial formulation in their paper.

Since the method of Fourier functional analysis uses a two-level gradient method to determine the model coefficients for all linear and nonlinear terms in the general model, questions arise as to the uniqueness of results. In other words

- are the model coefficients sensitive to the initial guesses?
- If the solutions are sensitive to initial guesses, are the results obtained with different initial guesses acceptable?
- If not all results by different initial guesses are acceptable, what would the constraint and criteria be to determine the "best" set of coefficients?

In this research, two more sets of test data obtained at NASA Langley Research Center will be used to conduct a more extensive testing on the method of Fourier functional analysis as well as the indicial

formulation. The results have shown that an outer optimization procedure with constraints should be added to the original Fourier functional analysis due to the complexity of the present highly-nonlinear optimization problem with constraints. In addition, the results in validating the indicial formulation also show that some special treatments should be made in the practical applications of the indicial formulation.

2. FOURIER FUNCTIONAL ANALYSIS

2.1 Theoretical Model

In the Chin and Lan's study, a general formulation for a response C_L at time t can be written as

$$C_L(t) = C_L(0) + \text{zero-lag response} + \int_0^t C_{L_\alpha}[t-\tau;\ \alpha(\tau),\ \dot{\alpha}(\tau)]\ \frac{d\alpha(\tau)}{d\tau}d\tau + \frac{\ell}{V_\infty}\int_0^t C_{L_{\dot{\alpha}}}[t-\tau;\ \alpha(\tau),\ \dot{\alpha}(\tau)]\ \frac{d\dot{\alpha}(\tau)}{d\tau}d\tau \qquad (1)$$

Here, the zero-lag response represents the virtual mass effect in 2-D incompressible flow which includes the effect of $\ddot{\alpha}$ and is identical in every harmonic motion. Therefore, it is independent of the time history of motion. The last two terms involving the time integrals represent the summation of indicial responses at time t due to changes in α and $\dot{\alpha}$ in the prior motions. The key task to determine the time integrals in Eq.(1) is to find an analytical form for C_L in terms of $\alpha(t)$ and $\dot{\alpha}(t)$. Then, the time response at a given time t can be calculated through the integrals by substituting the derivatives of C_L.

According to the linear theory of unsteady aerodynamics, an unsteady aerodynamic response can be separated into a product of an amplitude function and a phase function in harmonic motion. The amplitude function is a function of motion variables as well as their time

rate of change. On the other hand, the phase function is a function of frequency and depends on the phase lag between the response and the excitation. For 2-D incompressible flow, Theodorsen introduced a phase function(Ref.4 and 5) which can be determined numerically by analyzing the responses obtained at different frequencies with the same amplitude in harmonic oscillations. Chao and Lan(Ref.11) used this approach successfully to calculate the indicial lift function for a plunging wing.

Based on a similar idea, a more general model which is applicable to nonlinear aerodynamic responses involving dynamic stall and vortex lag is formulated to be a sum of the products of amplitude functions and phase functions for frequencies which are multiples of the test frequency in harmonic motion, instead of only taking the response to the test frequency as in the linear theory. That is,

$$C_L = C_0 + \sum_j (\text{amplitude function})_j * (\text{phase function})_j \qquad (2)$$

For a harmonic motion at a given frequency, the response can be decomposed in terms of k and t' by Fourier-analyzing this response over one period. The complete expression is written as

$$\begin{aligned} C_L = A_0 &+ A_1\cos(kt') + A_2\cos(2kt') + A_3\cos(3kt') \\ &+ B_1\sin(kt') + B_2\sin(2kt') + B_3\sin(3kt') \\ &+ \ldots \end{aligned} \qquad (3a)$$

$$\alpha_1=\alpha_m+\alpha_o\cos(kt') \tag{3b}$$

$$\alpha=\alpha_o\cos(kt') \tag{3c}$$

$$\dot{\alpha}=(-\alpha_o k)\sin(kt') \tag{3d}$$

Here, k is the reduced frequency, t' is the nondimensional time, α_m is the mean angle of attack, and α_0 is the amplitude of angle-of-attack change. Following the convention in the classical airfoil theory, the analysis is best performed in complex form as follows:

$$C_L=A_0+(A_1-iB_1)\,e^{ikt'}+(A_2-iB_2)\,e^{i2kt'} + (A_3-iB_3)\,e^{i3kt'}+\ldots \tag{4a}$$

$$\alpha=\alpha_0\,e^{ikt'} \tag{4b}$$

$$\dot{\alpha}=(i\alpha_0 k)\,e^{ikt'} \tag{4c}$$

An important step herein is to convert Eq.(4) into a formula in terms of $\alpha(t')$ and $\dot{\alpha}(t')$. A "successive Fourier analysis" has been used effectively to split $\cos(n\theta)$ and $\sin(n\theta)$ into n+1 terms which include $\cos^n\theta$ and $\sin^n\theta$ and other cross-product terms. Once the coefficients A_j,B_j at different frequencies are obtained by Fourier analysis, the next question is what the appropriate expression is for the phase function to represent the lag effects throughout

the whole range of k. From past experience(Ref.10 and 12), it was found that Padé approximants provide an accurate approximation of the theoretical phase functions. Therefore, in the present model the response will be put in the following form including the products of amplitude functions and phase functions:

$$
\begin{aligned}
C_L \equiv\ & A_0(k) \\
& + C_1 * [E_{11}\alpha + E_{21}\dot{\alpha} + (H_{11}\alpha + H_{21}\dot{\alpha}) * (1 - PD_1)] \\
& + C_2 * [E_{12}\dot{\alpha}_2 + E_{22}\ddot{\alpha}_2 + (H_{12}\alpha^2 + H_{22}\alpha\dot{\alpha} + H_{32}\dot{\alpha}^2) \\
& \qquad * (1 - PD_2)] \\
& + C_3 * [E_{13}\dot{\alpha}_3 + E_{23}\ddot{\alpha}_3 + (H_{13}\alpha^3 + H_{23}\alpha^2\dot{\alpha} + H_{33}\alpha\dot{\alpha}^2 + H_{43}\dot{\alpha}^3) \\
& \qquad * (1 - PD_3)] \\
& \qquad + \ . \ . \ .
\end{aligned}
\tag{5}
$$

where PD's are Padé approximants of order 2 and are defined as

$$
PD_j = \frac{P_{1j}\,(ik)^2 + P_{2j}\,(ik)}{P_{3j}\,(ik)^2 + (ik) + P_{4j}} \tag{6}
$$

$E_{11}\dot{\alpha}_j + E_{21}\ddot{\alpha}_j$ etc. are the zero-lag response; and the variables $\dot{\alpha}_j$ and $\ddot{\alpha}_j$ are defined as

$$\dot{\alpha}_j = ik\,\alpha_0^{\,j}\,e^{ijkt'}$$

$$\ddot{\alpha}_j = -k^2\,\alpha_0^{\,j}\,e^{ijkt'}$$

to be consistent with higher order terms.

Finally, a general expression for the nonlinear aerodynamic models is constructed. This expression is to interpolate a complete set of harmonic-

oscillatory data with different frequencies to result in a formula for all frequencies. The response calculated at the test frequency encompasses the classical linear theory. It is noted that the response in time domain is given by the real part of the summation from each mode in Eq.(5). The expressions for all aerodynamic force and moment models are similar and will be determined with the following optimization procedures.

2.2 Inner Optimization Procedure Without Constraints

The main objective in the inner optimization procedure is to determine the E and H values for each mode independently by data-fitting the A_j and B_j at different frequencies.

In the previous study, the first term in Eq.(5) was assumed to be constant based on a set of experimental data for a 70-deg. delta wing. After two more sets of experimental data have been examined in this research, it is found that a linear polynomial function of k for $A_0(k)$ is better than a constant, especially in modeling C_D responses. The C_j, which are given and unchanged in the inner procedure, are reference values and used to normalize the response given by A_j-iB_j in the least-squared-error method.

The inner optimization procedure mainly consists of two major methods. They are

(1)Least-squared-error method: For fixed E and H values etc., the P_{1j},P_{2j},P_{3j},P_{4j} are determined by minimizing the sum of squared errors.

(2)Gradient method: The values of E and H etc. are varied so that the sum of squared error is minimum.

According to the previous study, a two-level gradient method is more effective than a straightforward gradient method because of the type of nonlinearity in this optimization problem. The detail about the least-squared-error method and gradient method are discussed in the following. The idea is illustrated in the flow chart of Fig.2.

2.2.1 Least-Squared-Error Method

At a specified reduced frequency, the magnitude of Fourier components in Eq.(4a) written in complex form is A_j-iB_j. So

$$A_j - iB_j = C_j \alpha_0^j * [E_{1j} ik + E_{2j}(-k^2) + (\text{amplitude function})_j * (1-PD_j)] \quad (7)$$

For the assumed values of E and H etc., the only unknown variables in Eq.(7) are the coefficients of Padé approximants. Eq.(7) is rearranged as follows with all known values being on one side:

$$V_j + iW_j \equiv 1 - \frac{A_j - iB_j - E_{1j}\, ik - E_{2j}\,(-k^2)}{(\text{amplitude function})_j} = \frac{P_{1j}\,(ik)^2 + P_{2j}\,(ik)}{P_{3j}\,(ik)^2 + (ik) + P_{4j}} \quad (8)$$

It should be noted that A_j-iB_j in Eq.(8) has been normalized by $C_j\alpha_0^j$. If both sides of Eq.(8) are multiplied by the denominator of the Padé approximant and separated into real and imaginary parts, Eq.(8) becomes

$$Re \equiv P_{1j}k^2 - P_{3j}V_jk^2 + P_{4j}V_j - W_j k = 0 \tag{9a}$$

and

$$Im \equiv P_{2j}k + P_{3j}W_jk^2 - P_{4j}W_j - V_jk = 0 \tag{9b}$$

Then, the coefficients of Padé approximants, i.e. P_{ij} , are chosen by minimizing the sum of squared errors with different k's. That is,

$$Err \equiv \Sigma\, Re(k_i)^2 + \Sigma\, Im(k_i)^2 \tag{10}$$

By equating the first derivatives of Eq.(10) with respect to variables P_{1j},P_{2j},P_{3j} and P_{4j} to zero, the coefficients of Padé approximants can be determined from the following equation:

$$\begin{bmatrix} \Sigma k_i^4 & 0 & -\Sigma V_i k_i^4 & \Sigma V_i k_i^2 \\ 0 & \Sigma k_i^2 & \Sigma W_i k_i^3 & -\Sigma W_i k_i \\ -\Sigma V_i k_i^4 & \Sigma W_i k_i^3 & \Sigma (V_i^2 k_i^4 + W_i^2 k_i^4) & -\Sigma (V_i^2 k_i^2 + W_i^2 k_i^2) \\ \Sigma V_i k_i^2 & -\Sigma W_i k_i & \Sigma (V_i^2 k_i^2 + W_i^2 k_i^2) & \Sigma (V_i^2 + W_i^2) \end{bmatrix} \begin{bmatrix} P_{1j} \\ P_{2j} \\ P_{3j} \\ P_{4j} \end{bmatrix} = \begin{bmatrix} \Sigma W_i k_i^3 \\ \Sigma V_i k_i^2 \\ 0 \\ 0 \end{bmatrix} \tag{11}$$

where i is the index for different frequencies used in acquiring the experimental data, and the mode subscript j on V and W has been omitted.

2.2.2 Gradient method without constraints

Once the unknown coefficients P_{1j},P_{2j},P_{3j} and P_{4j} are found, a one-dimensional gradient method is adopted to find better E and H values which minimize the sum of squared errors. The sum of squared errors is defined as :

$$S = \sum [A_j - (A_j)_{numerical}]^2 + \sum [B_j - (B_j)_{numerical}]^2 \quad (12)$$

where $(A_j)_{numerical}$ = Re[RHS of Eq.(7)]

$(B_j)_{numerical}$ = Im[RHS of Eq.(7)]

Because of the difficulty in locating a global minimum in a straightforward gradient method, a two-level gradient method described in the following is used in this investigation.

(1)First level

Step 1: The current E or H value is perturbed by a small amount ΔE or ΔH to find the gradient of sum of squared errors.

Step 2: Each E or H value advances one step to new value according to its local gradient obtained in step 1.

Step 3: Repeat Step 1 and Step 2 for each variable E or H until several iterations has been reached(it is set to be 5 in the current program)

(2)Second level

Repeat the first level until several iterations has been reached(it is

set to be 10 in the current program).

2.3 Outer Optimization Procedure With Constraints

As mentioned earlier in the introduction, the results for E and H values by the inner optimization procedure are not unique. They tend to vary with different initial guesses of E and H values. Moreover, not all of these results are acceptable due to the requirement that the denominators of Padé approximants must have real negative roots only. the latter requirement is necessary so that in time domain the corresponding exponential terms will die out at large time. A straightforward method which directly adds this requirement as constraints to the inner optimization loop has been tried. Unfortunately, for most cases, it was found that directly imposing constraints to the two-level gradient method tends to make the final results close to the initial guesses of E and H values. In other words, the constraints block the path of searching vector obtained in the gradient method so that a global minimum solution can not be reached in such a situation. To avoid this problem, an outer optimization loop has been added outside the inner optimization procedure. The outer optimization procedure is based on the same search technique as the inner one, i.e. the gradient method, except that additional constraints are imposed for the purpose of choosing proper initial values for E and H. A question arises as to what would be the objective function of the outer

optimization procedure. From the experience of validating the indicial formulation, an objective function which tends to minimize the lag effect of phase function in time domain at $\tau=0$ is chosen. That is, $(1.-a_{1j}-a_{2j})$ is minimized.

A further examination of Eq.(5) is needed at this time. The remaining variables which are not calculated by any optimization procedure are C_j. Theoretically, E and H values are inversely proportional to C_j for a given response A_j-iB_j, and can be adjusted to take appropriate values in the gradient method for a given reference value of C_j. But, numerical experimentation shows that this is not true. The reason is that the given response A_j-iB_j in Eq.(8) is normalized by $C_j\alpha_0^j$, while the E and H values always start from the same built-in initial guesses. In other words, the C_j must be properly chosen in a way to make the present method more workable and user-friendly in analyzing any given set of test data. Therefore, one more outer loop has been added outside the first outer gradient method to determine the best value of C_j within a feasible range of C_j. To illustrate the necessity of this additional outer optimization loop, test data for the 70-deg. delta wing(Ref.13) used in Chin and Lan's paper are reanalyzed by the modified method. Significant improvement at small time can be seen in the constant-rate pitch-up motion(Fig.3). The detail of the two-level outer optimization procedures are discussed in the following,

and the flow chart is presented in Fig.4.

2.3.1 Gradient Method With Constraints

Unlike the gradient method in the inner optimization loop, the gradient method used in the outer loop is imposed with a constraint which requires all roots of the denominators of Padé approximants to be real and negative. In addition, another special constraint which needs to be applied only to the analysis of C_D responses is that E_{11} can not be negative according to the classical linear theory. By treating the whole inner optimization procedure as a "function box", a gradient method with constraints which comprises a gradient-search process and a series of checking-up has been implemented. This includes the following three steps.

Step 1: Find an acceptable starting point

For a given C_j, the starting initial guesses for E and H values are assumed to be a set of optimal initial values from the previous C_j or a set of build-in initial data in case the search of the previous C_j finds no reasonable starting values. If this starting point violates the constraints, each of E and H values will take turn to advance one step(maximal number of steps is set to be 4) until a reasonable starting point is found.

Step 2: Construct an acceptable gradient vector

Once an acceptable starting point has been found, a gradient vector is constructed by separately perturbing a small amount ΔE or ΔH for the

current initial guess. If the perturbation in any of E or H values leads to an unacceptable result, the gradient in the corresponding direction will be set to zero. It is noted that the objective function in this gradient method is defined as

$$F_1=-1./(1.-a_{1j}-a_{j2}) \qquad (13)$$

from numerical experiments, where a_{1j} and a_{2j} represent the lag effects at very small time.

Step 3: Advance to a new acceptable point

Based on the gradient vector in Step 2, a new set of initial values for E and H are obtained by advancing a given step length DS. Once again, the reasonableness of the new point should be checked. If it is an unacceptable point, the searching procedure must be stopped; and the last acceptable point found in Step 1 would be recalled to be the optimal set of initial values of E and H for the given C_j. Otherwise, Step 2 to Step 3 would be repeated further until several iterations has been reached(it is set to be 10 iterations in the current program).

2.3.2 Determination of reference value C_j

In the search of the best reference value for C_j, no gradient method is needed. A simple way used in the present method is to evaluate different C_j over a feasible range. Based on the experience in analyzing the test data

presented in this report and the earlier test data(Ref.13) used by Chin and Lan, the optimal C_j usually satisfies the following inequality.

$$C_j \leq \frac{1}{\alpha_m j}$$

Here, α_m is in radian and j is the mode index. So, a set of feasible C_j for the second level search can be built up. Then, a cost function which is defined as

$$F_2 = |a_{1j} + a_{2j}| + |a_{1j}| + |a_{2j}| \qquad (14)$$

is used in the evaluation of C_j. The best reference value of C_j is determined by selecting the C_j with a minimum cost function.

3. INDICIAL FORMULATION

3.1 General Mathematical Formulation

According to Tobak(Ref.14), in linear theory exponential functions which are obtained by applying the Fourier integral to the phase functions in frequency domain are good representations in time domain for aerodynamic response corresponding to a step change due to the asymptotic nature of exponential functions. In Chin and Lan's paper this approach was applied to the nonlinear model and successfully set up a general mathematical formulation, called "indicial formulation". A brief review of this formulation will be given in the following.

Once the appropriate coefficients in Eq.(5) have been found for a set of harmonic responses, Eq.(5) can be rewritten in a compact form by absorbing C_j into E and H values as follows:

$$C_L = A_0(k) + \sum_{j=1}^{m} (E_{1j}\alpha_j + E_{2j}\dot{\alpha}_j) + \sum_{j=1}^{m} (\text{amplitude function})_j * (\text{phase function})_j \tag{15}$$

where phase functions are defined as

$$1 - \frac{P_{1j}\,(ik)^2 + P_{2j}\,(ik)}{P_{3j}\,(ik)^2 + ik + P_{4j}} = 1 - \frac{i(jk)\,a_{1j}}{i(jk) + ja_{3j}} - \frac{i(jk)\,a_{2j}}{i(jk) + ja_{4j}} \tag{16}$$

Based on a step input (Ref.4), the phase function will be converted into exponential functions in time domain but the amplitude function is kept unchanged. Therefore, an indicial response C_L for the circulatory lift, i.e. the third term in Eq.(15), can be defined as

$$C_{L_{indicial}} \cong \sum_{j=1}^{m} (\text{amplitude function})_j * (1.-a_{1j}e^{-a_{2j}jt}-a_{2j}e^{-a_{4j}jt}) \tag{17}$$

From Eq.(1), it is known that aerodynamic response at time t is made of three parts. The first part is the initial response at the starting point. The second part is the response without hysteresis effect; while the last part is the indicial response due to changes in α and $\dot{\alpha}$ in the prior motion. The initial response $C_L(0)$ is obtained by setting the running variable τ to zero in the indicial response C_L and the zero-lag response term is identical in every harmonic motion. Then, the integrands in the third part can be determined explicitly by taking derivatives with respect to α and $\dot{\alpha}$ from Eq.(17). It should be noted that an average value C_{ave} also will be added in Eq.(1) because α in the amplitude functions of Eq.(17) denotes only a perturbation from α_m in the harmonic model. Therefore, the final form of indicial formulation for arbitrary motions is given as

$$C_L(t') = C_{L_{indicial}}[t'-\tau,\ \alpha(\tau),\ \alpha(\tau)]_{\tau=0} + C_{ave} + \sum_{j=1}^{m}(E_{1j}\alpha_j + E_{2j}\dot{\alpha}_j)$$
$$+ \sum_{j=1}^{m}\int_0^{t'} \frac{d\,(a.f.)_j}{d\alpha} * (1-a_{1j}e^{-a_{3j}j(t'-\tau)} - a_{2j}e^{-a_{4j}j(t'-\tau)})\ \frac{d\alpha(\tau)}{d\tau}\,d\tau$$
$$+ \frac{\ell}{V_\infty}\sum_{j=1}^{m}\int_0^{t'} \frac{d\,(a.f.)_j}{d\,\alpha} * (1-a_{1j}e^{-a_{3j}j(t'-\tau)} - a_{2j}e^{-a_{4j}j(t'-\tau)})\ \frac{d\alpha(\tau)}{d\tau}\,d\tau \qquad (18)$$

3.2 Implementations of Indicial Formulation

To perform the time integration in Eq.(18) for arbitrary motions, some special numerical implementations have been made in the present program. First of all, a 3-point Simpson rule is chosen to evaluate numerical integration. Secondly, an arbitrary motion has to be represented locally by a cosine function in order to utilize the results of harmonic modeling. At a certain time of an arbitrary motion, the total angle of attack α_1 and $\dot{\alpha}_1$ can be described by the cosine and sine functions as

$$\alpha_1(\tau) = \alpha_m + \alpha_o \cos(k\tau + \phi) \qquad (19a)$$

$$\alpha_1(\tau) = -\alpha_o k \sin(k\tau + \phi) \qquad (19b)$$

By knowing the harmonic model's mean angle of attack α_m and amplitude α_0, an equivalent frequency k and an equivalent phase angle ϕ at a given instantaneous time τ can be solved by Newton's method. To smooth out possible discontinuity in response when the given motion has a sudden change in $\dot{\alpha}$, an α_0 which is slightly greater than the actual amplitude is frequently used. It should be emphasized that this dose not change the instantaneous values of α_1 and $\dot{\alpha}_1$ in the actual time history of motion. It merely changes the values of equivalent frequency k and phase function ϕ. Finally, the C_{ave} in Eq.(18) which was assumed to be a constant in the previous study has been reformulated. A constant term A_0 in the harmonic modeling is now replaced with a linear polynomial function of k for $A_0(k)$. Based on the similar concept in the indicial response, the C_{ave} at a given t' should be made of all $A_0(k)$ of prior states in the motion up to the current time. So, a simple way to calculate C_{ave} is to take an average, i.e.

$$C_{ave} = [\sum_{m=1}^{M} A_0(k_m)]/M \qquad (20)$$

where m is an index for running time, and k_m is the equivalent frequency based on the original amplitude in the harmonic model.

In addition to the above-mentioned general implementations in the indicial formulation, several special treatments used in some particular motions will be discussed in the next chapter.

4. RESULTS AND DISCUSSION

4.1 Test Data

In the present study, test data for three kinds of motions obtained at the NASA Langley Research Center are taken to be analyzed or compared with numerical results calculated from simulations of the specified motion. They are described in detail as follows:

(1)Large Amplitude Harmonic Motions: Test data of harmonic motions with large amplitude are used for numerical modeling in Fourier functional analysis. In this category, there are two groups of test data, and each group includes three sets of aerodynamic data for C_L,C_D and C_M with five reduced frequencies. The first group is for a 70-deg. delta wing, and the second one is for an F-18 model. Both test models are harmonically oscillated about 32.5 deg. of angle of attack with an amplitude of 30 degree. This large coverage in angle of attack which contains low α region, near-stall region and post-stall region exhibits a good characterization of hysteresis behaviors. In addition, the test data for a 70-deg. delta wing(Ref.13) used in Chin and Lan's paper also have been reanalyzed for the purpose of comparison.

(2)Constant-Rate Pitching Motions: Test data of constant-rate pitching motions are used for validation of the indicial formulation in arbitrary motions. The experimental data in this category were taken from

the same models as described in the large amplitude harmonic motions. Responses with three pitch rates for each model have been measured in pitch-up motions as well as pitch-down motions. The angle of attack starts from 2.5 degree and stops at 62.5 degree in the pitch-up motions; but moves in reverse in the pitch-down motions.

(3)Medium Amplitude Harmonic Motions: An additional group of forced harmonic oscillation data for an F-18 model provides a further examination of the interpolative property of the mathematical model. The mean angle of attack and amplitude of oscillation in this harmonic motion are intentionally set to be different from those in the large amplitude harmonic motions. In the present test, the F-18 model was harmonically oscillated about 22.5 degree angle-of-attack with an amplitude of 20 degree.

4.2 Fourier Functional Analysis

As pointed out in chapter 2, a constant term for $A_0(k)$ in the previous study is replaced by a linear polynomial function of k, especially while analyzing C_D responses. To show the necessity of this change, the term A_0 versus the test reduced frequencies for the F-18 C_D responses are plotted in Fig.5(a), and also the numerical results by both models are compared with experimental data at the highest k in Fig.5(b). Both figures show that a discrepancy of about 0.1 exists if an average value for $A_0(k)$ is applied. Regardless of the optimization procedures, other task to improve the

accuracy of the present method is to include the static test data as additional dynamic stall data at a very low reduced frequency, such as k=1.0E-6. The main purpose of this implementation is to avoid possible poor extrapolation at low reduced frequency.

The results by the Fourier functional analysis are presented in Fig.6 for the 70-deg. delta wing and Fig.7 for the F-18 model respectively. Five Fourier terms are used in this analysis and the calculated coefficients for the two aerodynamic models are listed in Table(1) and Table(2) respectively. All results were done by the same set of build-in initial data for E, H and C_j without any try-and-error guess by a user. The results show that the present method is able to capture all major hysteresis effects. Compared with the up-stroke data, most of the down-stroke data are modeled with less accuracy. The reason can be found by taking a further look at the C_L test data for the presently-used 70-deg. delta wing (see Fig.8(a)) and those for the other 70-deg. delta wing(Ref.13) used in Chin and Lan's paper (see Fig.8(b)). In Fig.8(b), it appears that the flow becomes attached in the low α region (0-20 deg.) during the down-strokes. On the contrary, strong hysteresis effects still exist under similar conditions in Fig.8(a). So, the trend of the hysteresis behavior on down-strokes is not as consistent as that on up-strokes in the presently-used test data. This may imply that a higher order Padé approximant could be needed to model responses which have

more complicated hysteresis effects. It is noted that the mismatched part of F-18 C_M responses at k=0.015(see Fig.7(c)) is due to the even more inconsistent trend of the hysteresis behavior from one frequency to the other occurring in the region of high angle of attack.

4.3 Indicial Formulation

4.3.1 Harmonic Motion and Harmonic Ramp Motion

The harmonic motion is used to compare with Fourier modeling results which have been well fitted with test data. On the other hand, the harmonic ramp motion can be used to show how good the agreement with the static value is at the time when the motion stops.

As mentioned in chapter 2, discontinuity could happen in the calculation of time integral if the given motion has a sudden change in $\dot{\alpha}$. This can be easily solved by slightly increasing the amplitude of the original model, such as by 2.5 degree. In the following calculations, the amplitude (α_0) which was 30 degree in the testing is set to be 30.5 degree for the harmonic ramp calculation and 32.5 degree for the constant-rate pitching motions respectively.

The results of harmonic motions and harmonic ramp motions are plotted in Fig.9 for the delta wing and Fig.10 for the F-18 model respectively. In the harmonic ramp motions, all responses eventually approach the static value corresponding to the angle of attack when the

motion stops.

4.3.2 Constant-Rate Pitching Motion

This is used to compare with test data at the same pitch-rate.

Two special treatments about this type of motion should be mentioned here. First of all, a question arises about the results by Eq.(19), when the actual angle of attack (α_1 in Eq.(19)) is near the two ends of a harmonic model's α range, for example 2.5 or 62.5 deg. in the present test model. In such a situation, the equivalent k obtained from Eq.(19) tends to be high because the corresponding $\dot{\alpha}_1$ is too large comparing with $\dot{\alpha}$ in the harmonic model. From the experience in calculating the constant-rate pitching motions, it was found that an unreasonably extrapolated high value of k at a starting point would lead to an unacceptable result in simulation. So, one of the variables, α_m and α_0, must be treated as an unknown instead of k, when the extrapolated k-value is greater than a given allowable value k_{max}. Through a series of tests on both variables, the amplitude of harmonic model α_0 was chosen as the other unknown in case the extrapolated k-value exceeds the given allowable k_{max}. Therefore, Eq.(19) will be replaced by the following equation if the equivalent frequency k in Eq.(19) is larger than the given k_{max}:

$$\alpha_1(\tau) = \alpha_m + \alpha_o \cos(k_{max}\tau + \phi) \qquad (21a)$$

$$\alpha_1(\tau) = -\alpha_o k_{max} \sin(k_{max}\tau + \phi) \qquad (21b)$$

where α_0 and ϕ are the unknowns, and are, again, solved by Newton's method.

Secondly, as the constant-rate pitch-down motions start at a high angle of attack, the time integration should start from a static value by setting $t' \rightarrow \infty$ to the first term of Eq.(18).

The results of the constant-rate pitching motions are presented in Fig.11 for the delta wing and Fig.12 for the F-18 model respectively. As expected, all results for pitch-up motions are well predicted except in the region near the starting point. The reason for this is that the phase lag terms $(1.-a_{1j}-a_{2j})$ for $\tau=0$ in the first term of Eq.(17) are not able to perfectly represent a starting point which physically does not involve any hysteresis effects. On the other hand, some of the results for pitch-down motions are not as good as those for pitch-up motions. There are two possible reasons for this. Firstly, the harmonic model which does contain large hysteresis effects in the high angle-of-attack region can not precisely depict an initial response at the starting point in the high α region which definitely possesses a static value without any phase lag. Secondly, the poor

numerical modeling of harmonic motions in down-strokes which is caused primarily by the non-smooth variation of the response from one frequency to the other, especially at low and moderate k, also is a reason for these discrepancies.

4.3.3 Validation of the Interpolative Property

Harmonic responses with a lower mean angle of attack(α_m) and a smaller amplitude(α_0) for the F-18 model are calculated by using the indicial formulation to compare with the test data in the same conditions. The aerodynamic models are still those based on the test data with α_m=32.5 degree and α_0=30 degree.

Since the α range and reduced frequencies still are within the range of the original harmonic model, no extrapolated equivalent reduced frequencies are expected. For the known α_1 and $\dot{\alpha}_1$ time histories, the equivalent k and ϕ at certain time τ can obtained from Eq.(19) without any change in α_0 and α_m of the original harmonic model. To avoid the error which usually happens at a small time, the integral in Eq.(18) are evaluated from the third cycle and only over one period for the periodical motion.

The results are plotted in Fig.13. Comparing with the experimental data, the simulation by using the indicial formulation shows reasonably good agreement. It is also shown that the higher the reduced frequency is,

the better the calculated responses are. The reason is that the simulation for higher reduced frequency includes higher equivalent k which are well modeled in the original harmonic modeling than the simulation for lower reduced frequency. Moreover, some other results should also be noted in this simulation. first of all, the results of C_D responses reveal that using a model containing large hysteresis effects to calculate a motion with less dynamic effect may not be as good as expected(see Fig.13(b)). Secondly, although the analysis for C_M responses fails to model accurately the high α region (α>40 deg.) at low and moderate reduced frequencies (see Fig.7(c)), the harmonic motions with a α-range below 42 deg. still can be well simulated by the indicial formulation.

5. CONCLUSIONS

In the present research, a method involving Fourier functional analysis and indicial formulation proposed by Chin and Lan has been extensively examined and modified for the purpose of applications to airplane configurations. Two sets of test data from NASA Langley Research Center which include a 70-deg. delta wing and an F-18 model have been used to show the applicability of Fourier functional analysis and validate the indicial formulation. Extensive examination of this method has led to the modification of the method by adding an outer optimization procedure with constraints to the original optimization loop to automatically choose appropriate starting values for the unknowns in the nonlinear optimization process.

The results from the Fourier functional analysis showed that the general expression for the aerodynamic response to harmonic motions throughout a range of k was capable of accurately modeling nonlinear responses with large phase lag except in the region with an inconsistent hysteresis behavior from one frequency to the other, such as the F-18 C_M responses at low reduced frequencies. The results by time integration of the indicial integral showed the applicability of the latter to harmonic motions and ramp-type motions. Moreover, all pitch-up motions with constant rate were well simulated by indicial formulation; while the results for the

corresponding pitch-down motions were produced with less accuracy but still in a correct trend. Finally, The results for the F-18 model's aerodynamic response to harmonic motions with different mean angle of attack and amplitude was indicative of good interpolative property of the present aerodynamic models.

6. REFERENCES

1. Herbst, W. B. "Supermaneuverability" DGLR 83-106, October 1983.

2. Tobak, M.;and Schiff, L. B. "Aerodynamic Mathematical Modeling - Basic Concepts." Dynamic Stability Parameters, AGARD-LS-114, 1981.

3. Hanff, E. S.;and Huang, X. Z. "Roll-Induced Cross-Loads on a Delta Wing at High Incidence." AIAA Paper No. 91-3223, Sept. 1991.

4. Bisplinghoff, Raymond L.; Ashley, Holt; and Halfman, Robert L. Aeroelasticity, Chapters 5 and 6, Addison-Wesly Publishing Company, Cambridge, Mass., 1955.

5. Dowell, Earl H.(editor). A Modern Course in Aeroelasticity, Chapter 4, Sijthoff & Noordhoft International Publishers, Rockville, Maryland, 1980.

6. Heaslet, M. A.; and Lomax, H. "Two-dimensional Unsteady Lift Problems in Supersonic Flight." NACA Rep.945, November 1949.

7. Mazelsky, B. "Numerical Determination of Indicial Lift of a Two-Dimensional Sinking Airfoil at Subsonic Mach Numbers from Oscillatory Lift Coefficients with Calculations for Mach Number 0.7." NACA TN 2562, December, 1951.

8. Tobak, M.; and Pearson, W. E. "A Study of Nonlinear Logitudinal Dynamic Stability." NASA TR R-209, September, 1964.

9. Chambers, J. R.; and Grafton, S. B. "Static and Dynamic Logitudinal Stability Derivatives of a Powered 1/9-Scale Model of a Tilt-wing V/Stol Transport." NASA TN D-3591, September 1966.

10. Chin, Suei;and Lan, C. E. "Fourier Functional Analysis for Unsteady Aerodynamic Modeling." AIAA Paper No. 91-2867, August 1991.

11. Chao, C. D.;and Lan, C. E. "Calculation of Wing Response to Gusts and Blast Waves with Vortex Lift Effect." NASA CR-172232, October 1983.

12. Vepa, R. "Finite State Modeling of Aeroelastic Systems." NASA CR-2779, Feb. 1977.

13. Soltani, M. R.;Bragg, M. B.;and Brandon J. M. "Experimental Measurements on an Oscillating 70-degree Delta Wing in Subsonic Flow." AIAA Paper No. 88-2576, June 1988.

14. Tobak, M. "On the Use of the Indicial Function Concept in the Analysis of Unsteady Motions of Wings and Wing-Tail Combination." NASA Rep. 1188, 1954.

(a) C_L Responses

$A_0(k)=0.567+0.140*k$

j	C_j	E_{1j}	E_{2j}	H_{1j}	H_{2j}	H_{3j}	H_{4j}	H_{5j}	H_{6j}
1	2.5	-0.415	-0.232	0.150	0.750				
2	1.5	0.479	0.048	-0.850	-0.948	-1.026			
3	2.05	-0.268	0.114	0.350	-0.650	1.050	0.850		
4	13.0	-0.095	-0.043	0.050	0.377	0.930	-0.082	-0.057	
5	16.0	-0.075	0.042	-0.050	1.378	1.092	-0.961	-0.052	0.850
j	P_{1j}	P_{2j}	P_{3j}	P_{4j}	a_{1j}	a_{2j}	a_{3j}	a_{4j}	
1	-16.71	0.941	15.134	0.0010	0.9883	-2.093	-.0010	-.0651	
2	3.789	0.018	13.813	0.0010	0.0142	0.2601	-.0010	-.0714	
3	11.952	0.927	7.579	0.0010	0.9293	0.6477	-.0010	-.1310	
4	-1.216	0.450	6.477	0.0236	0.7792	-.9669	-.0291	-.1252	
5	4.821	0.681	5.296	0.0361	0.9196	-.0093	-.0486	-.1402	

(b) C_D Responses

$A_0(k)=0.476+0.8248*k$

j	C_j	E_{1j}	E_{2j}	H_{1j}	H_{2j}	H_{3j}	H_{4j}	H_{5j}	H_{6j}
1	1.3	1.129	1.166	0.650	0.034				
2	2.2	0.175	-0.237	-0.150	1.050	0.650			
3	2.8	0.309	-0.009	-0.050	-0.123	-0.354	0.877		
4	11.0	0.068	-0.025	0.050	-0.661	0.854	-0.059	-0.053	
5	21.0	0.012	-0.010	-0.050	-0.050	-0.050	-0.050	-0.050	-0.05
j	P_{1j}	P_{2j}	P_{3j}	P_{4j}	a_{1j}	a_{2j}	a_{3j}	a_{4j}	
1	-6.240	-0.067	8.550	0.001	-0.062	-0.668	-.0010	-0.116	
2	5.295	-0.203	6.065	0.001	-0.211	1.084	-.0010	-0.164	
3	-11.78	-4.079	4.015	0.042	-6.067	3.132	-.0538	-0.195	
4	12.31	-0.224	18.868	0.004	-0.324	0.977	-.0041	-0.049	
5	1.247	1.079	3.063	0.001	1.084	-0.677	-.0010	-0.325	

Table(1) Model Coefficients for A 70-deg. Delta Wing.

(c) C_M Responses

$A_0(k)=0.046+0.0773*k$

j	C_j	E_{1j}	E_{2j}	H_{1j}	H_{2j}	H_{3j}	H_{4j}	H_{5j}	H_{6j}
1	1.5	-0.923	1.127	-0.050	-0.476				
2	2.5	-0.475	0.263	-0.050	1.050	-0.050			
3	3.25	-0.022	-0.015	0.050	-0.667	-0.053	-0.048		
4	11.0	-0.138	-0.003	0.050	1.050	-0.050	-0.050	-0.050	
5	9.0	0.023	-0.025	-0.050	-0.150	-0.050	-0.050	-0.050	-0.05
j	P_{1j}	P_{2j}	P_{3j}	P_{4j}	a_{1j}	a_{2j}	a_{3j}	a_{4j}	
1	9.234	2.908	3.404	0.062	5.206	-2.494	-.0877	-0.206	
2	0.954	-0.340	3.512	0.001	-0.343	0.615	-.0010	-0.283	
3	11.594	0.312	11.369	0.001	0.307	0.712	-.0010	-0.087	
4	3.533	0.811	8.148	0.001	0.821	-0.387	-.0010	-0.122	
5	0.361	0.785	0.874	0.001	0.786	-0.373	-.0010	-1.143	

Table(1) Concluded.

(a) C_L Responses

$A_0(k) = 1.131+0.804*k$

j	C_j	E_{1j}	E_{2j}	H_{1j}	H_{2j}	H_{3j}	H_{4j}	H_{5j}	H_{6j}
1	1.9	1.068	1.262	0.350	0.819				
2	1.7	0.480	-0.238	-0.950	-0.250	-0.950			
3	1.45	-0.057	-0.110	0.150	1.050	1.050	-0.950		
4	1.0	-0.310	-0.062	0.850	-0.950	-0.950	1.050	0.550	
5	12.0	0.045	-0.017	0.050	0.652	1.096	-0.068	-0.050	-.050
j	P_{1j}	P_{2j}	P_{3j}	P_{4j}	a_{1j}	a_{2j}	a_{3j}	a_{4j}	
1	-17.22	0.244	14.046	0.001	0.2696	-1.496	-.0010	-.0702	
2	-0.142	-0.005	0.572	0.001	-.0044	-.2436	-.0010	-1.748	
3	50.422	-0.226	16.683	0.001	-.2882	3.311	-.0010	-.0589	
4	0.1656	0.710	1.784	0.001	0.7127	-.6199	-.0010	-.5596	
5	0.3468	1.456	0.204	0.001	1.4559	0.2427	-.0010	-4.898	

(b) C_D Responses

$A_0(k)=0.916+1.552*k$

j	C_j	E_{1j}	E_{2j}	H_{1j}	H_{2j}	H_{3j}	H_{4j}	H_{5j}	H_{6j}
1	2.5	0.162	-0.023	0.750	0.077				
2	2.5	0.511	0.259	-0.150	-0.250	0.250			
3	1.0	-0.115	-0.037	-0.950	1.050	1.050	1.050		
4	7.0	0.063	-0.003	0.050	-0.750	-0.050	-0.050	-0.050	
5	28.0	-0.007	-0.002	0.050	-0.150	-0.050	-0.050	-0.050	-0.05
j	P_{1j}	P_{2j}	P_{3j}	P_{4j}	a_{1j}	a_{2j}	a_{3j}	a_{4j}	
1	-5.174	0.009	9.309	0.001	0.014	-.5699	-.0010	-.1064	
2	56.012	0.746	19.232	0.001	0.717	2.1958	-.0010	-.0510	
3	-0.146	0.287	2.023	0.001	0.288	-.3602	-.0010	-.4932	
4	10.592	-0.411	17.481	0.001	-.4377	1.0437	-.0010	-.0562	
5	-0.307	0.929	2.756	0.001	0.934	-1.046	-.0010	-.3619	

Table(2) Model Coefficients for An F-18 Model.

(c) C_M Responses

$A_0(k)=-0.07614+0.7105*k$

j	C_j	E_{1j}	E_{2j}	H_{1j}	H_{2j}	H_{3j}	H_{4j}	H_{5j}	H_{6j}
1	2.5	-0.942	-0.954	-0.150	-0.850				
2	1.1	-0.098	-0.269	-0.350	0.780	-1.001			
3	1.75	-0.117	-0.112	-0.250	-0.050	0.250	-0.050		
4	3.0	-0.098	0.021	-0.050	0.798	0.994	-0.056	-0.050	
5	23.0	-0.018	-0.005	0.050	0.856	-0.066	-0.050	-0.050	-0.05
j	P_{1j}	P_{2j}	P_{3j}	P_{4j}	a_{1j}	a_{2j}	a_{3j}	a_{4j}	
1	-1.464	0.667	1.015	0.001	0.6702	-2.112	-.0010	-.9840	
2	22.400	0.141	23.931	0.001	0.1241	0.8119	-.0010	-.0408	
3	35.605	0.277	26.874	0.001	0.2543	1.0705	-.0010	-.0362	
4	4.007	1.086	5.440	0.018	1.2947	-0.558	-.0207	-.1631	
5	3.289	0.926	4.790	0.001	0.9316	-0.245	-.0010	-.2077	

Table(2) Concluded.

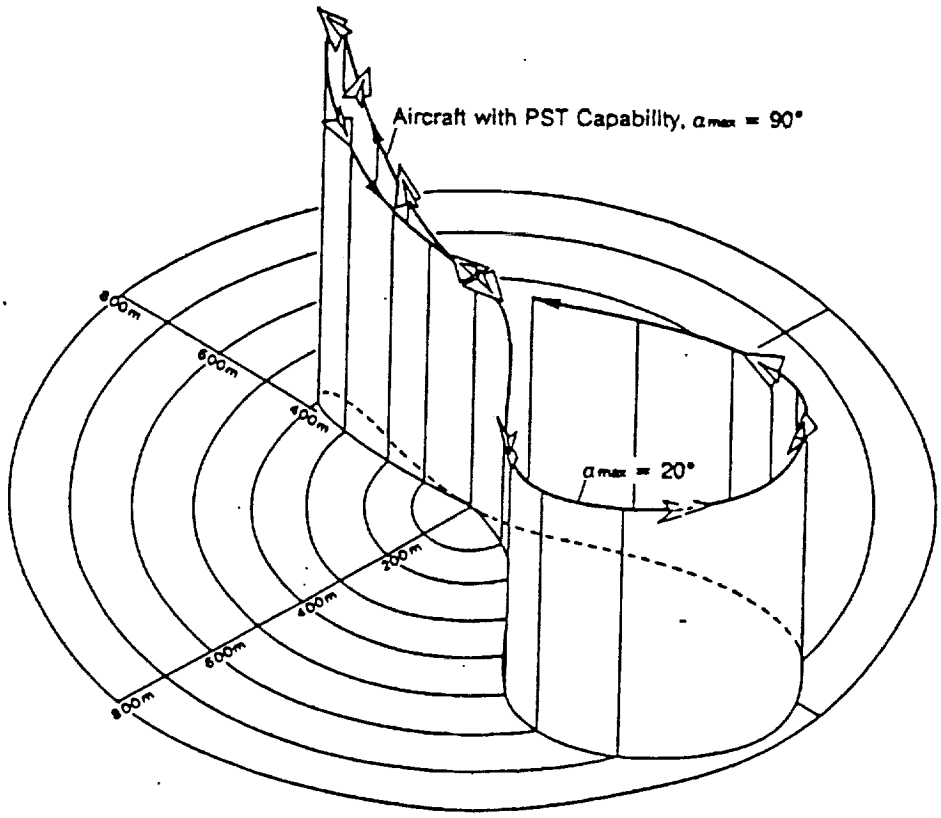

Figure 1 A New Air Combat Tactic with Post-Stall Maneuvering

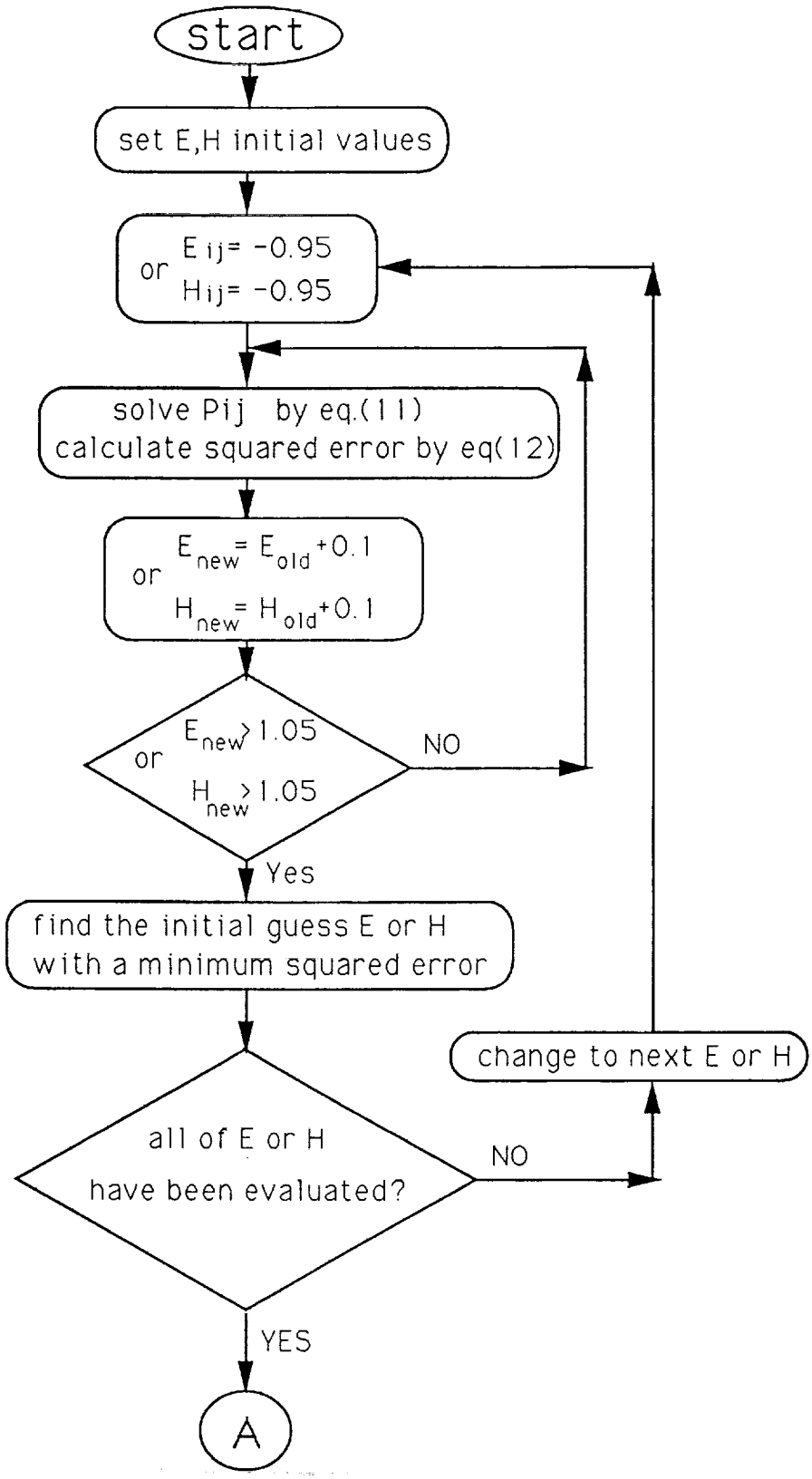

Figure 2 Flow Chart for The Inner Optimization Procedure.

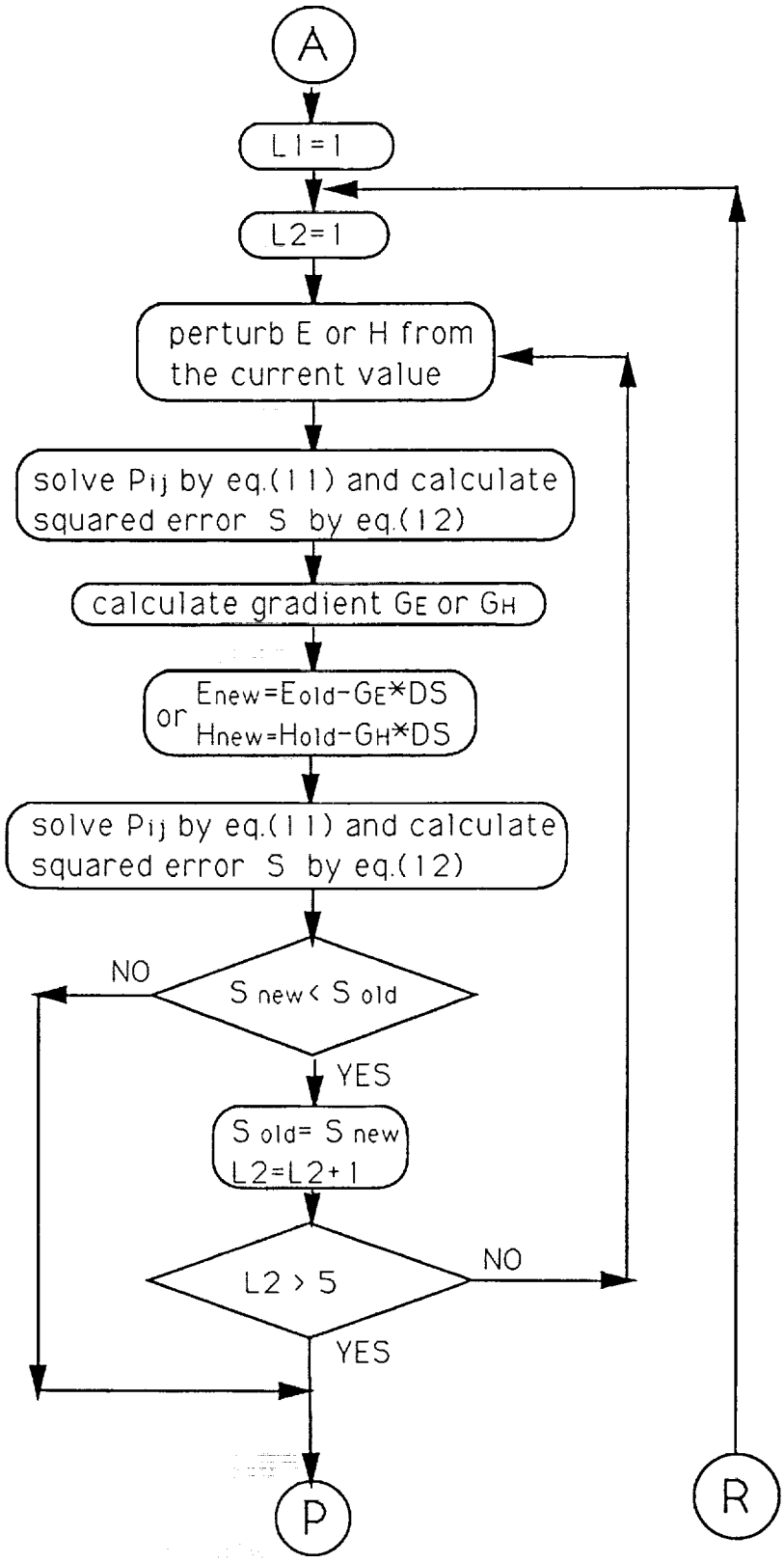

Figure 2 Continued.

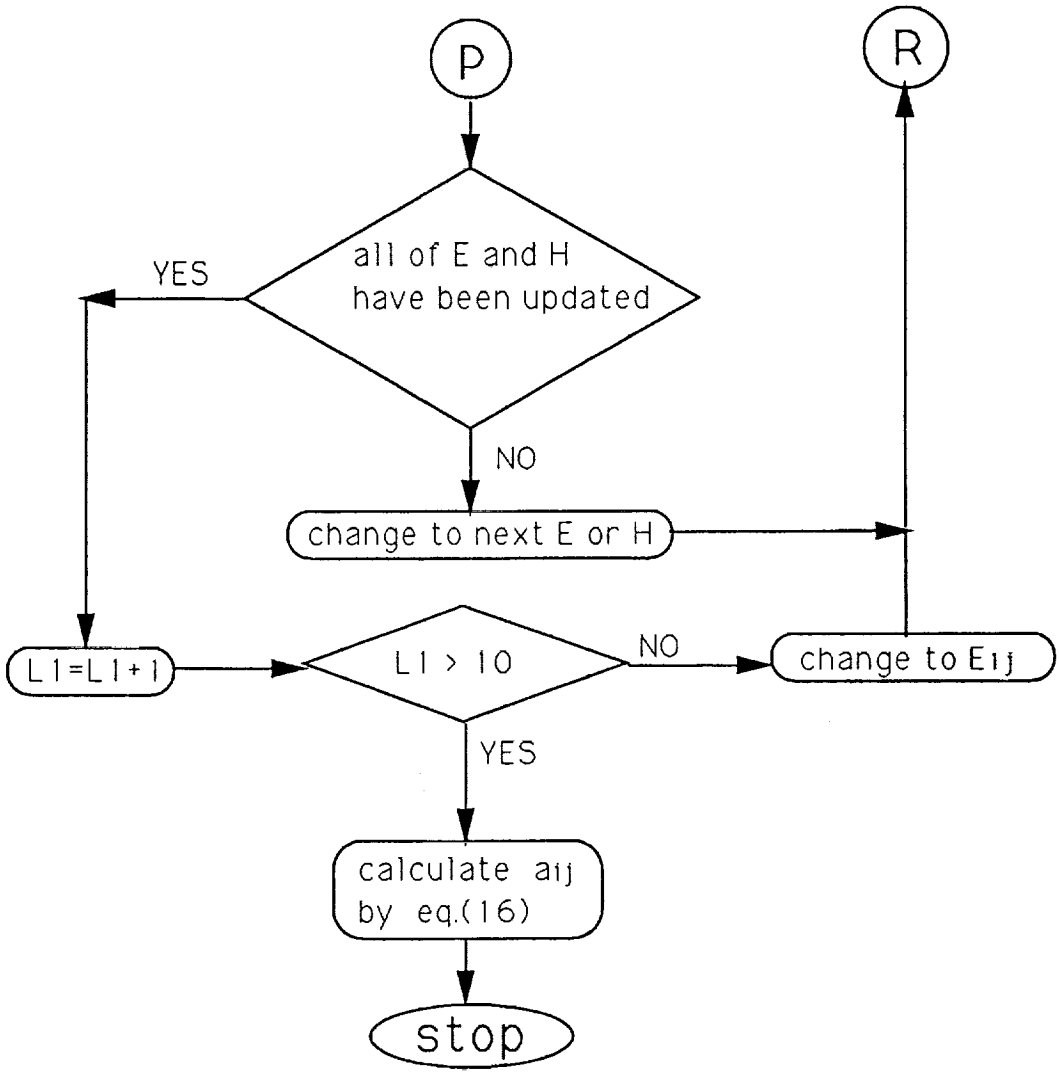

Figure 2 Concluded.

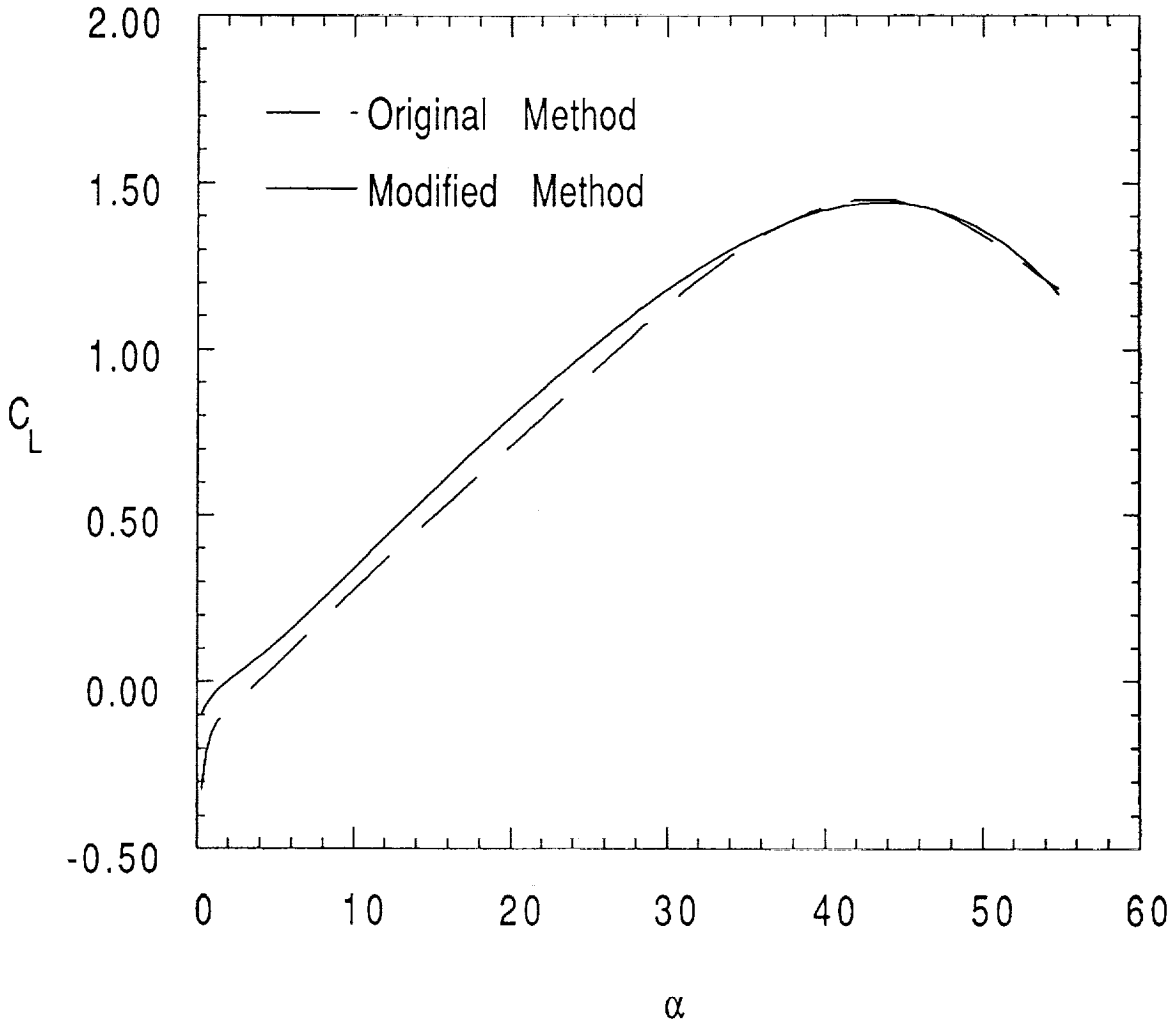

Figure 3 Comparison of Unsteady Lift Coefficient in Constant-Rate Pitch-up Motion by The Modified Method with The Results by The Original Method for A 70-deg. Delta Wing.

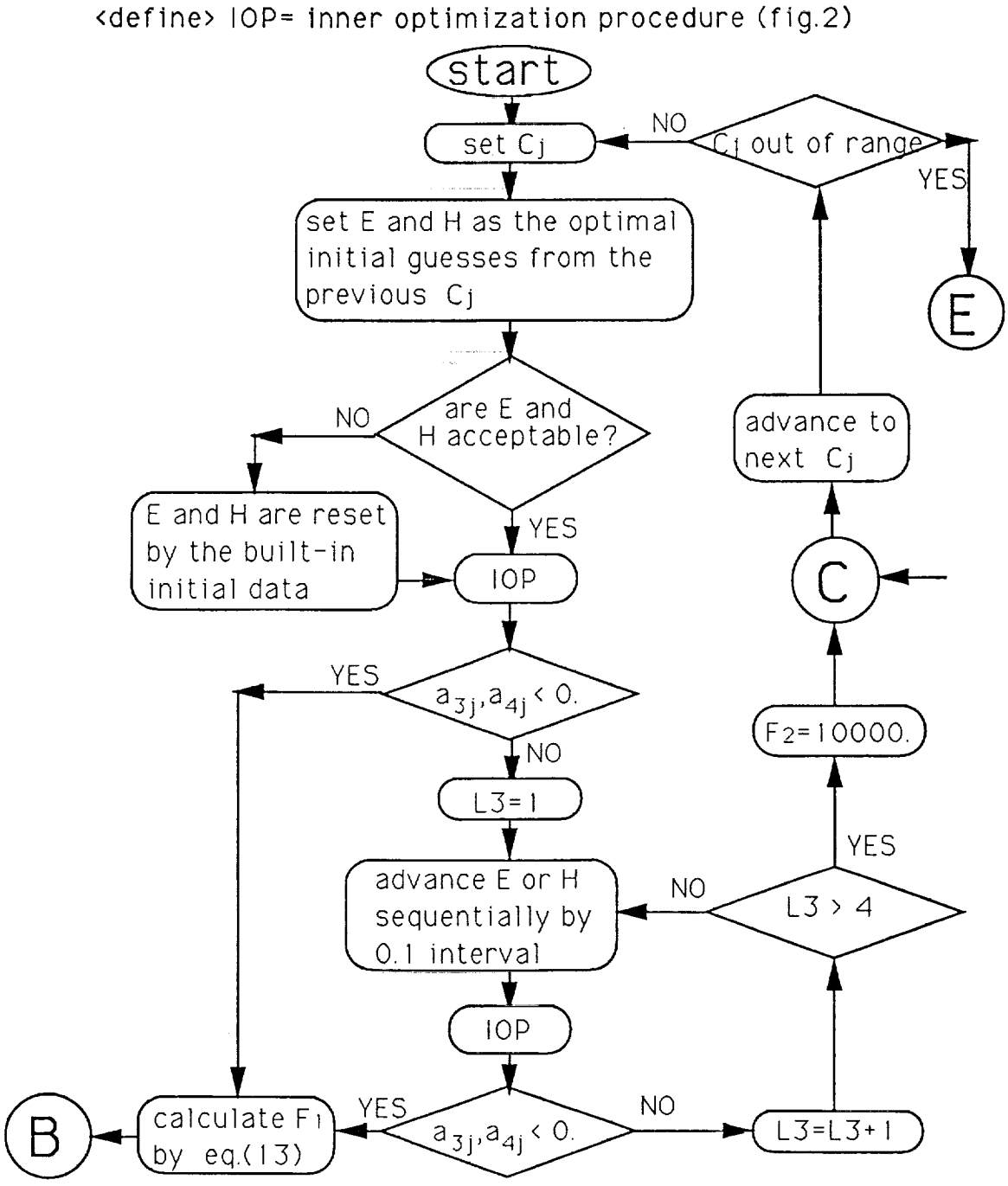

Figure 4 Flow Chart for The Outer Optimization Procedure.

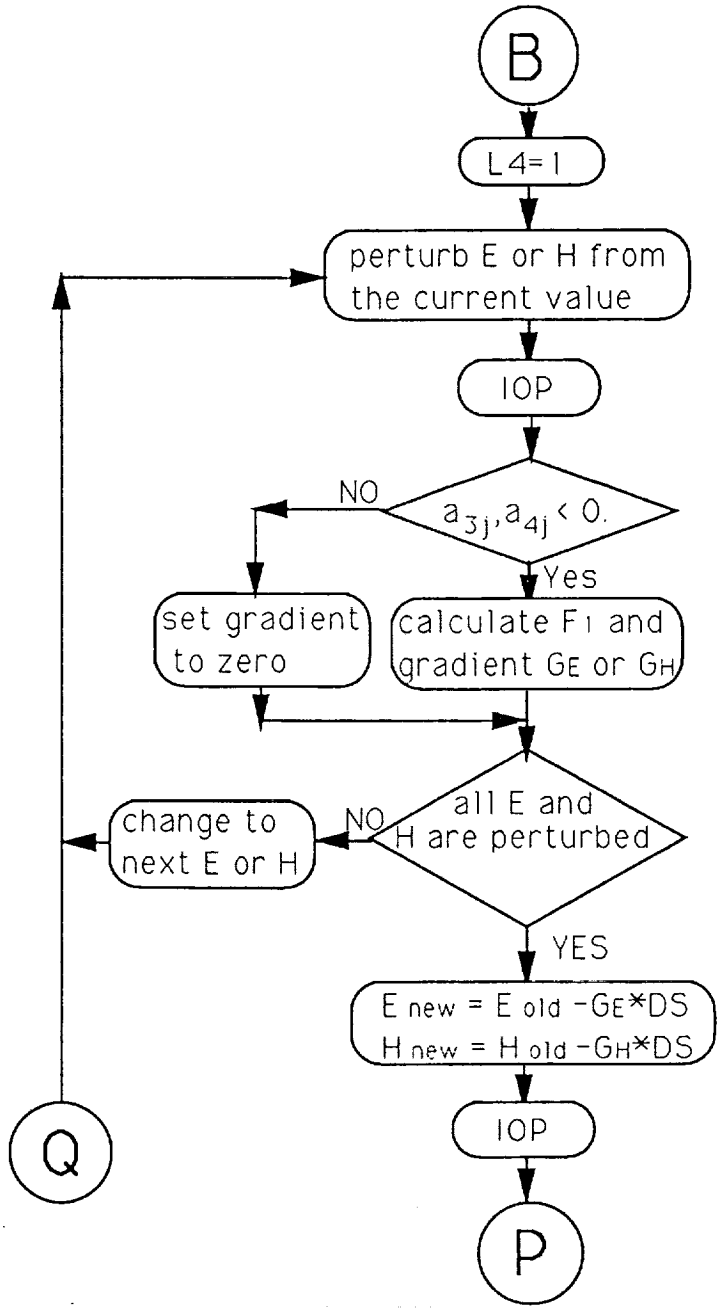

Figure 4 Continued.

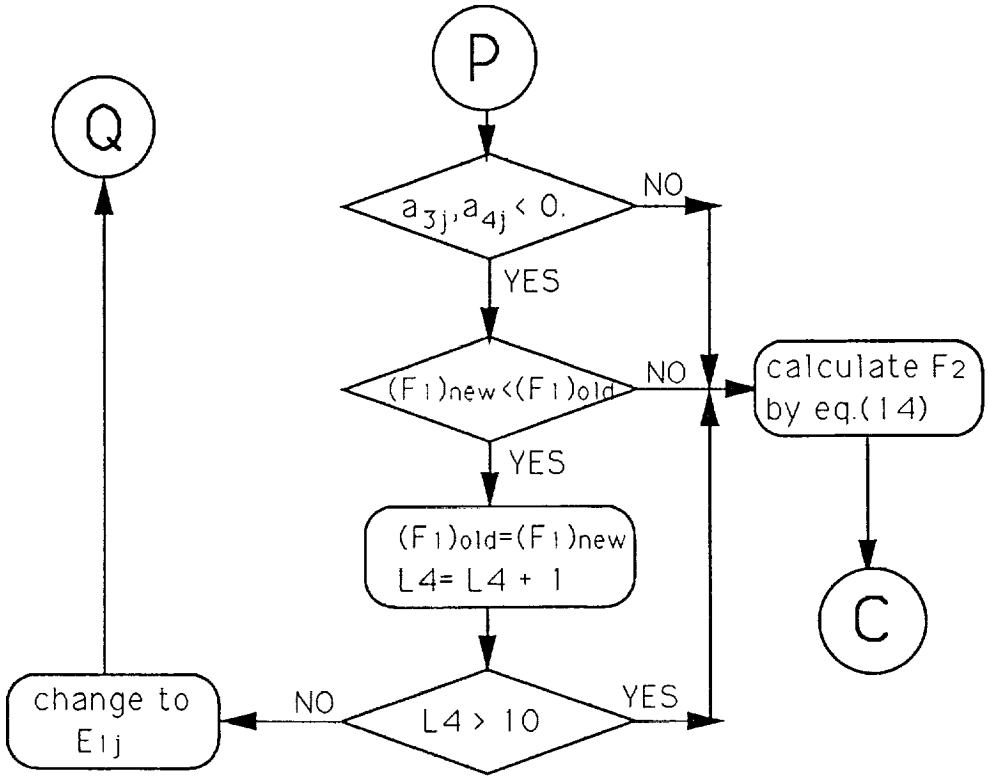

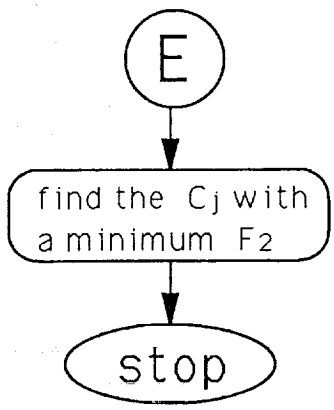

Figure 4 Concluded.

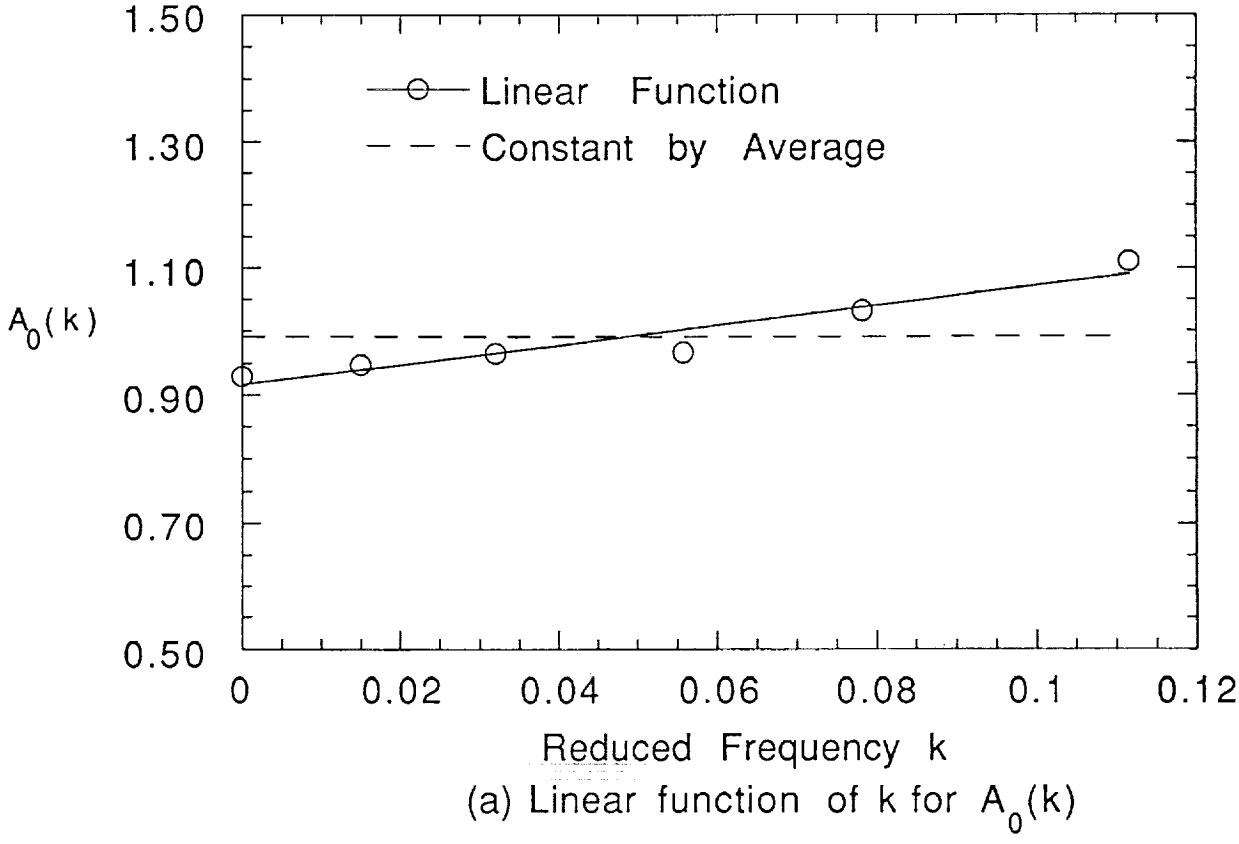

(a) Linear function of k for $A_0(k)$

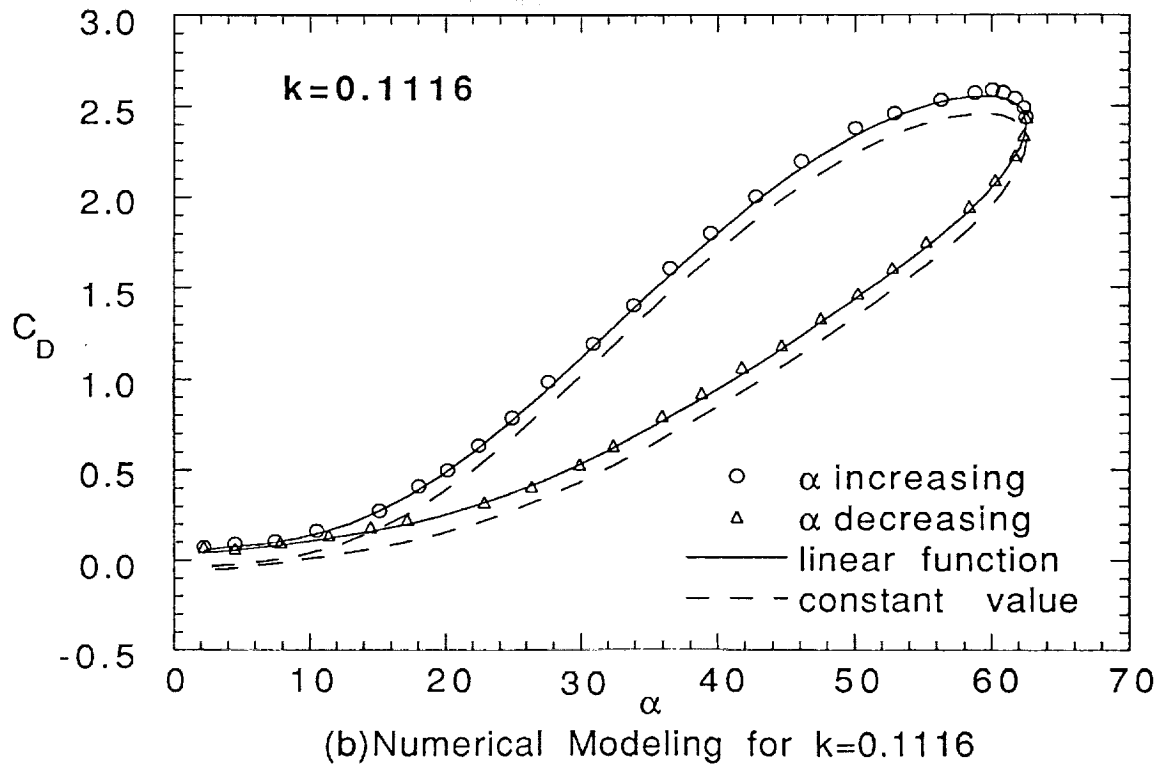

(b)Numerical Modeling for k=0.1116

Figure 5 Comparison of Different Models of $A_0(k)$ for The F-18 C_D Harmonic Responses.

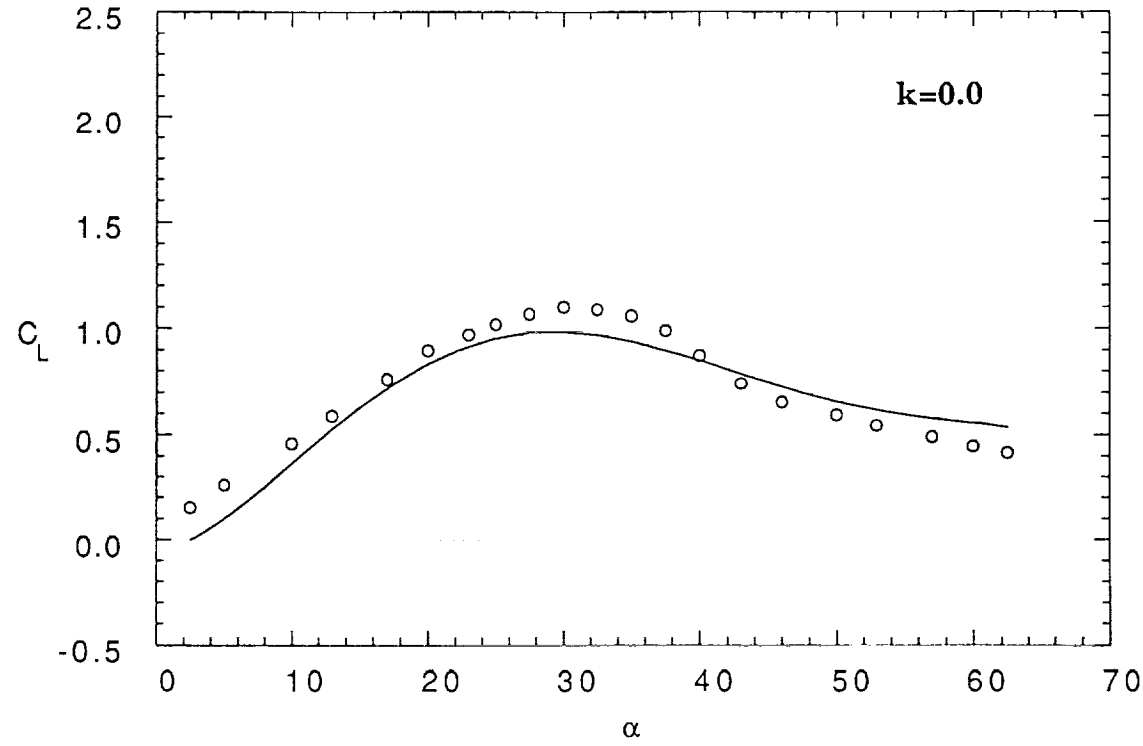

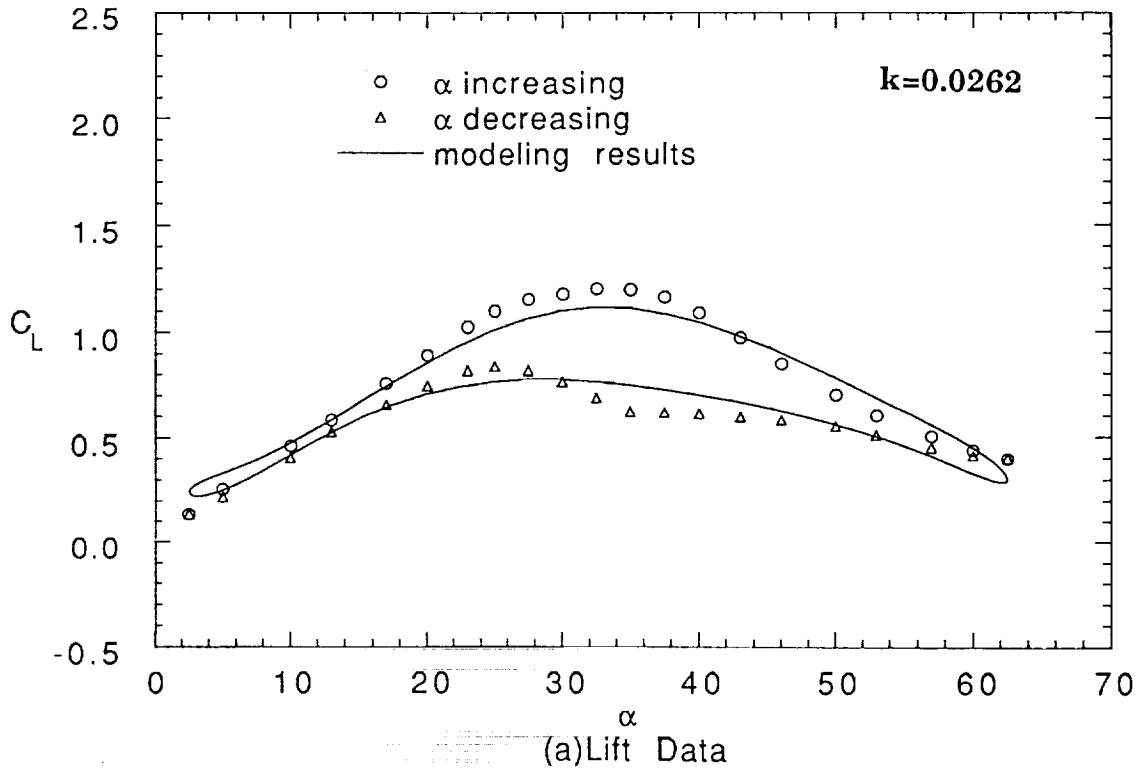

(a)Lift Data

Figure 6 Analysis of The Harmonic Responses for A 70-deg. Delta Wing.

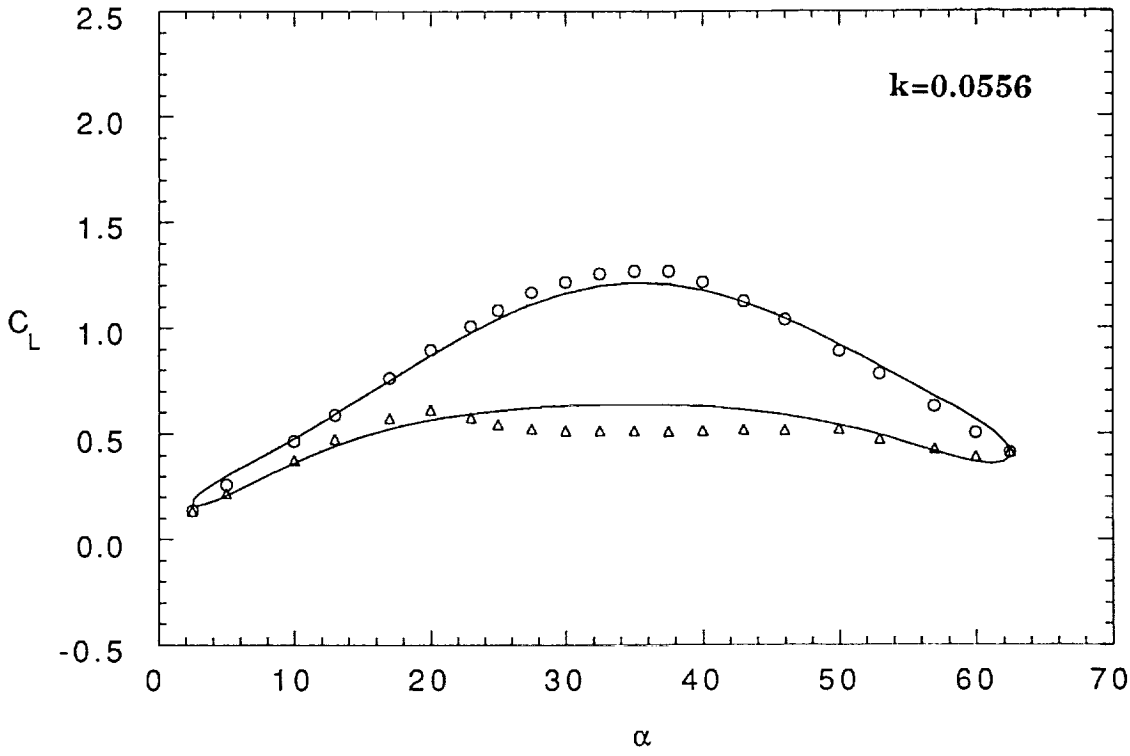

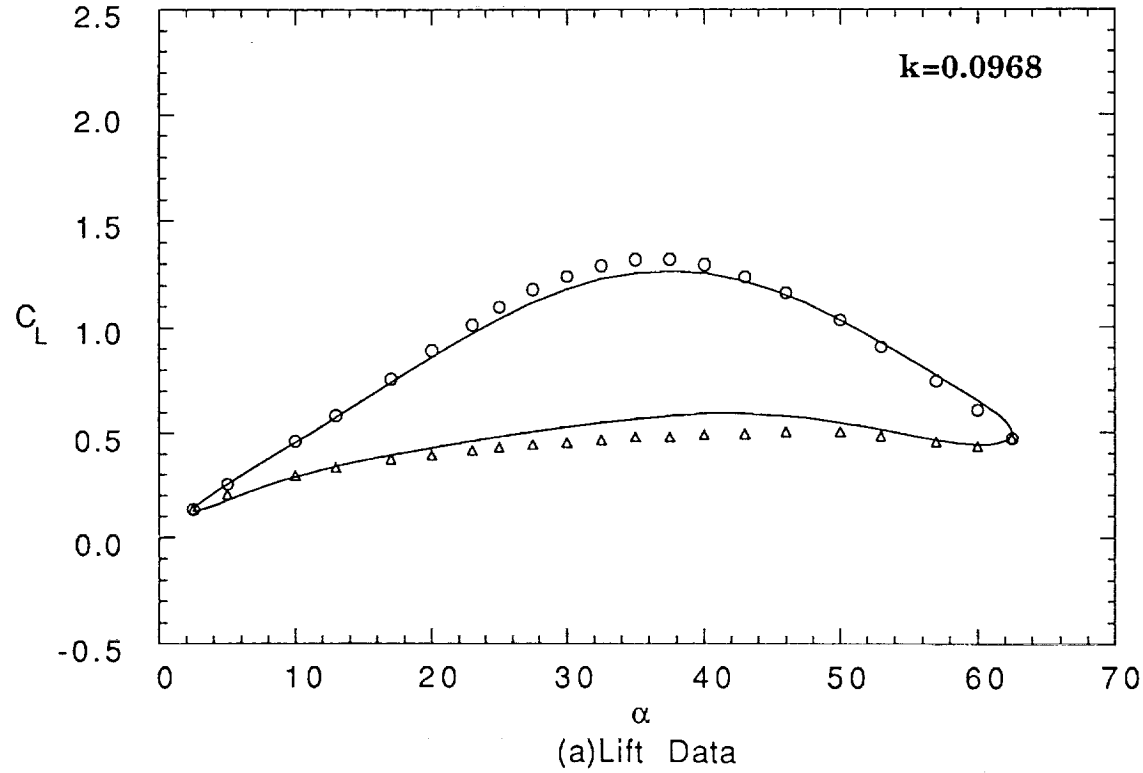

(a)Lift Data

Figure 6 Continued.

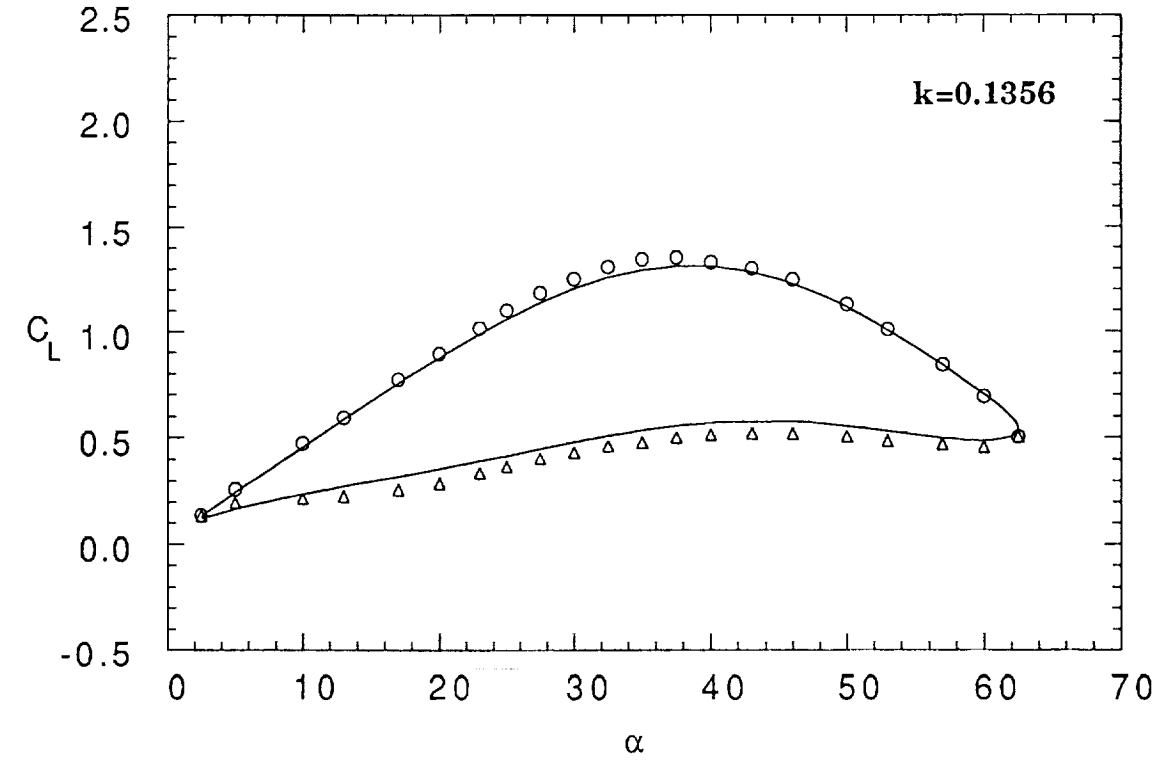

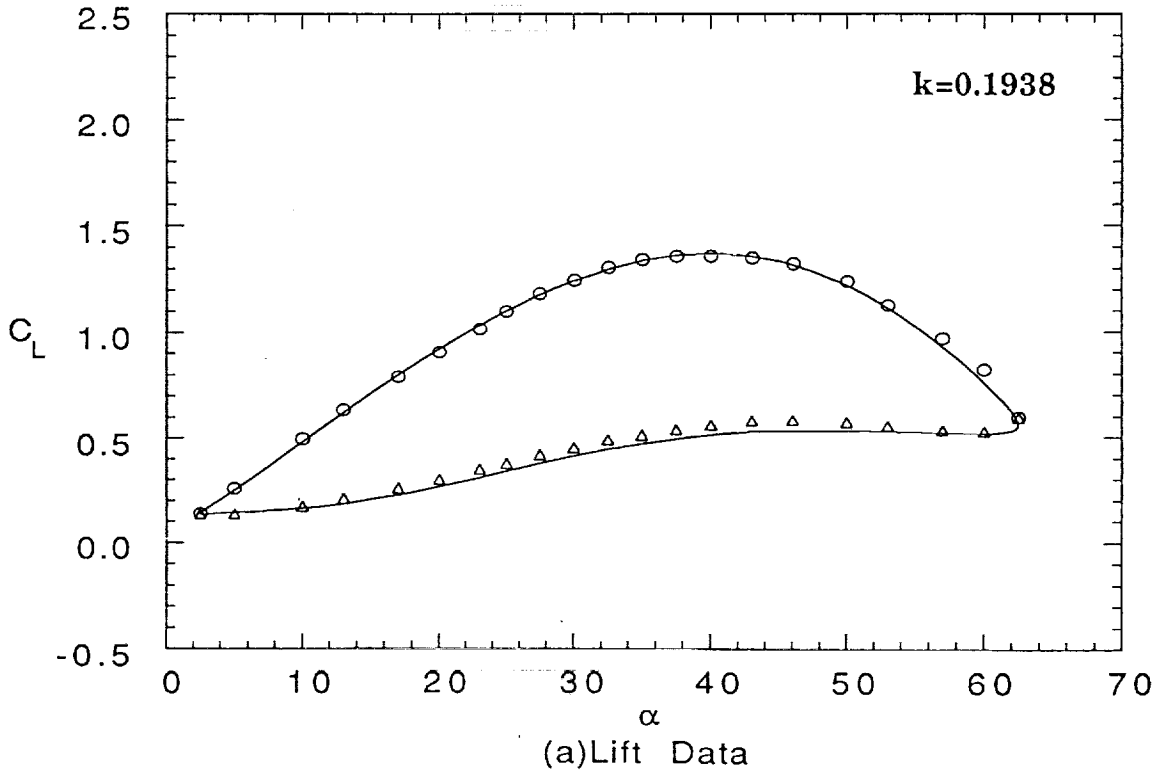

(a)Lift Data

Figure 6 Continued.

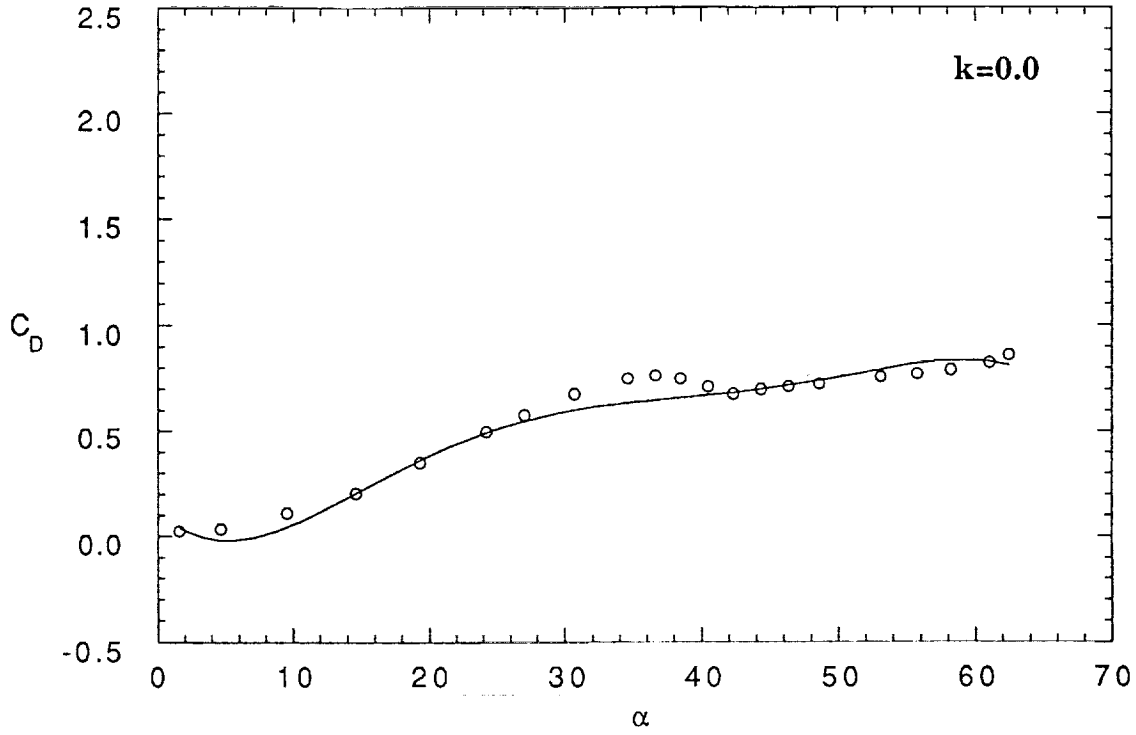

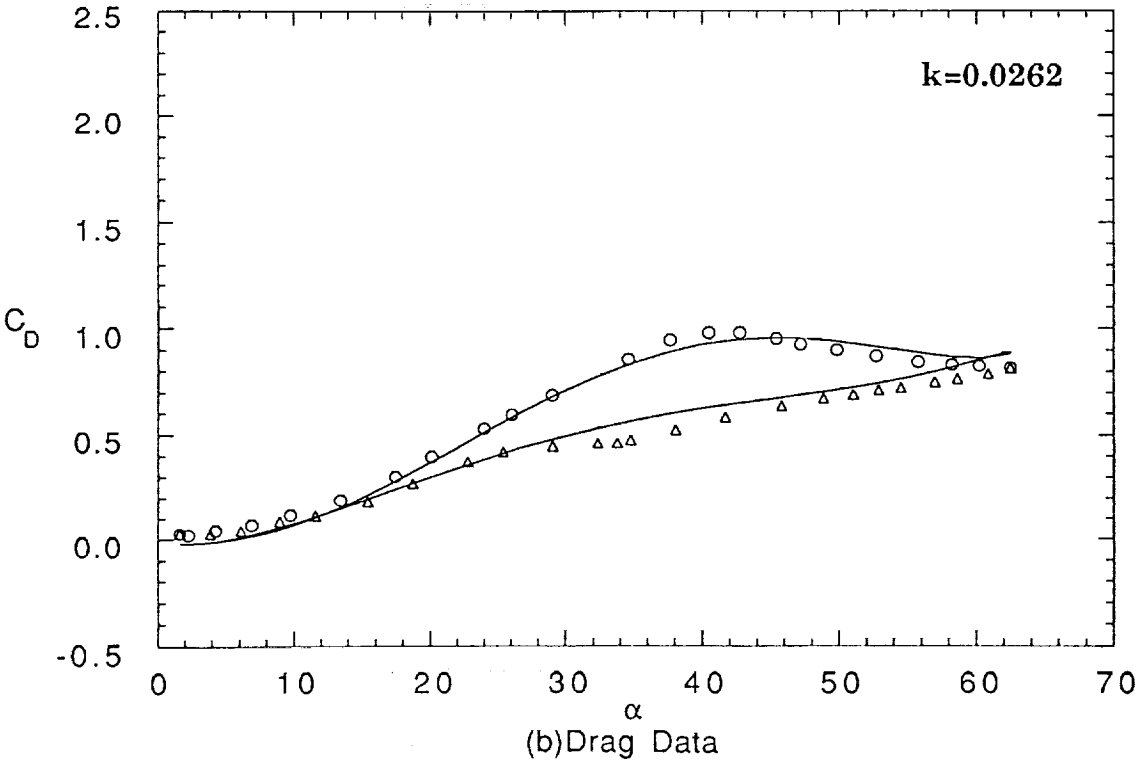

(b)Drag Data

Figure 6 Continued.

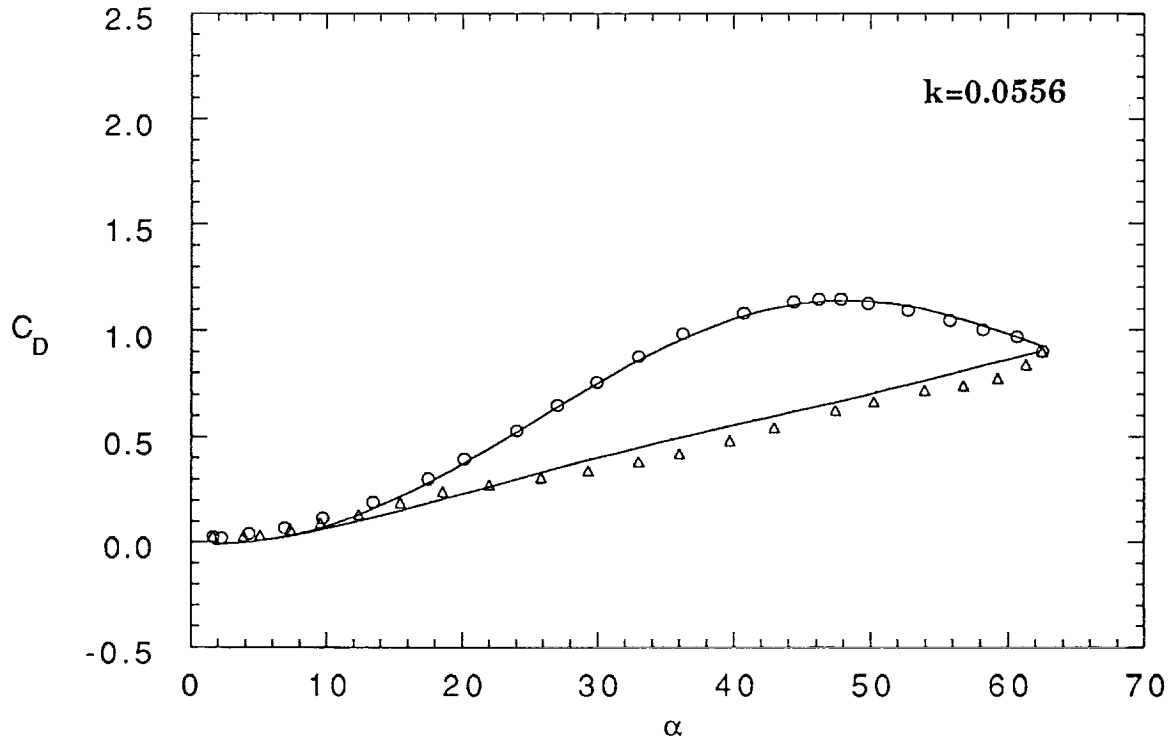

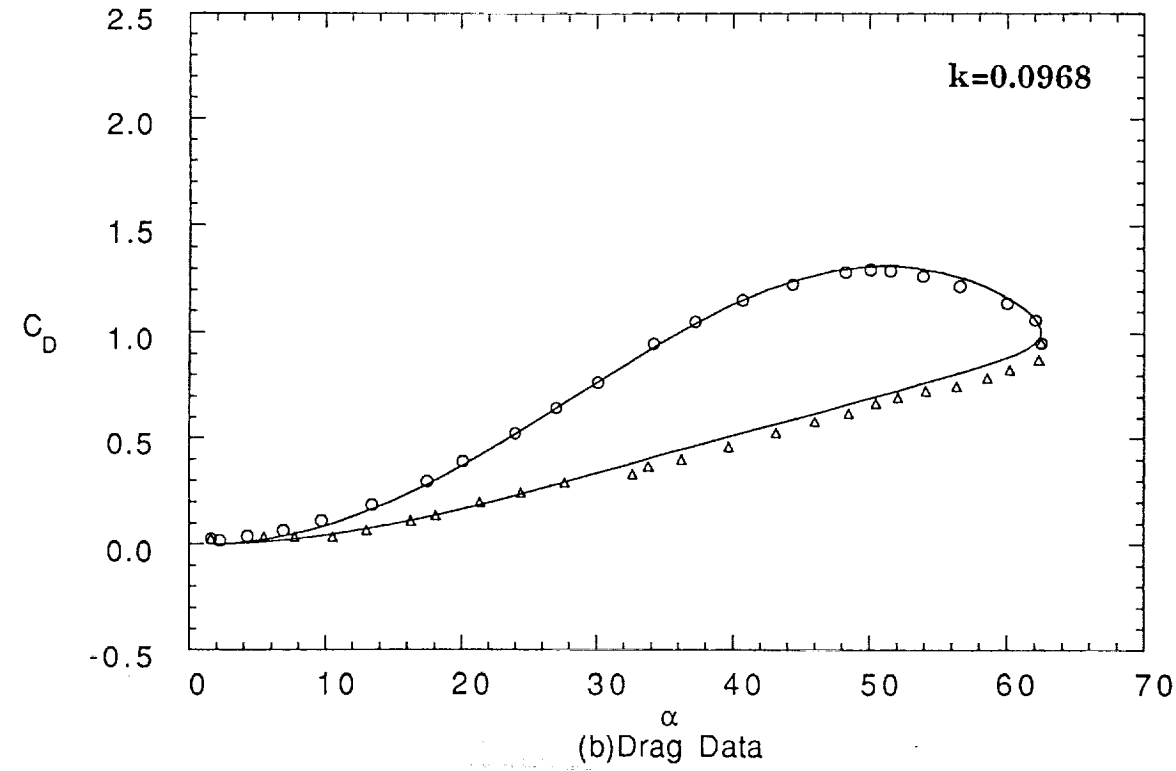

(b)Drag Data

Figure 6 Continued.

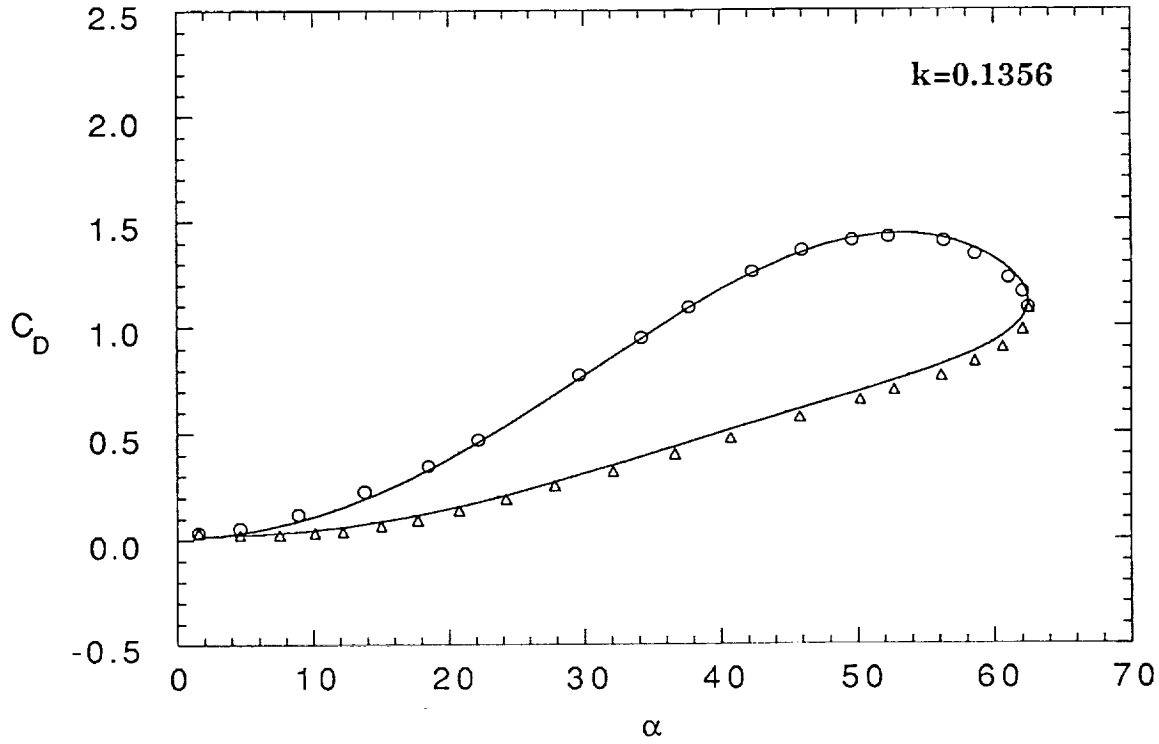

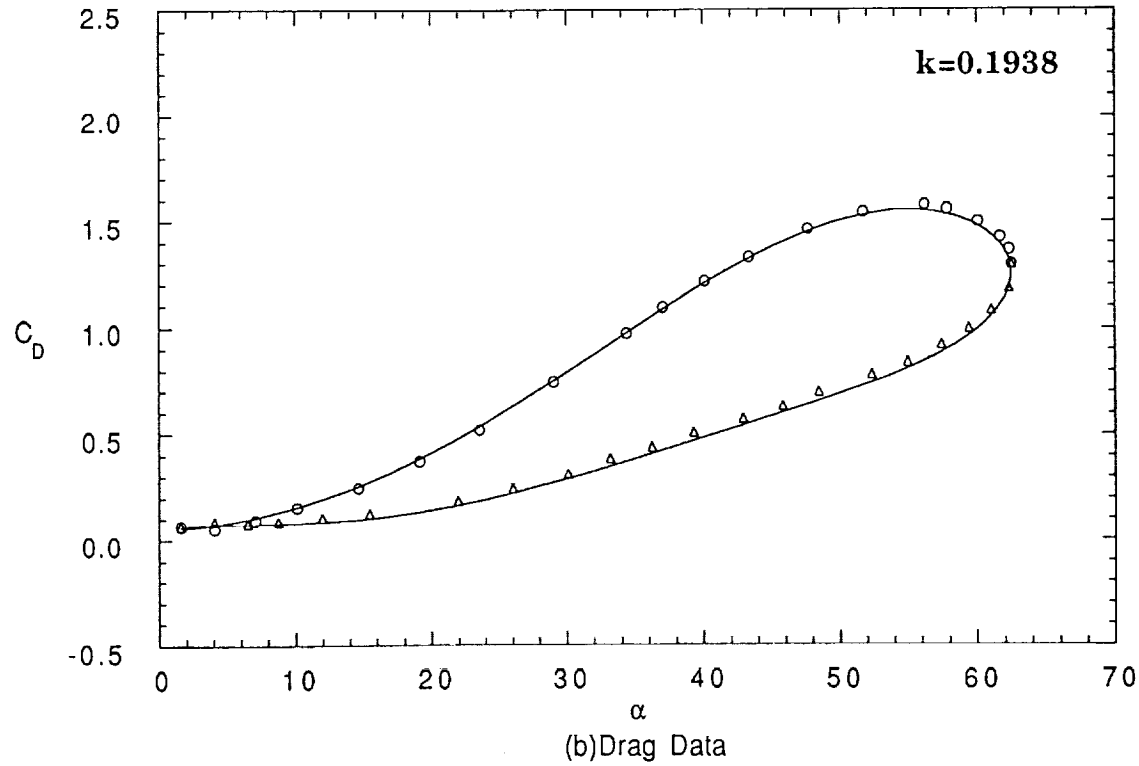

(b)Drag Data

Figure 6 Continued.

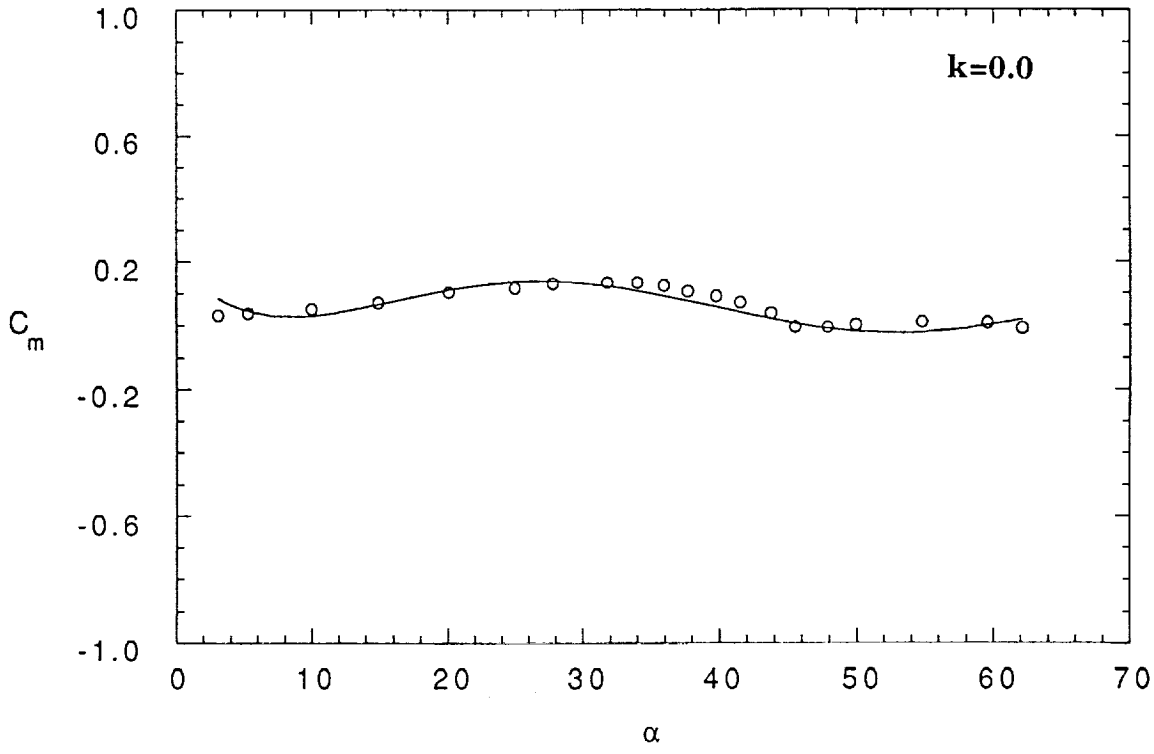

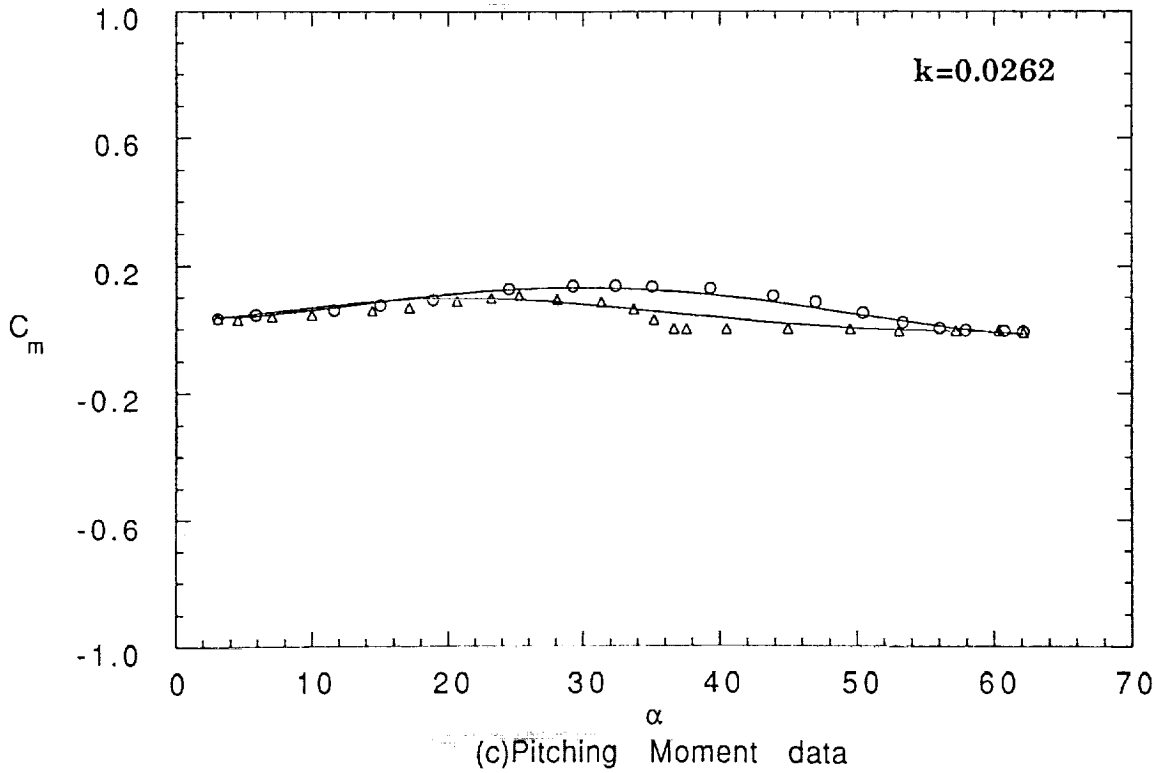

(c)Pitching Moment data

Figure 6 Continued.

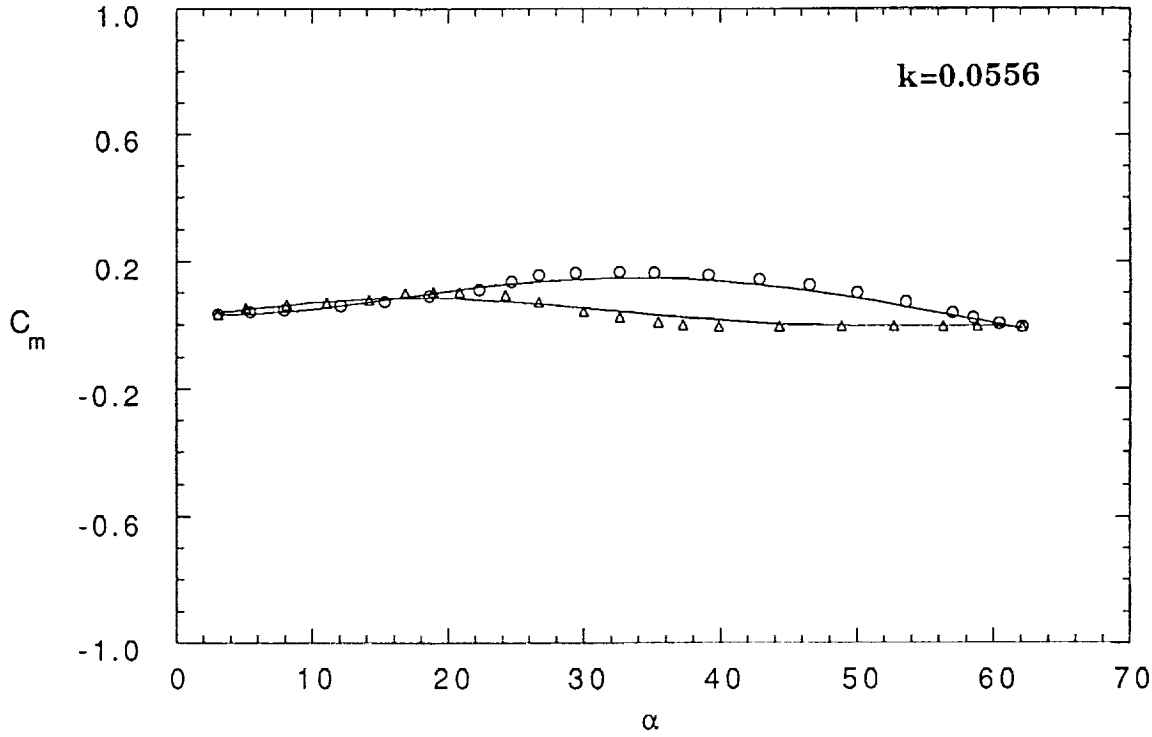

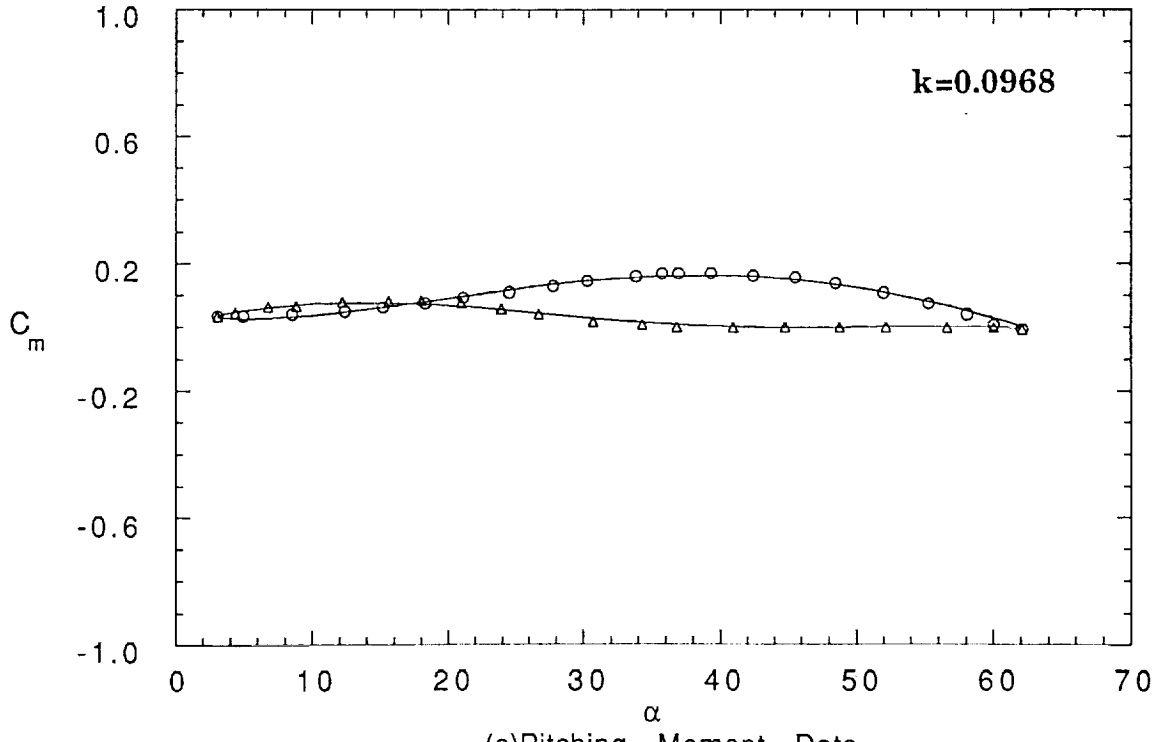

(c)Pitching Moment Data

Figure 6 Continued.

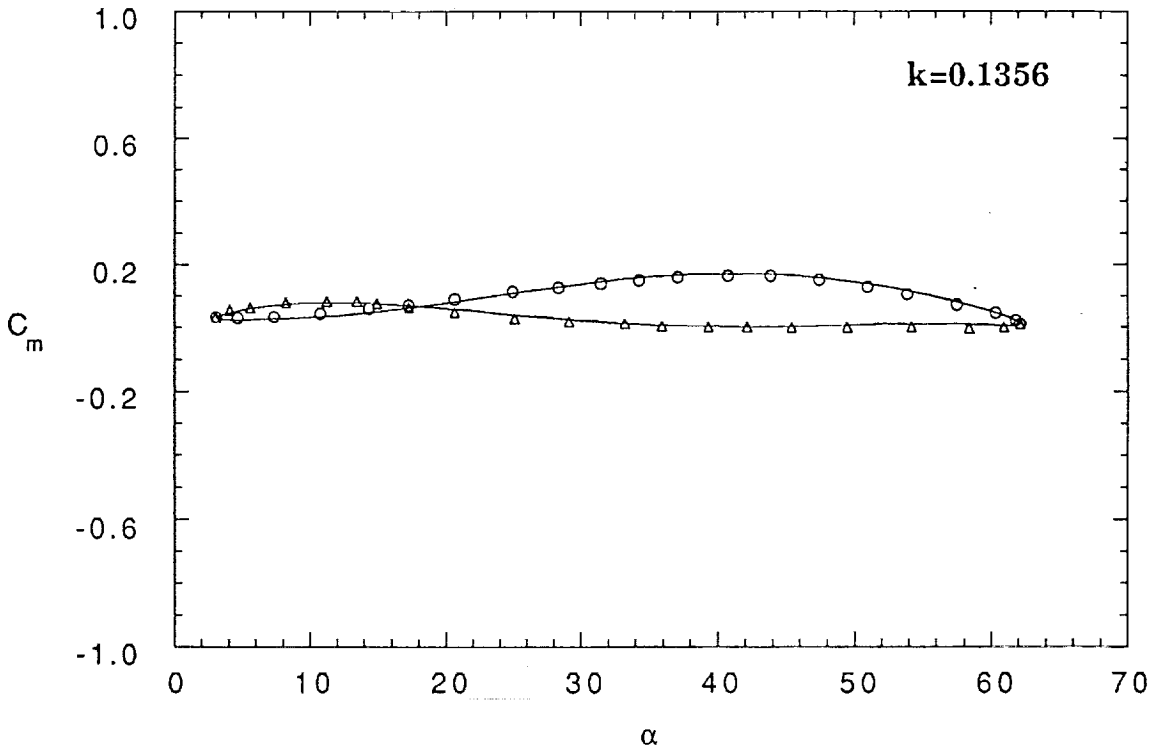

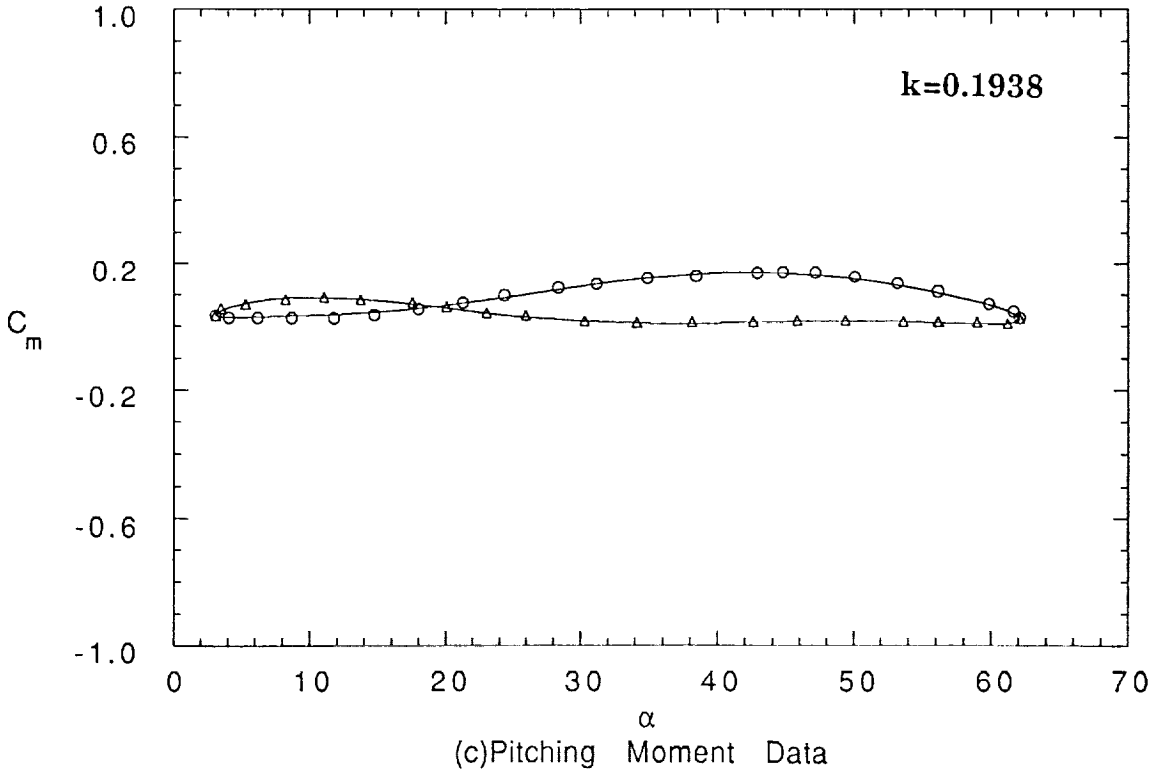

(c)Pitching Moment Data

Figure 6 Concluded.

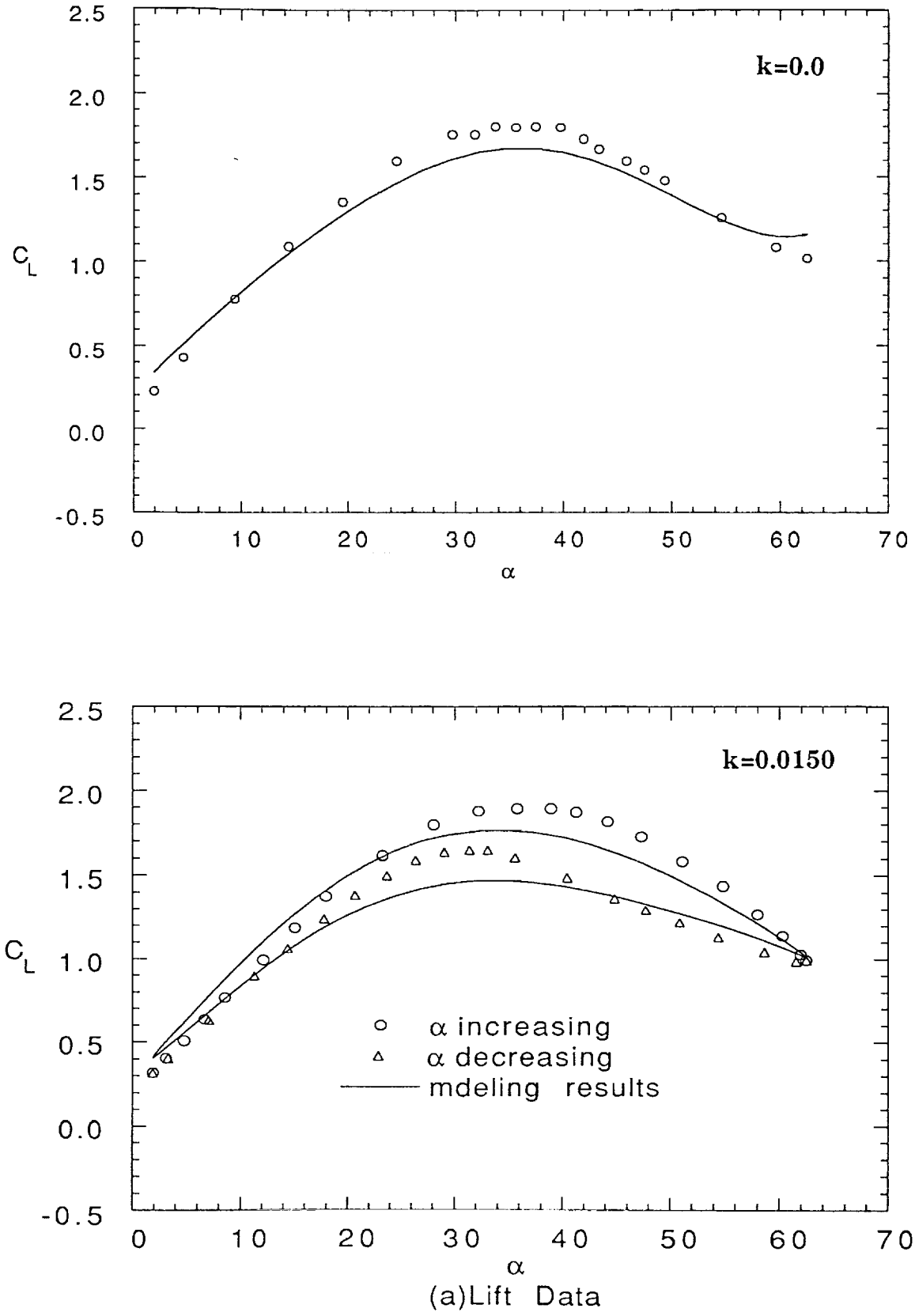

Figure 7 Analysis of The Harmonic Responses for An F-18 Model.

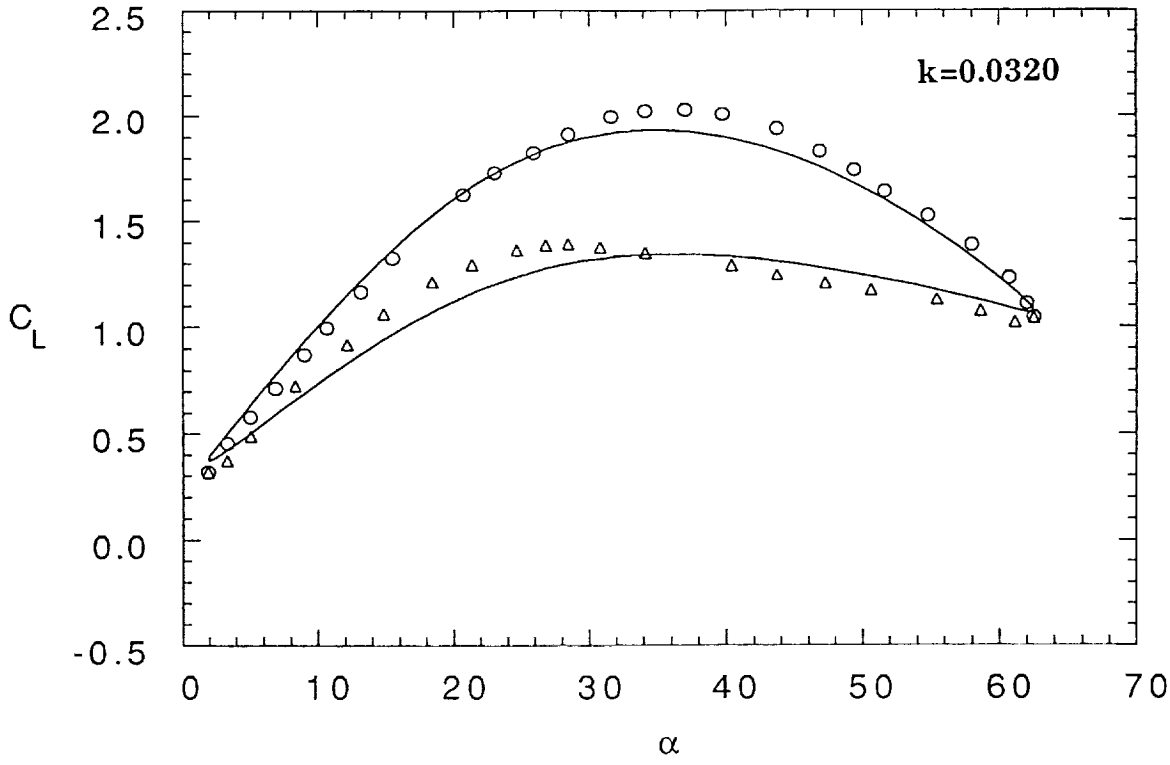

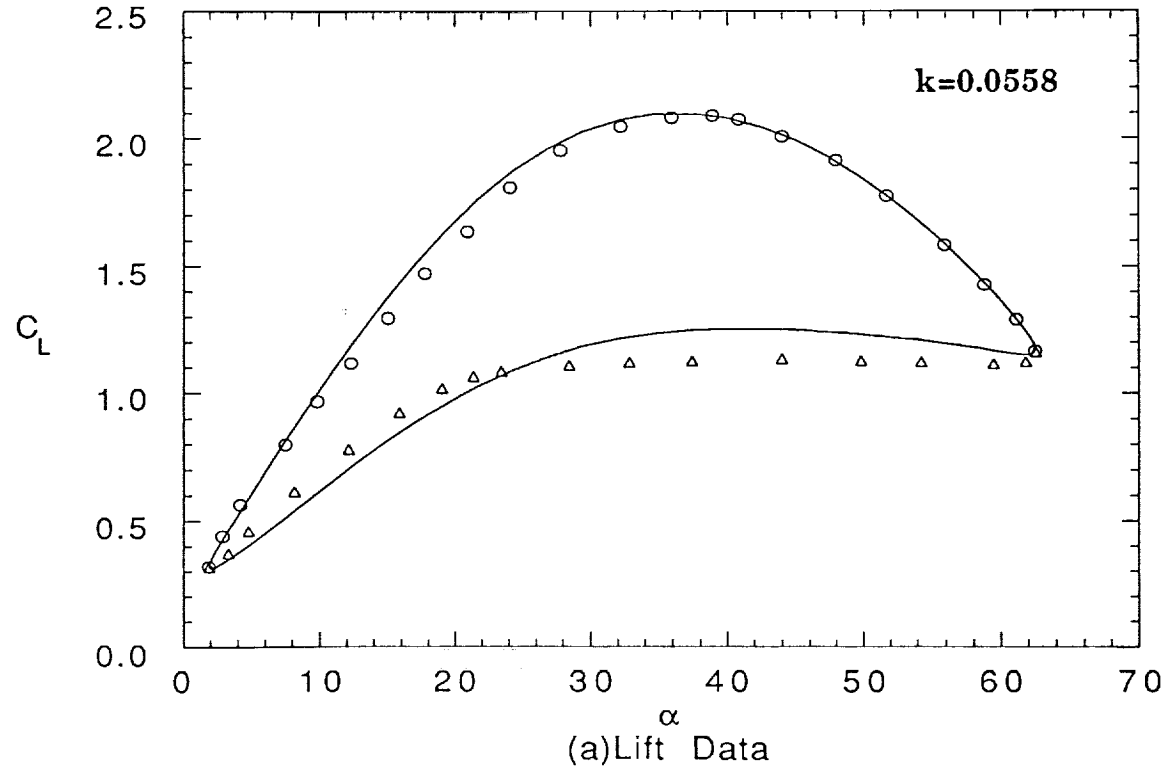

(a)Lift Data

Figure 7 Continued.

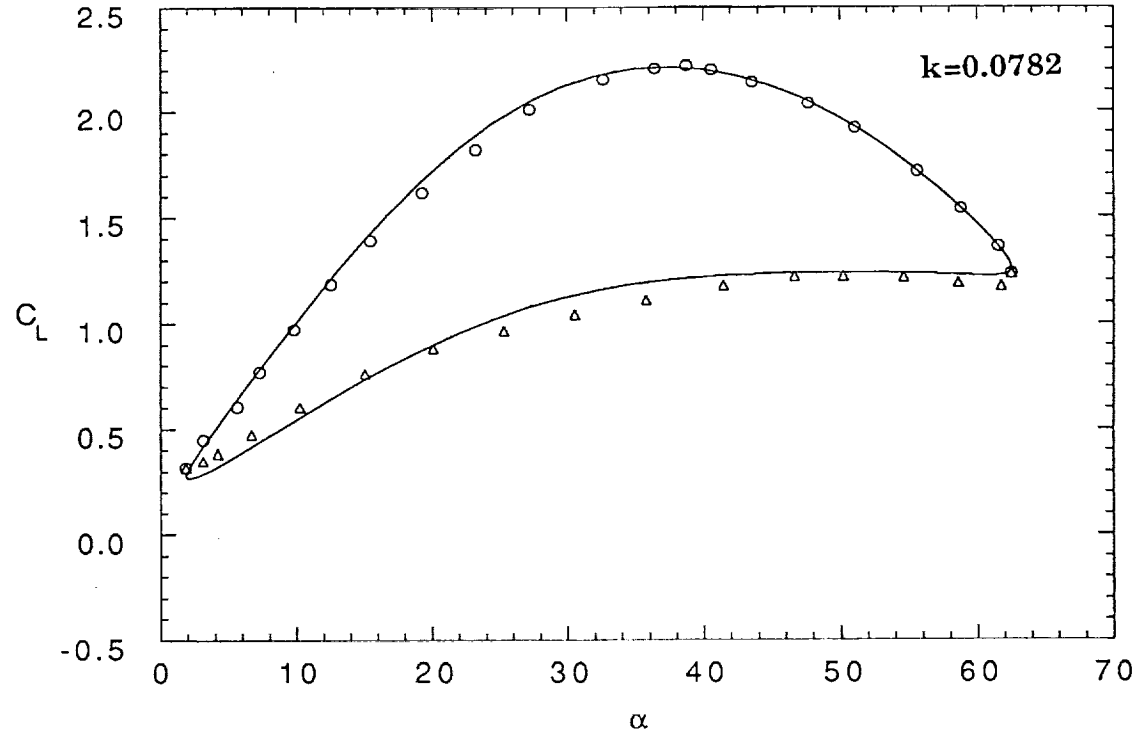

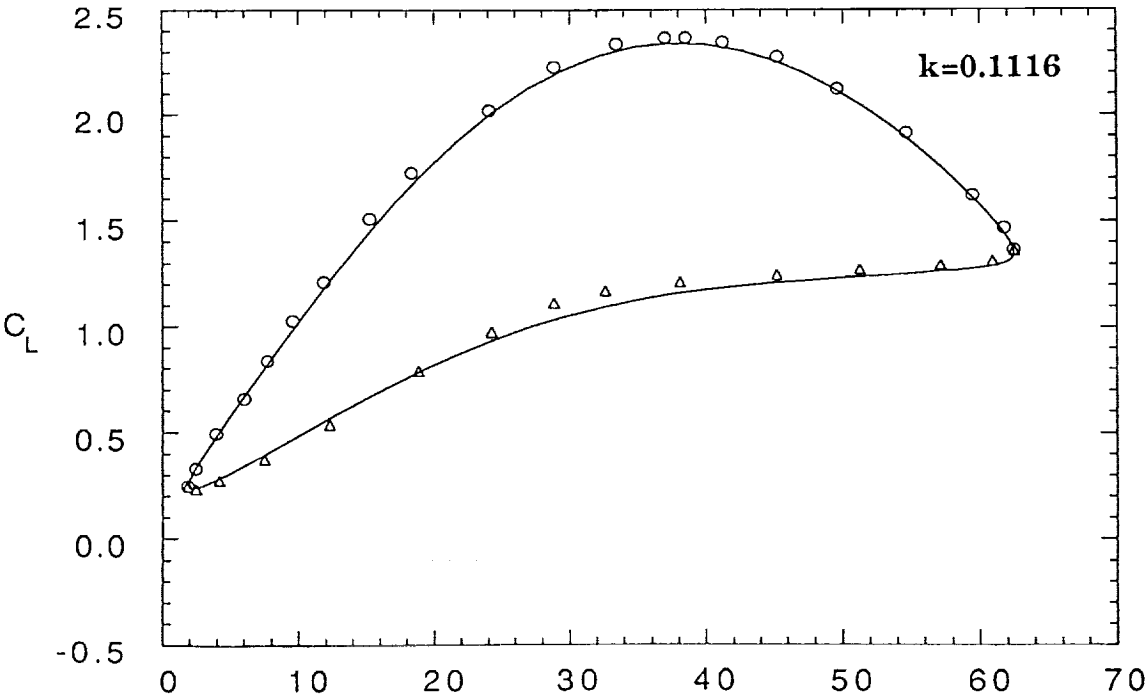

(a)Lift Data

Figure 7 Continued.

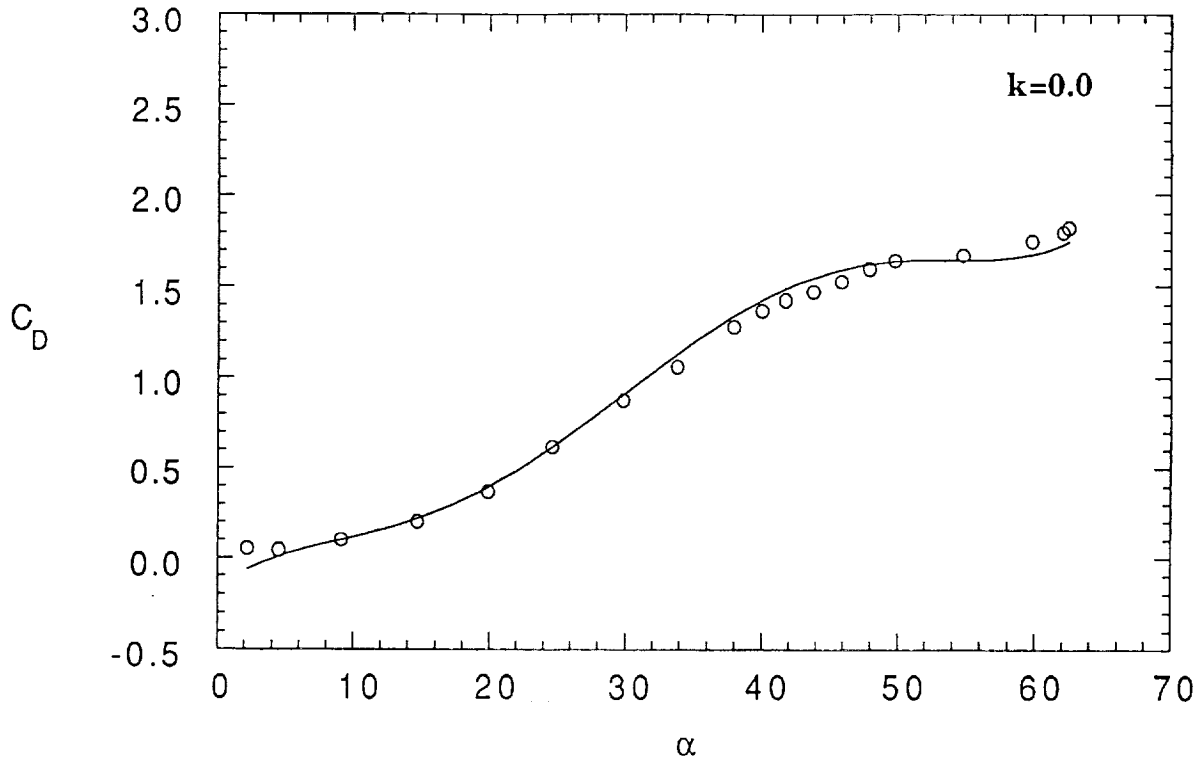

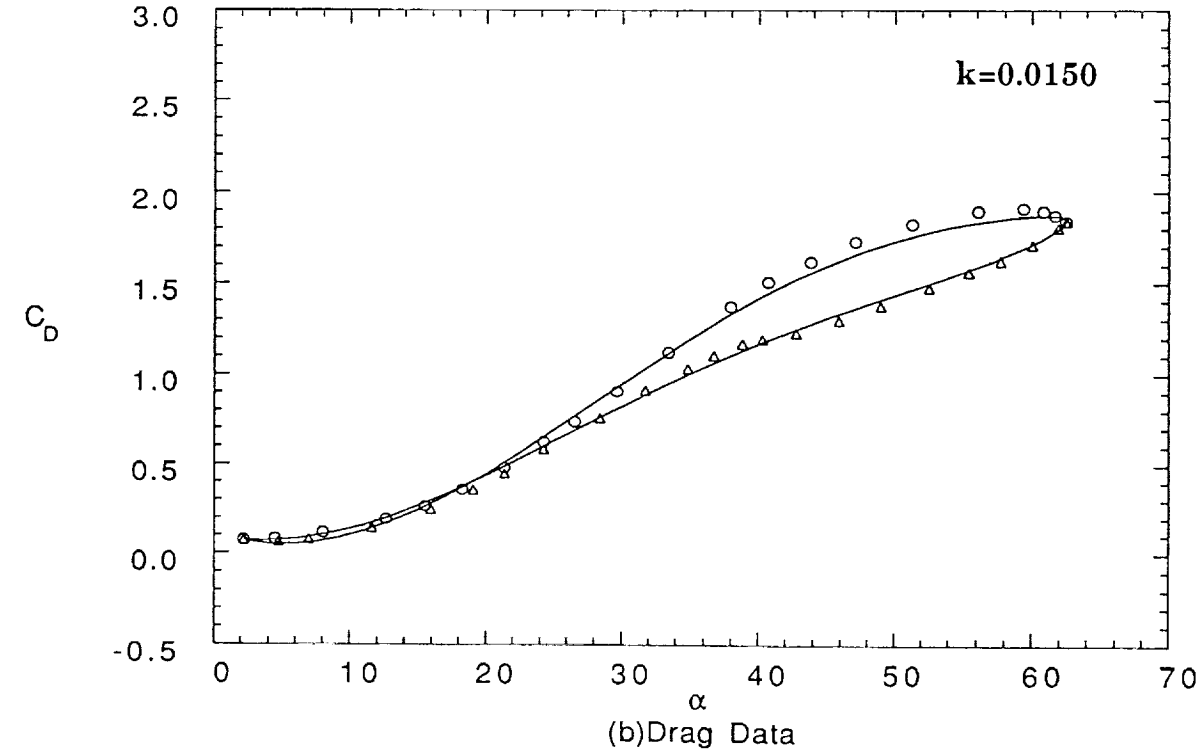

(b)Drag Data

Figure 7 Continued.

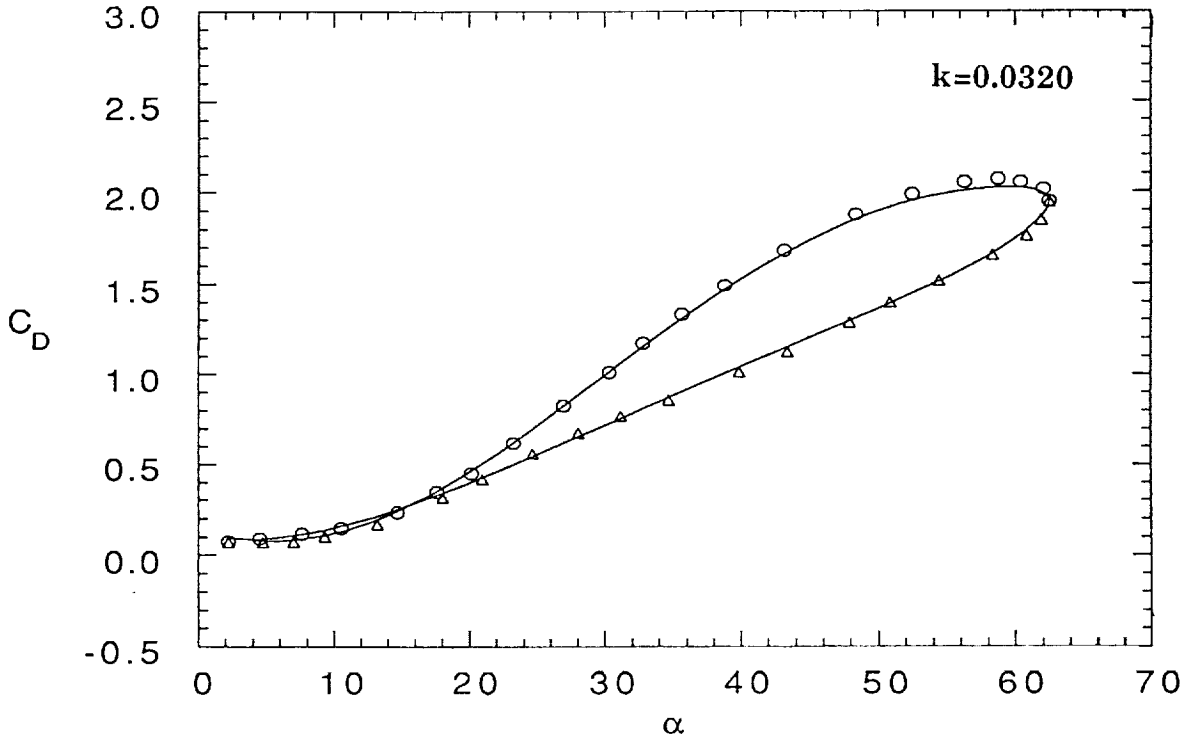

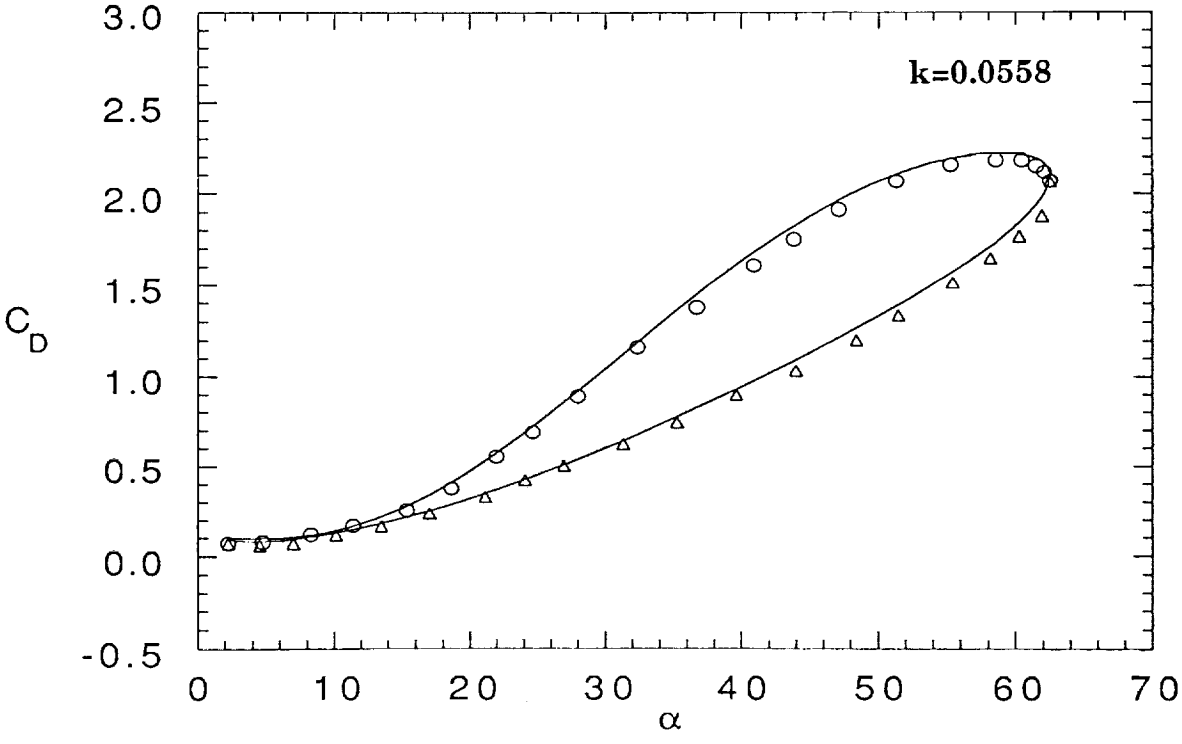

(b)Drag Data

Figure 7 Continued.

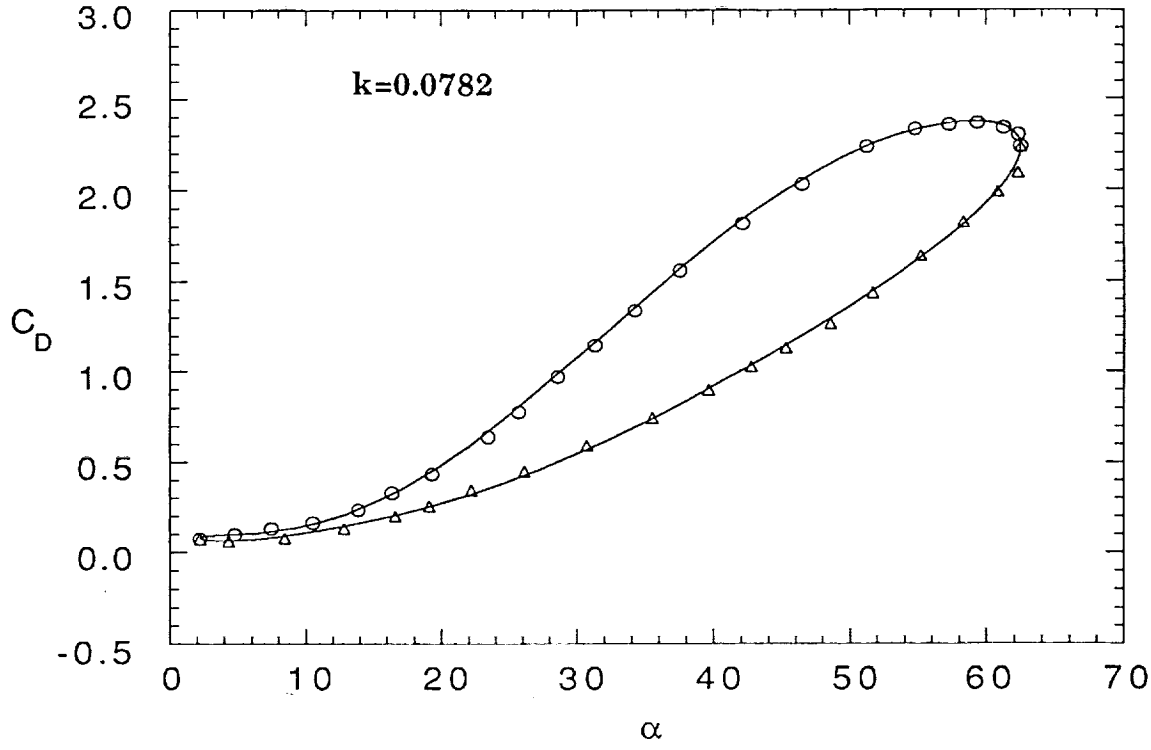

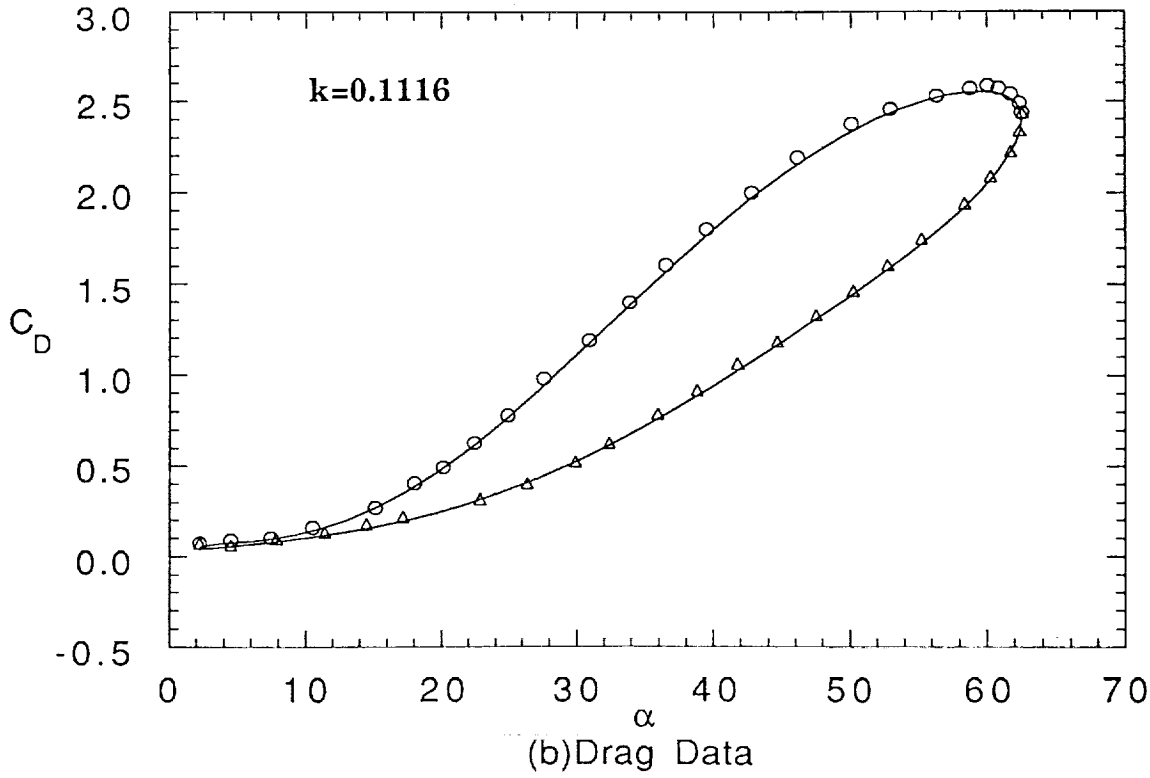

(b)Drag Data

Figure 7 Continued.

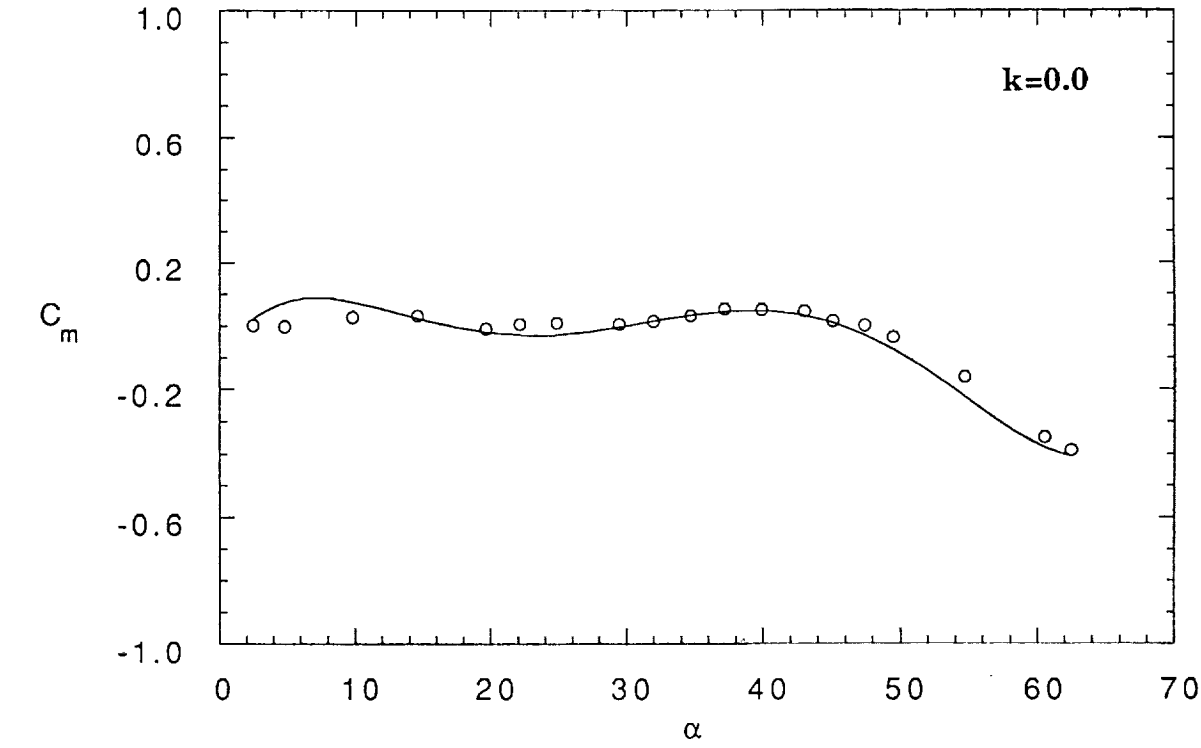

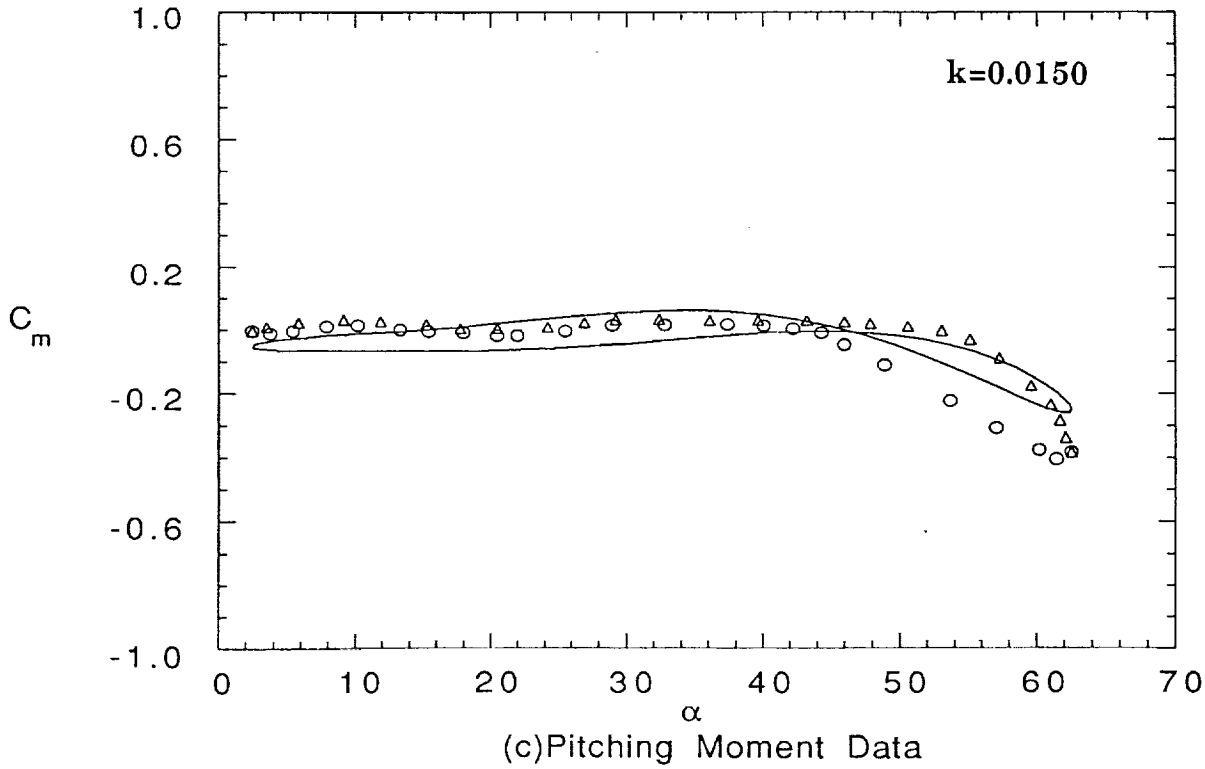

(c)Pitching Moment Data

Figure 7 Continued.

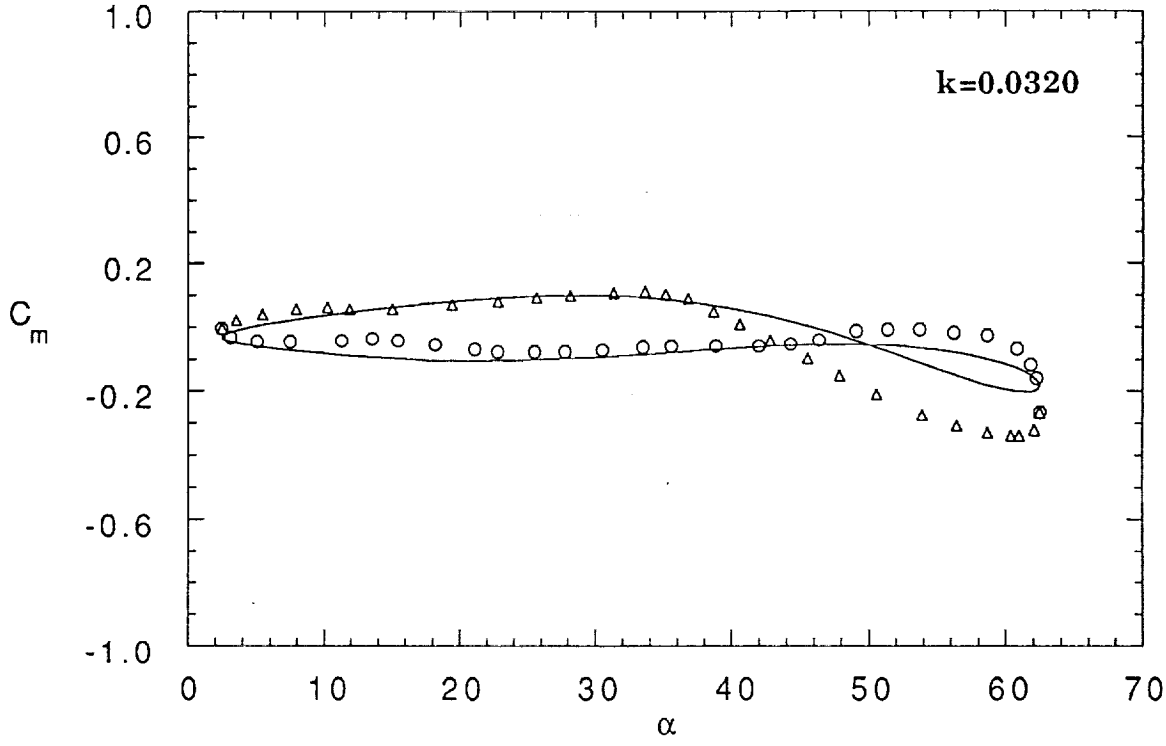

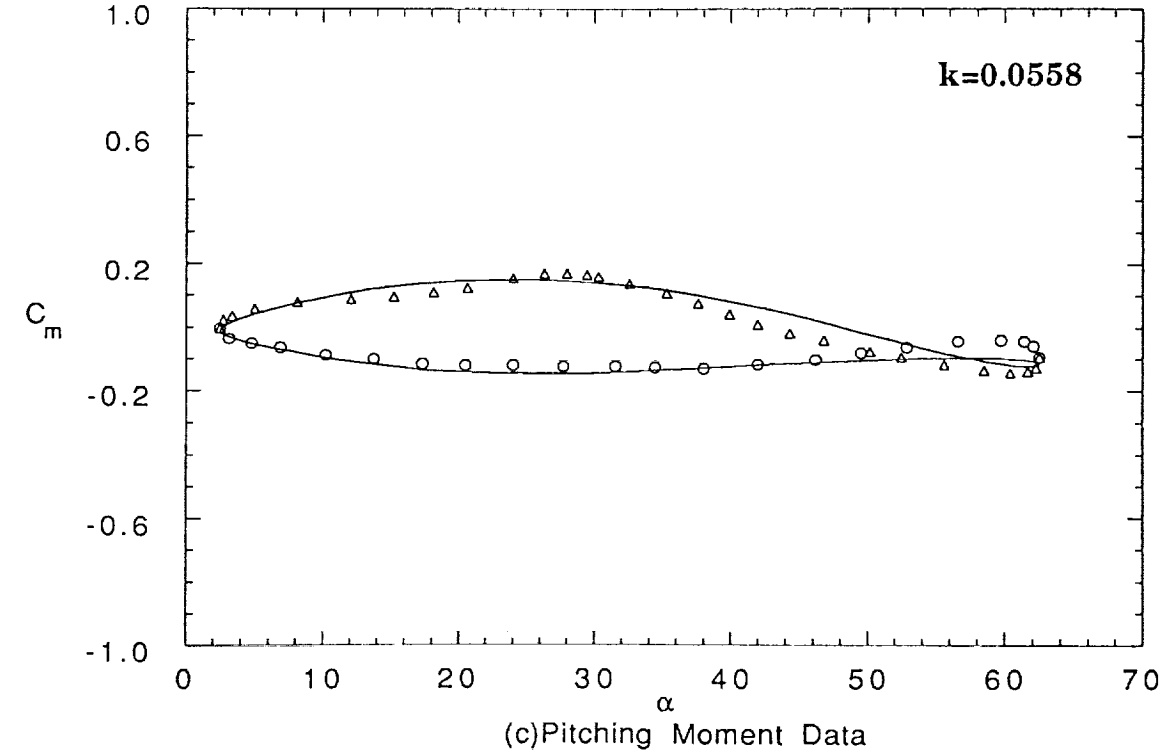

(c)Pitching Moment Data

Figure 7 Continued.

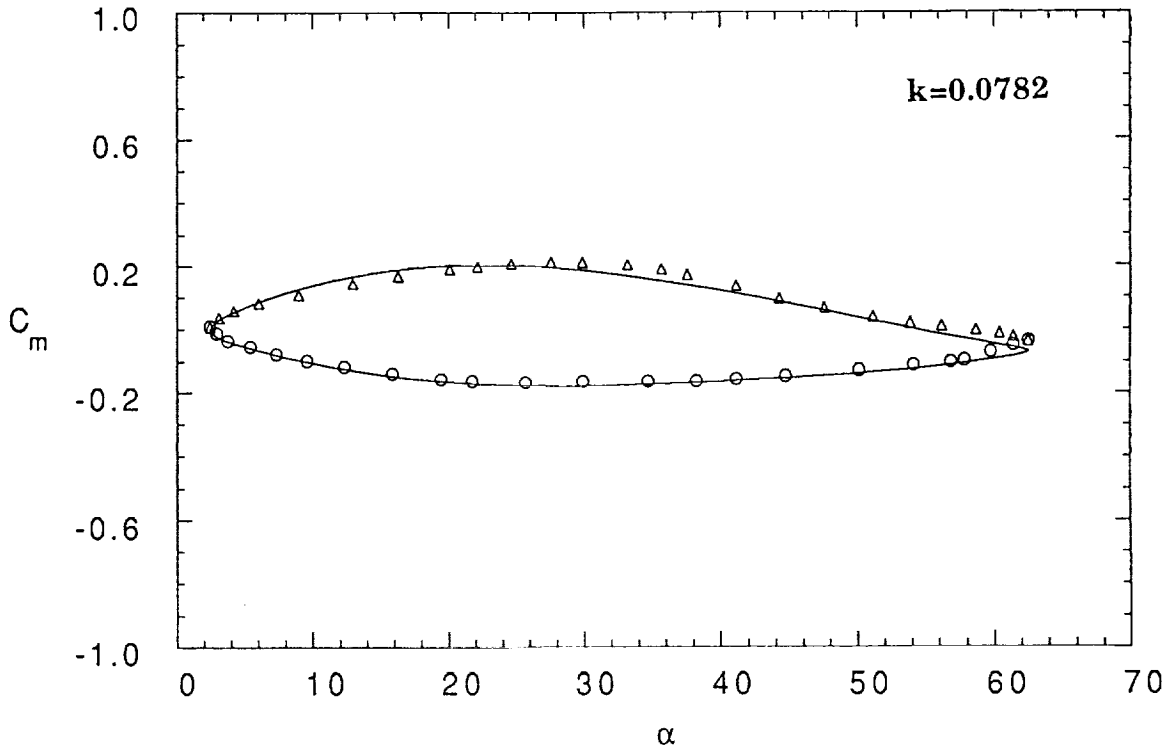

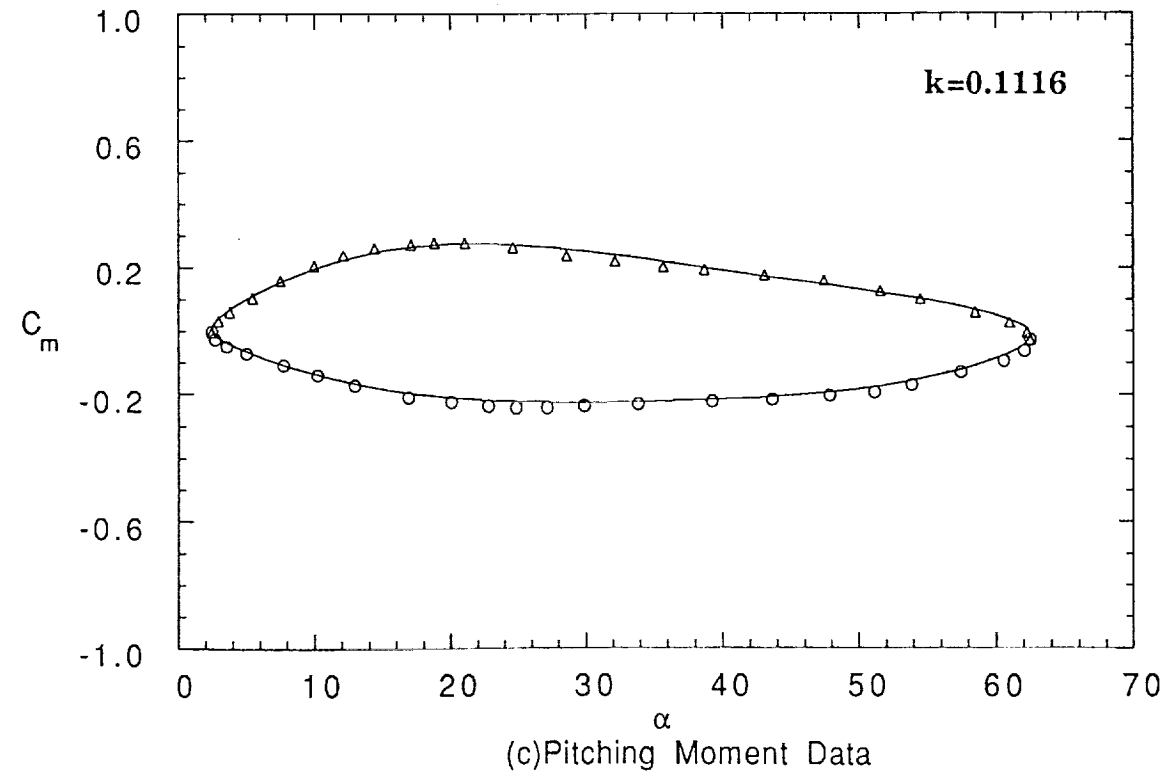

(c)Pitching Moment Data

Figure 7 Concluded.

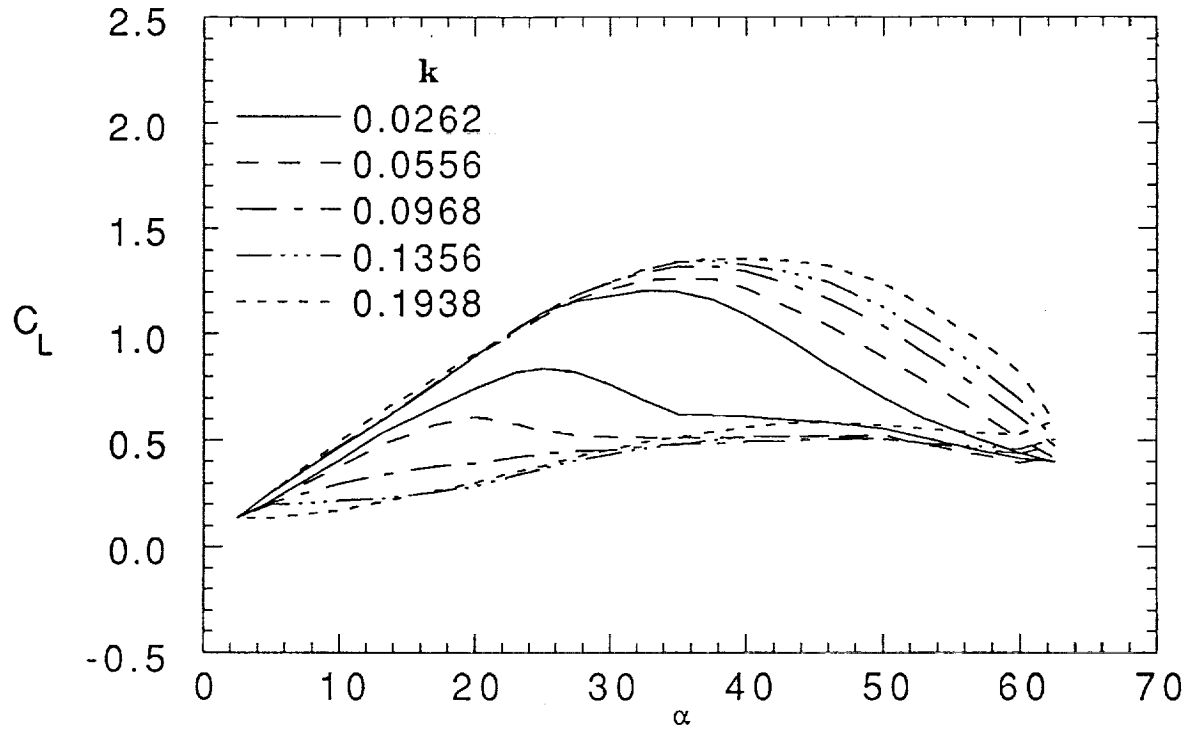

(a)C_L responses for the 70-deg. delta wing tested at NASA Langley Research Center

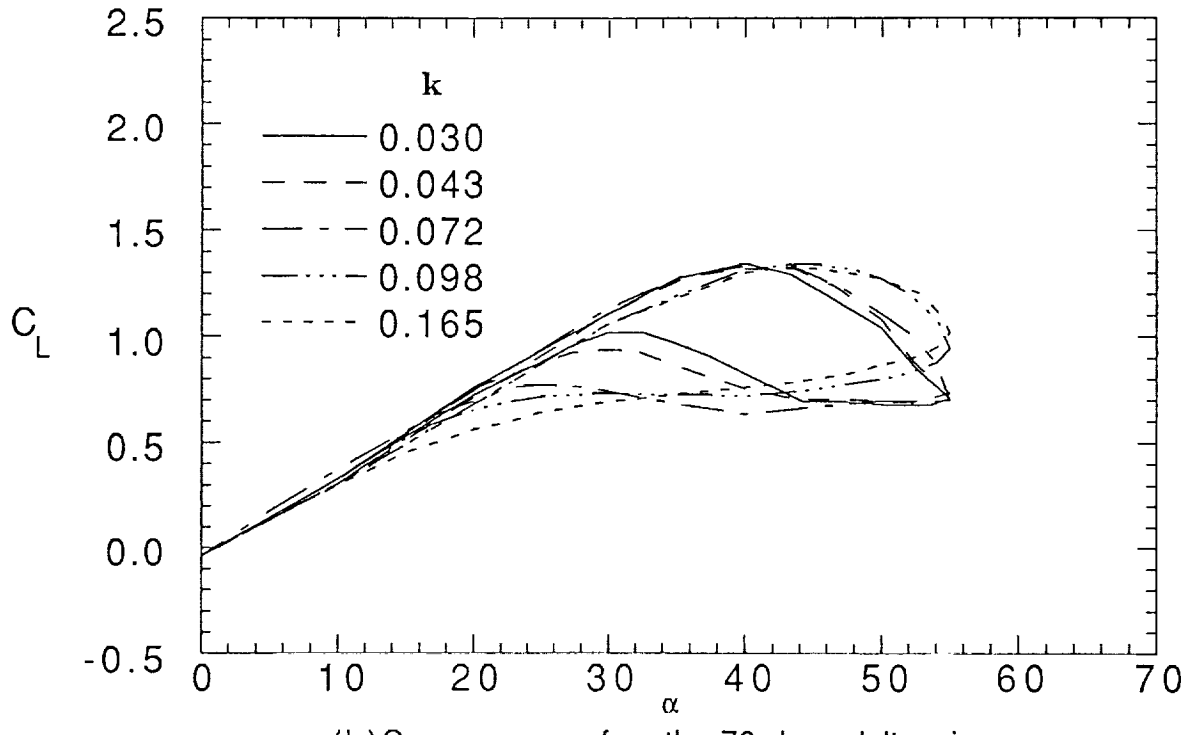

(b)C_L responses for the 70-deg. delta wing tested at Ohio State University(Ref.13)

Figure 8 Comparison of The Hysteresis Behavior of Lift Responses Between Two 70-deg. Delta Wings.

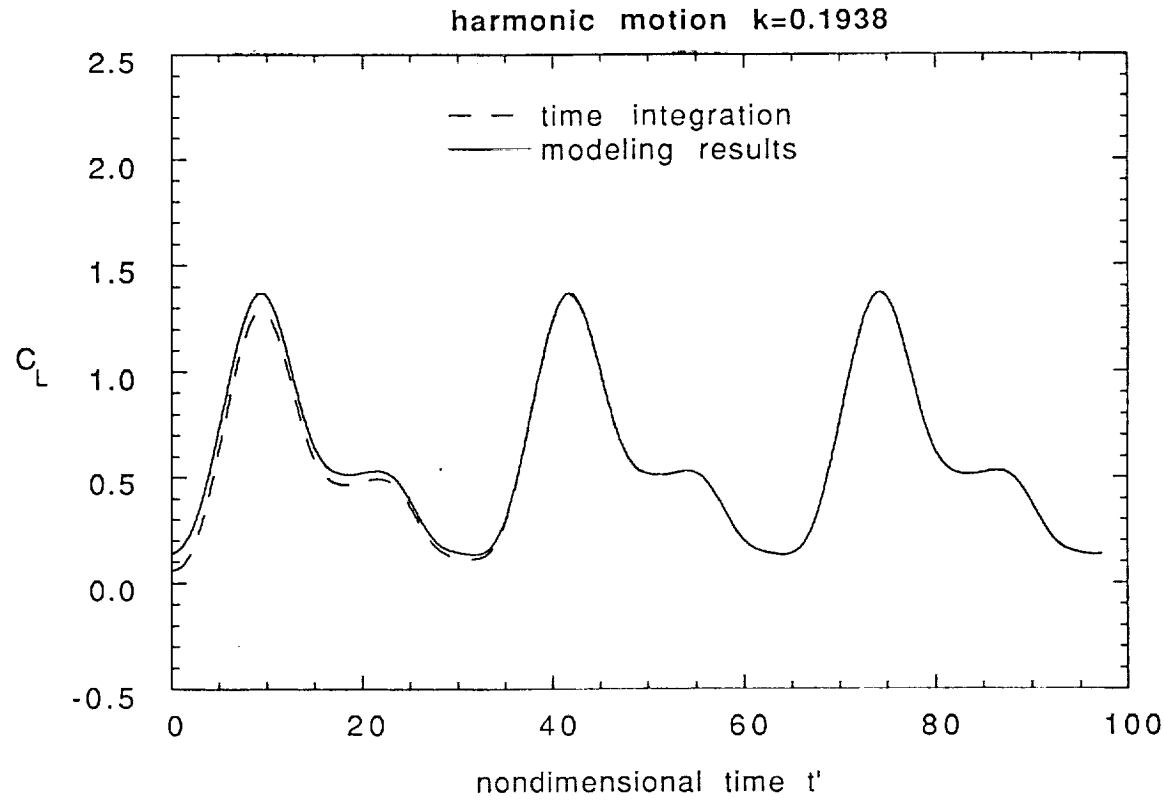

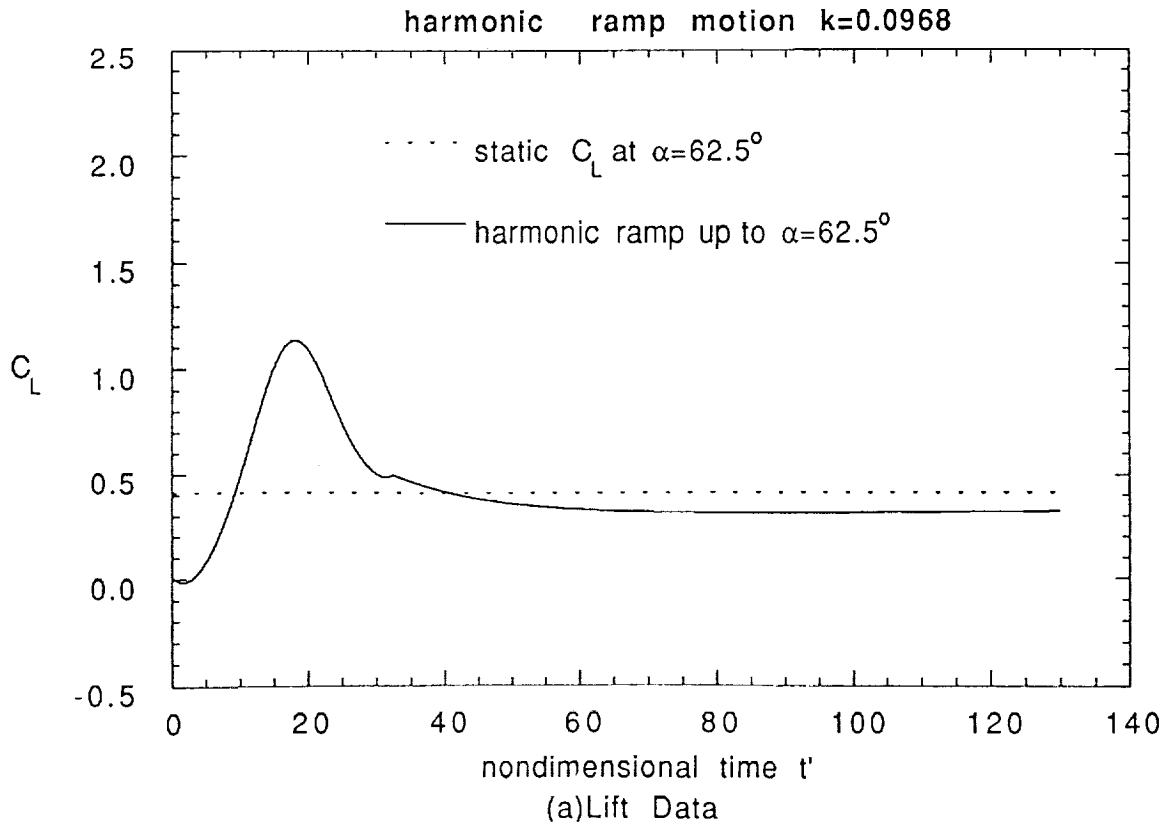

(a)Lift Data

Figure 9 Harmonic Motion and Harmonic Ramp Motion Responses by Indicial Formulation for A 70-deg. Delta Wing.

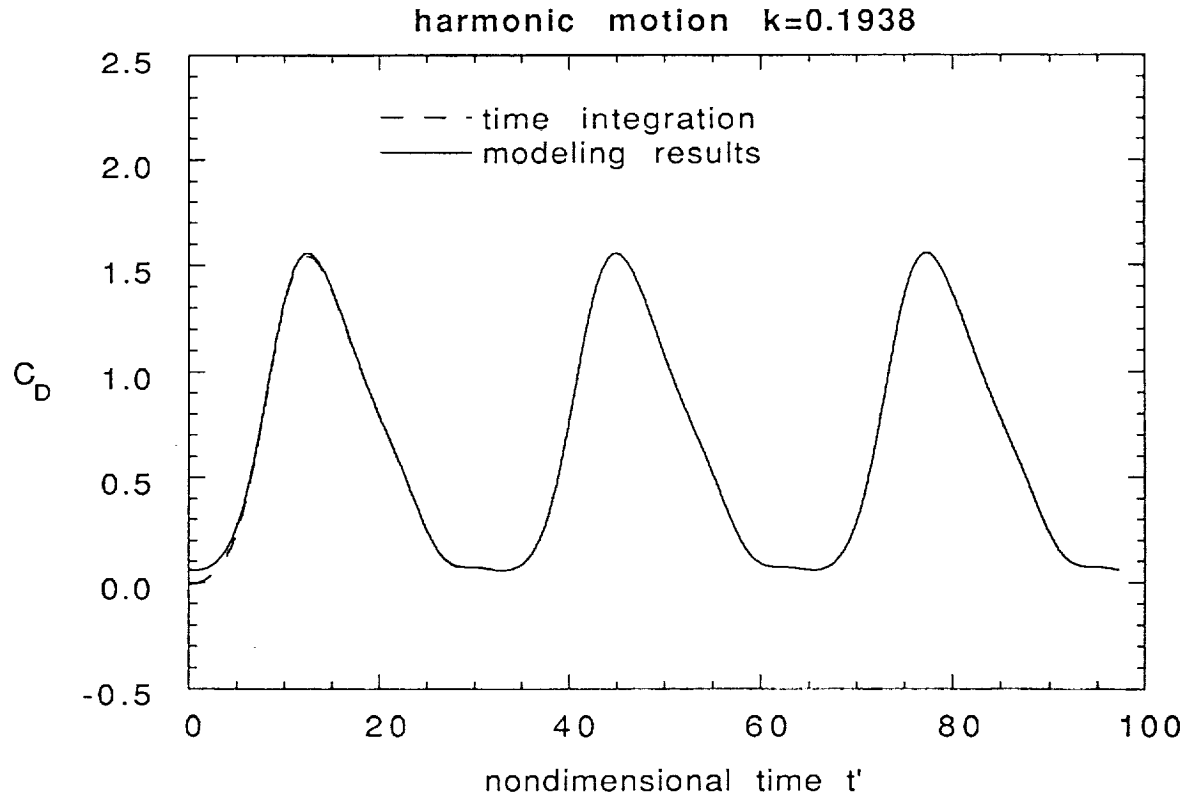

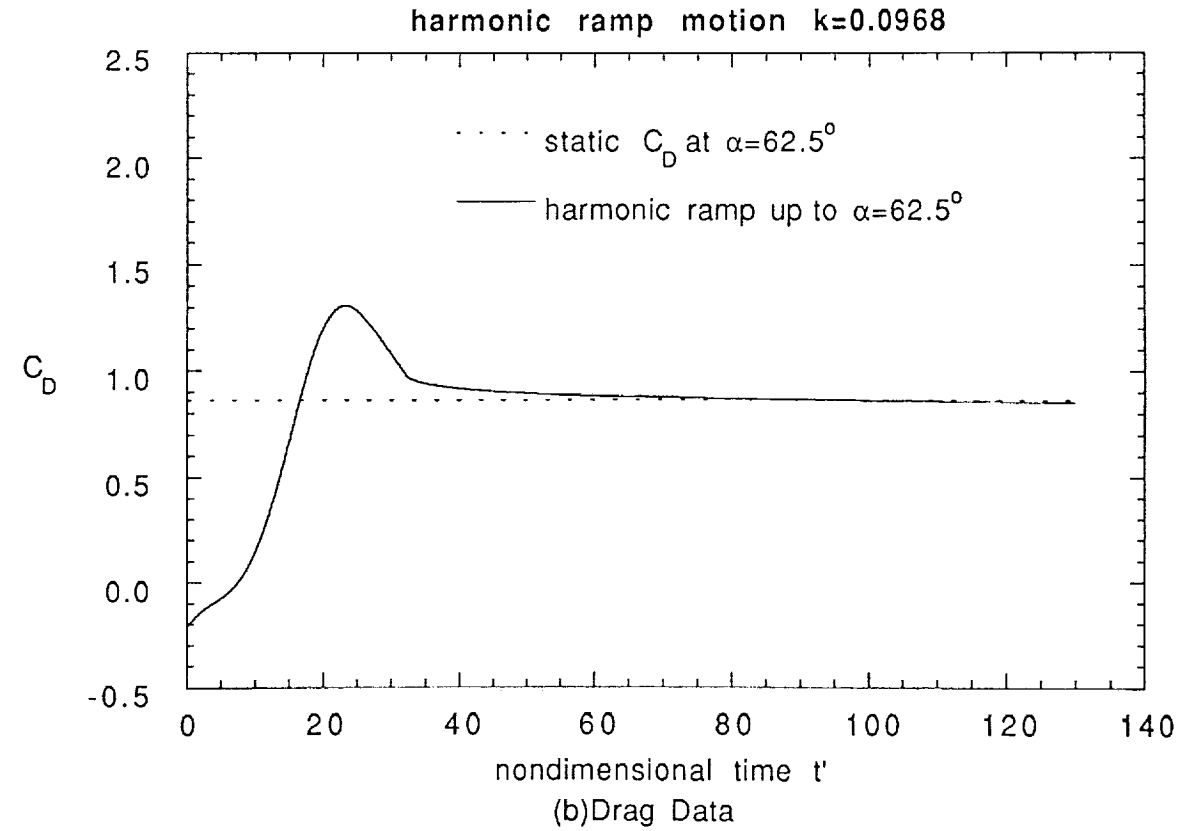

(b)Drag Data

Figure 9 Continued.

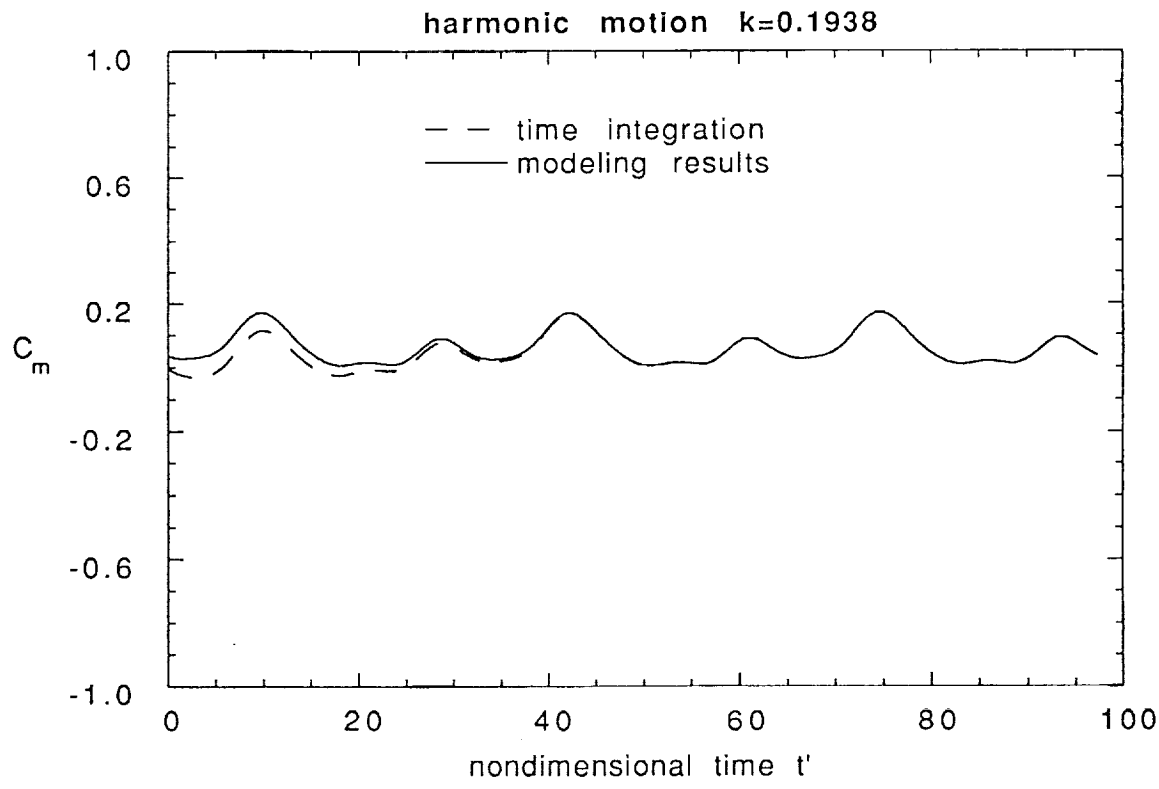

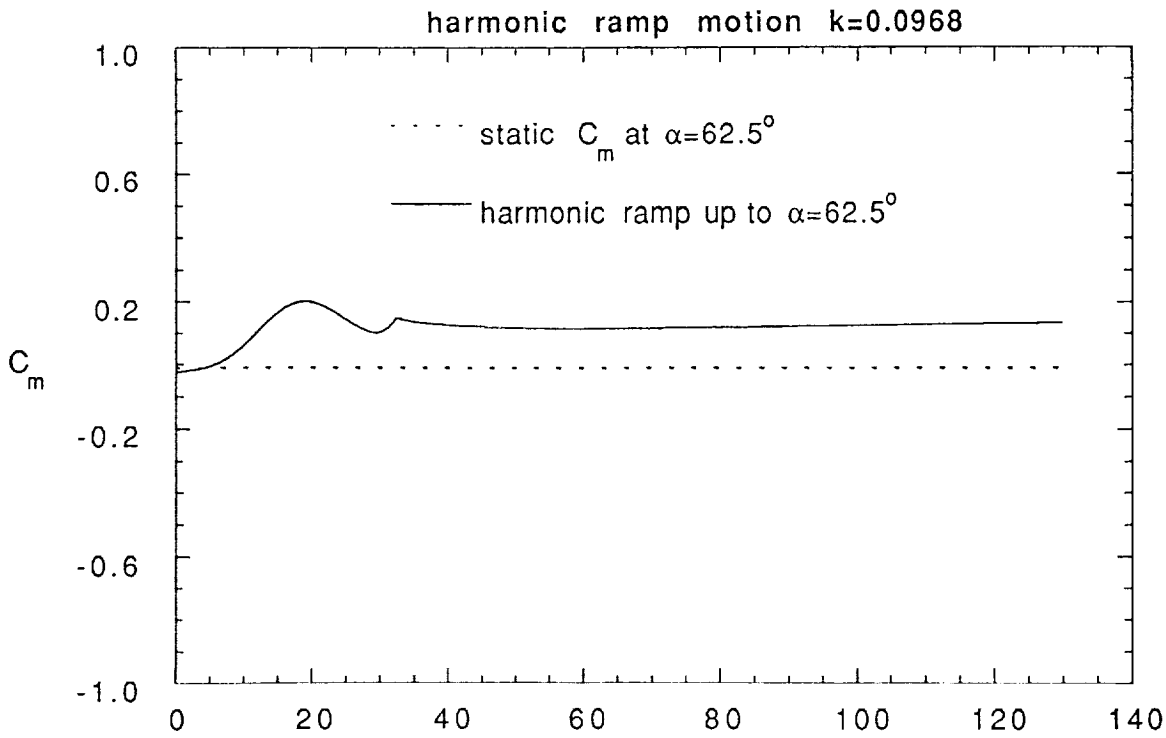

(c)Pitching Moment Data

Figure 9 Concluded.

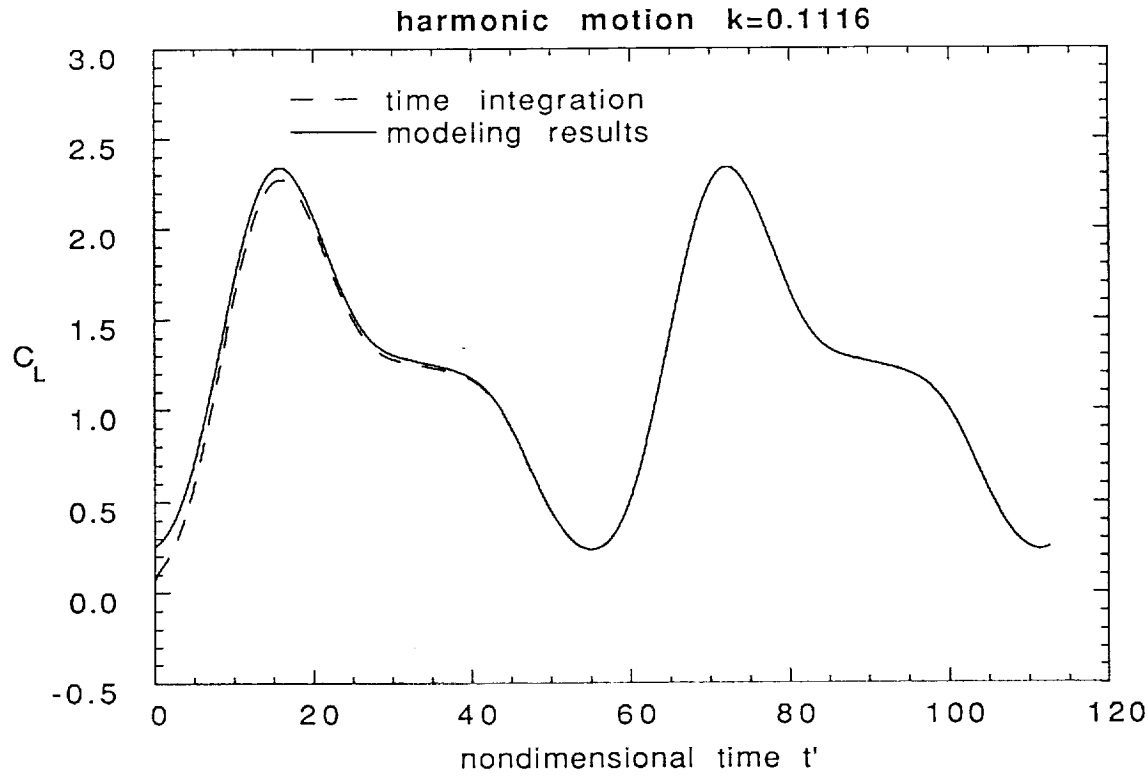

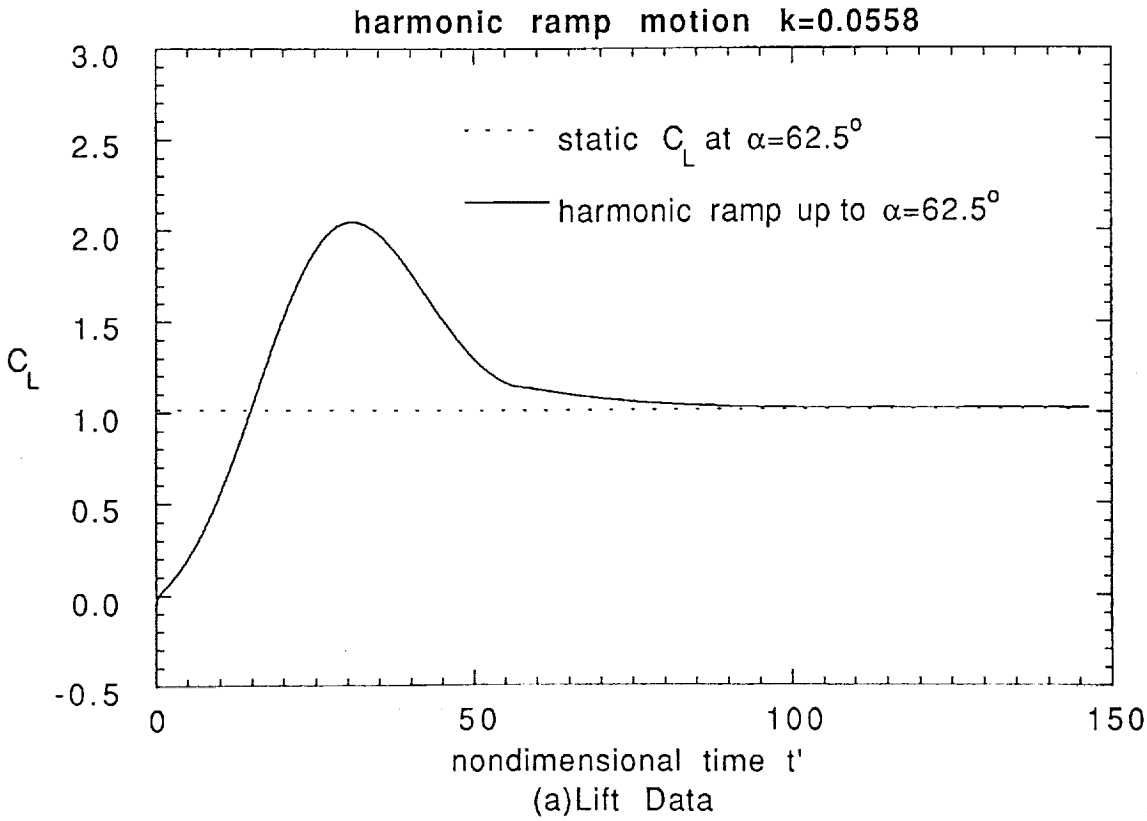

(a)Lift Data

Figure 10 Harmonic Motion and Harmonic Ramp Motion Responses by Indicial Formulation for An F-18 Model.

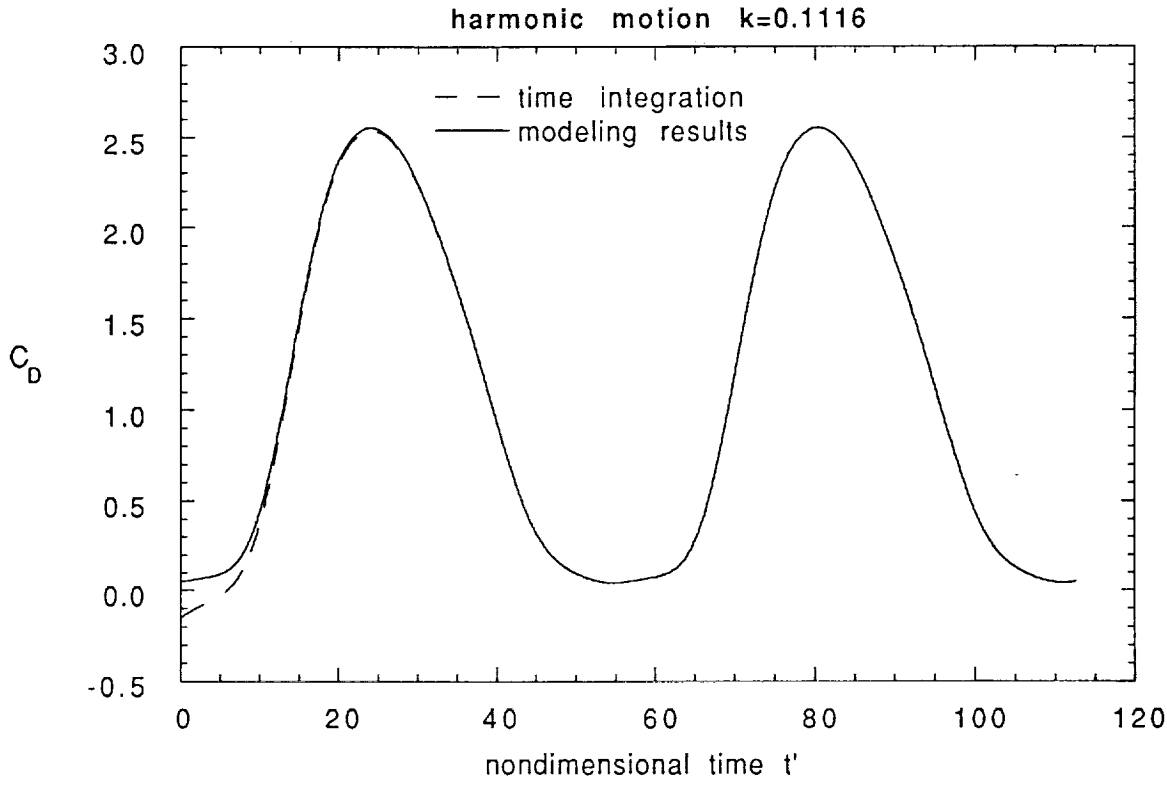

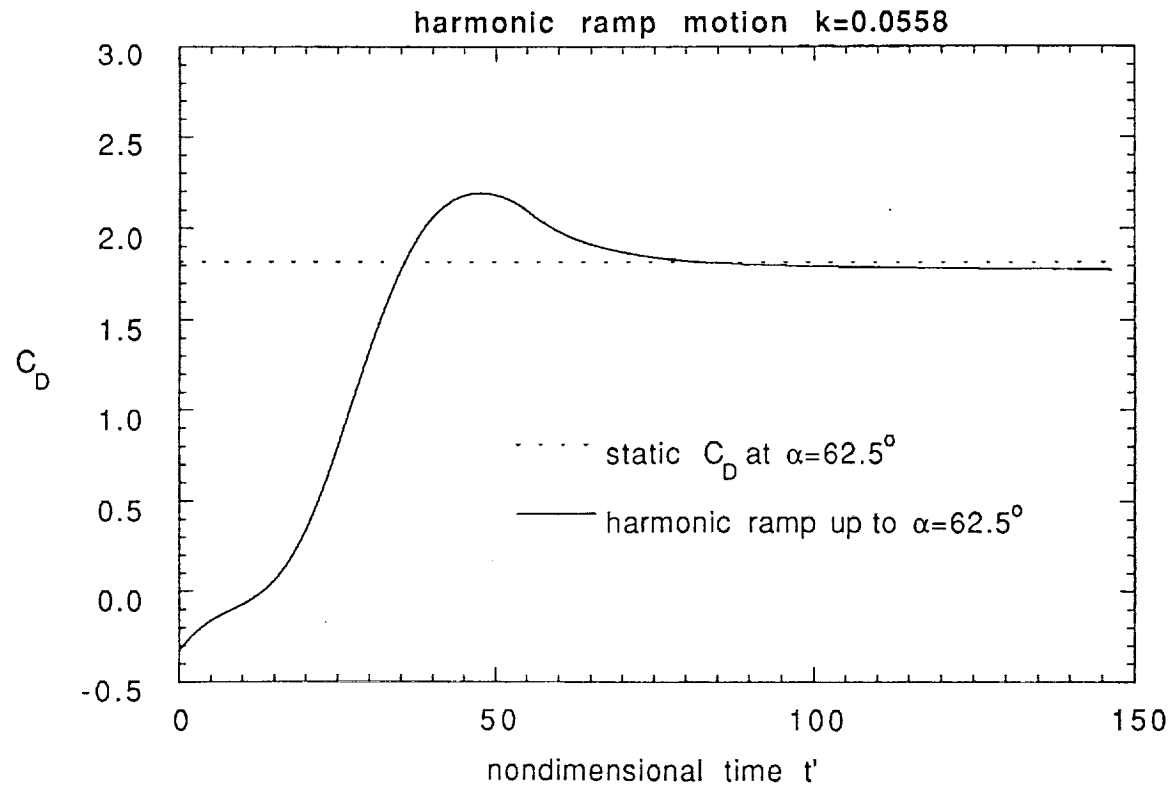

(b)Drag Data

Figure 10 Continued.

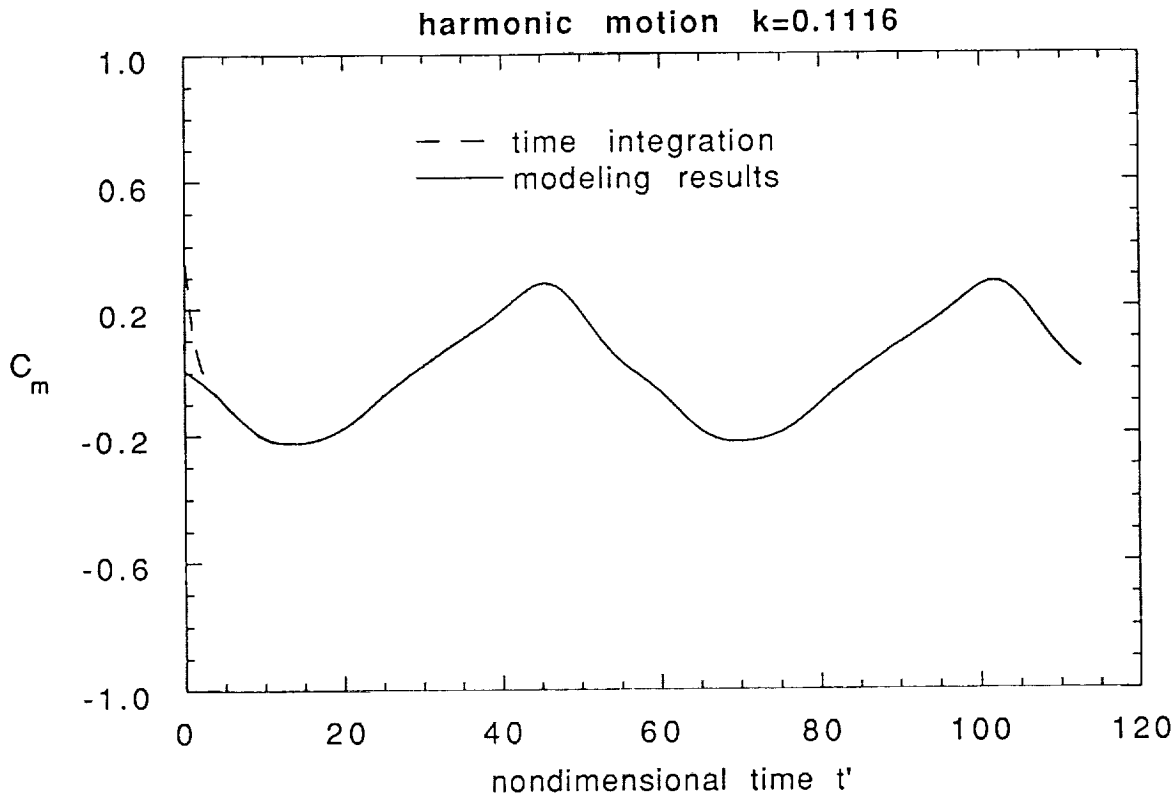

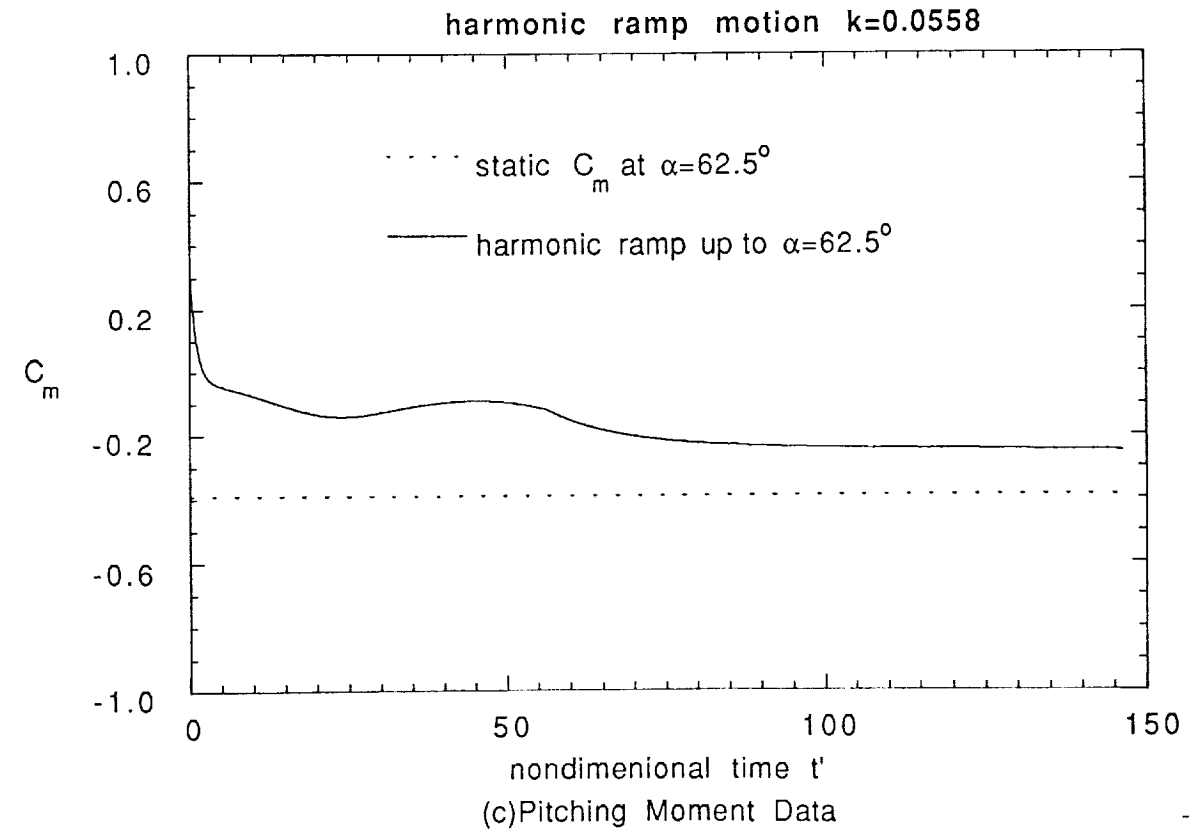

(c)Pitching Moment Data

Figure 10 Concluded.

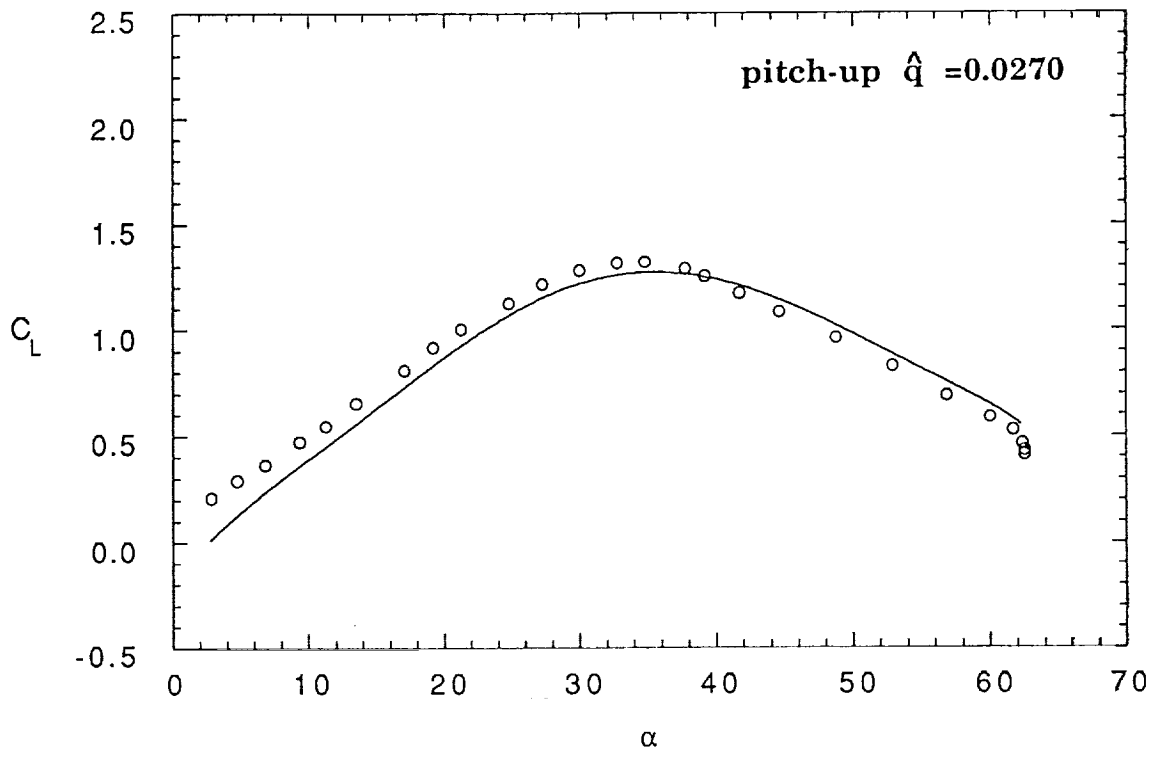

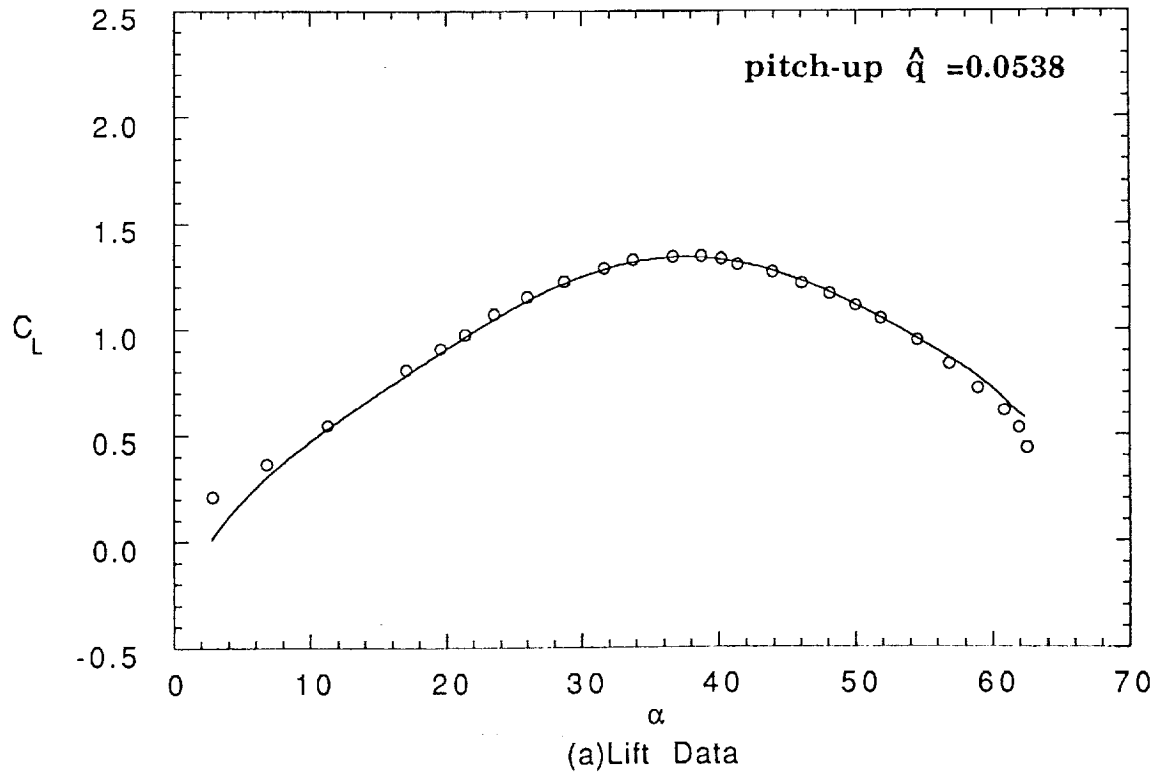

(a)Lift Data

Figure 11 Constant-Rate Pitching Motion Responses by Indicial Formulation for A 70-deg. Delta Wing.

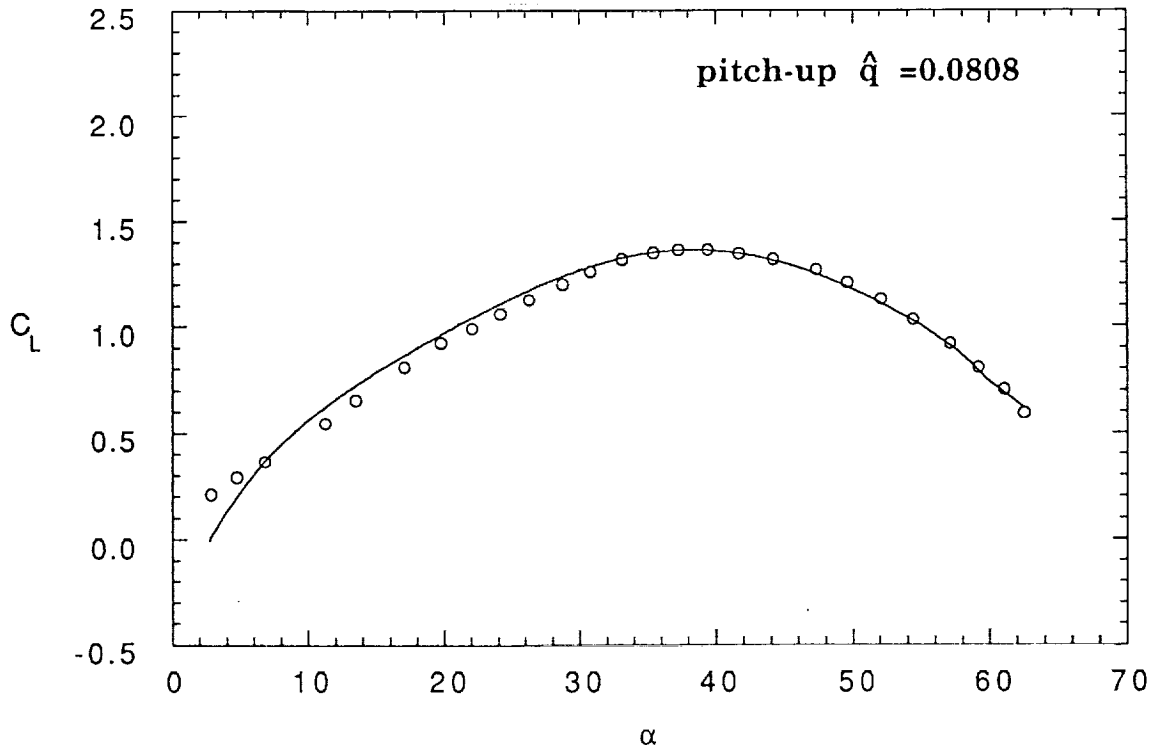

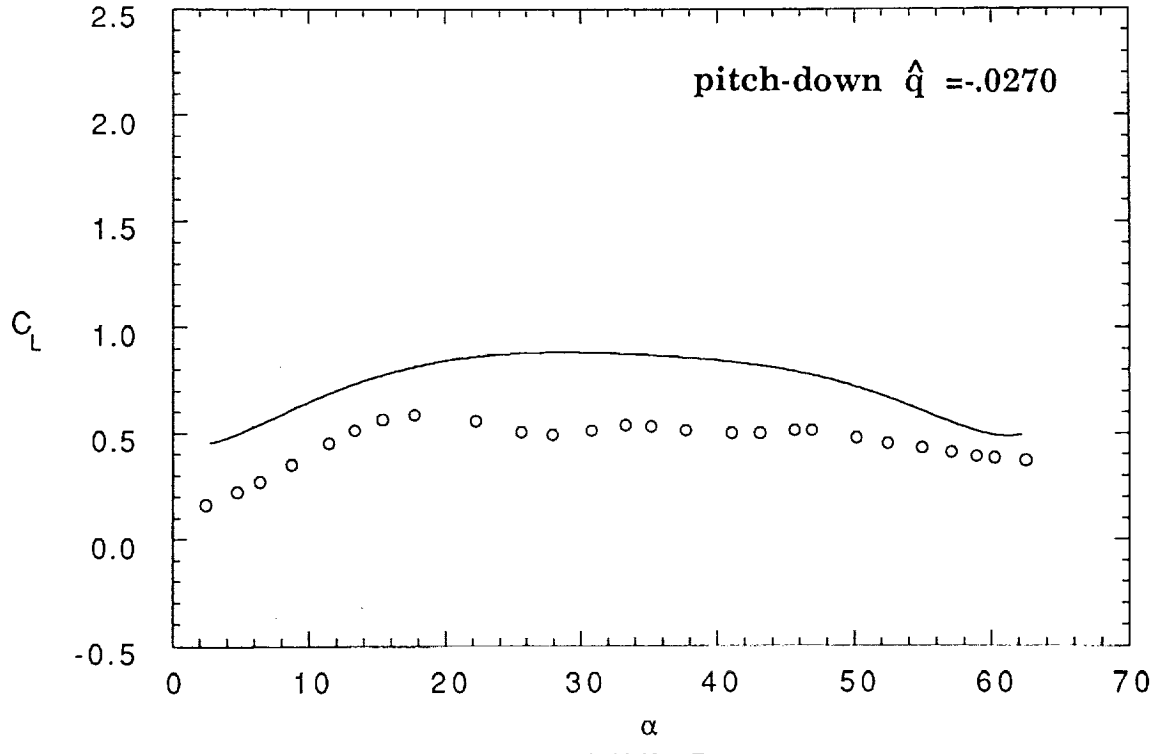

(a)Lift Data

Figure 11 Continued.

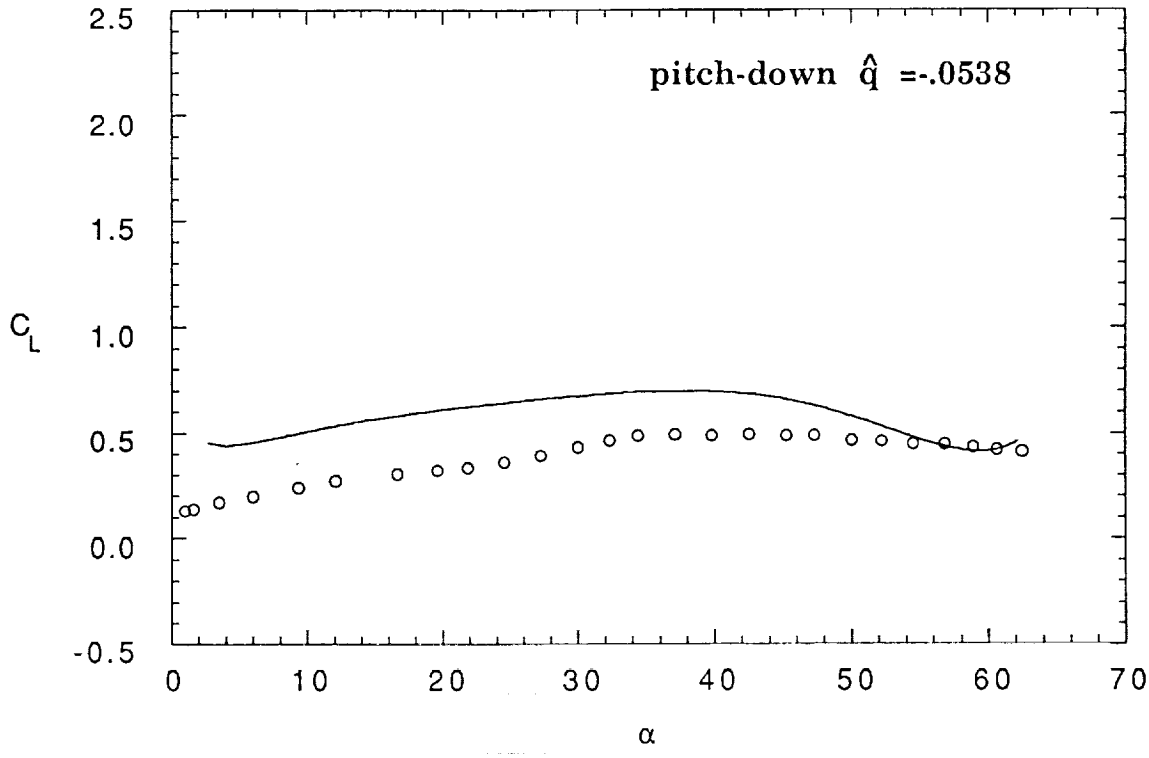

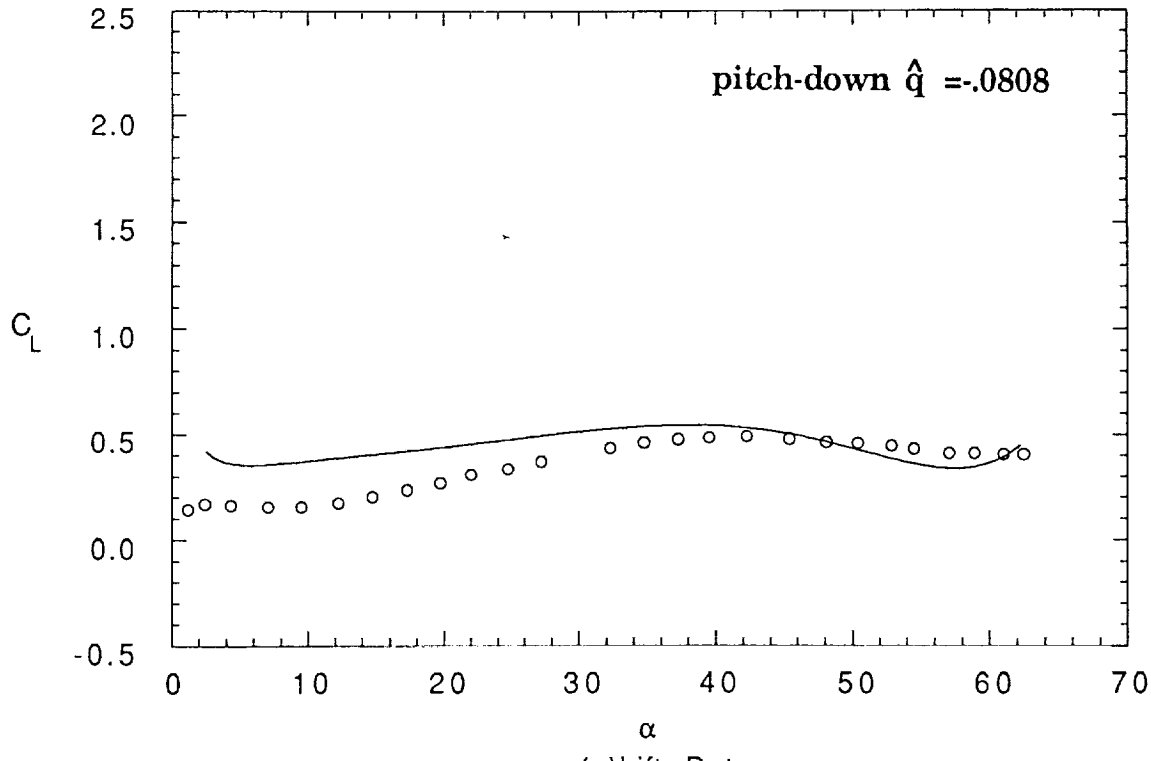

(a)Lift Data

Figure 11 Continued.

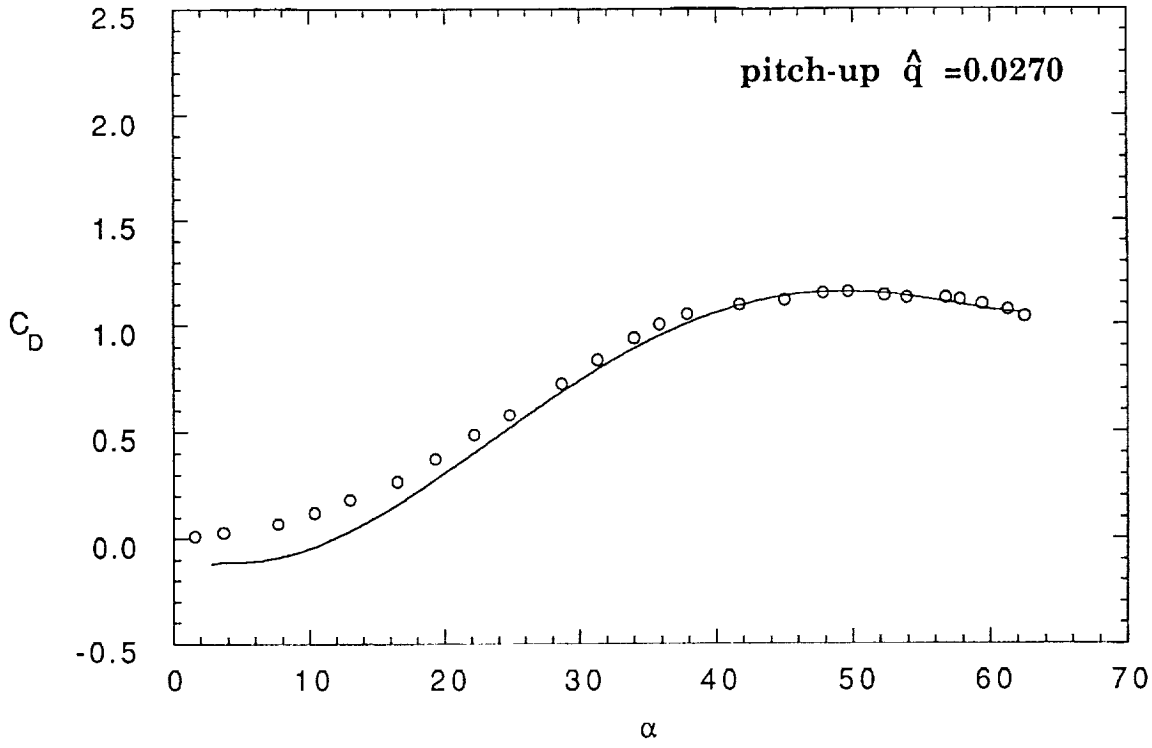

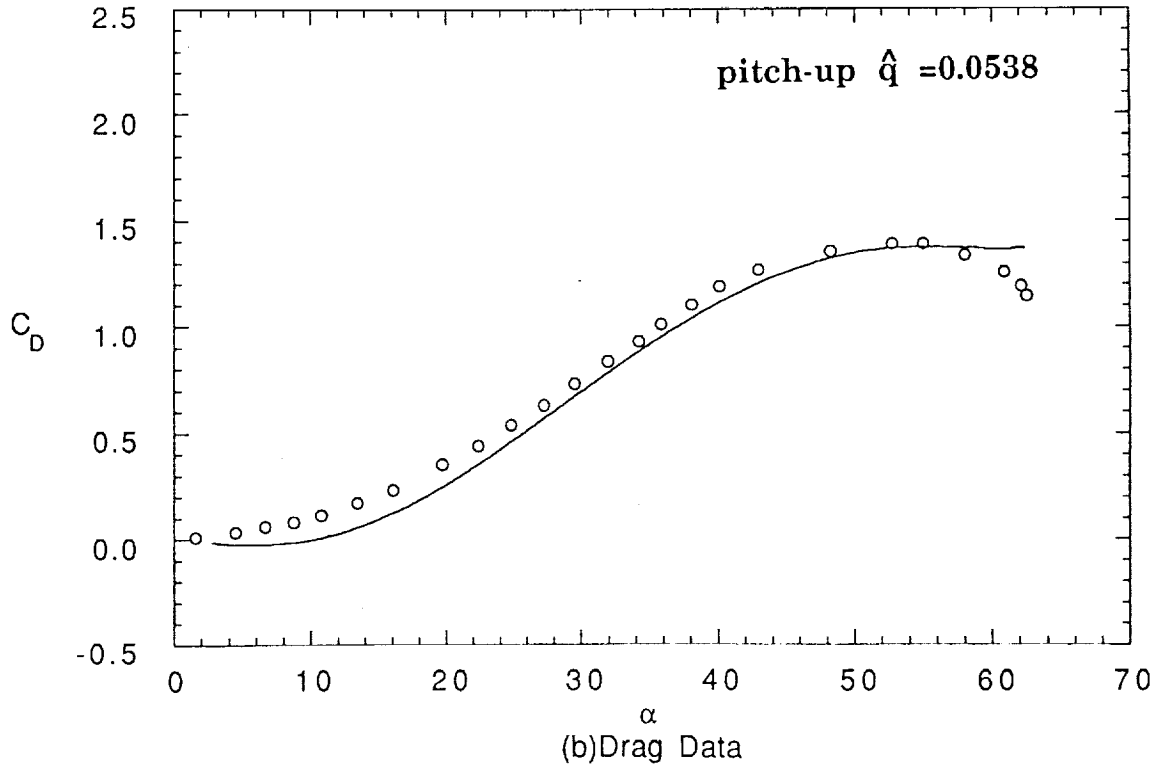

(b)Drag Data

Figure 11 Continued.

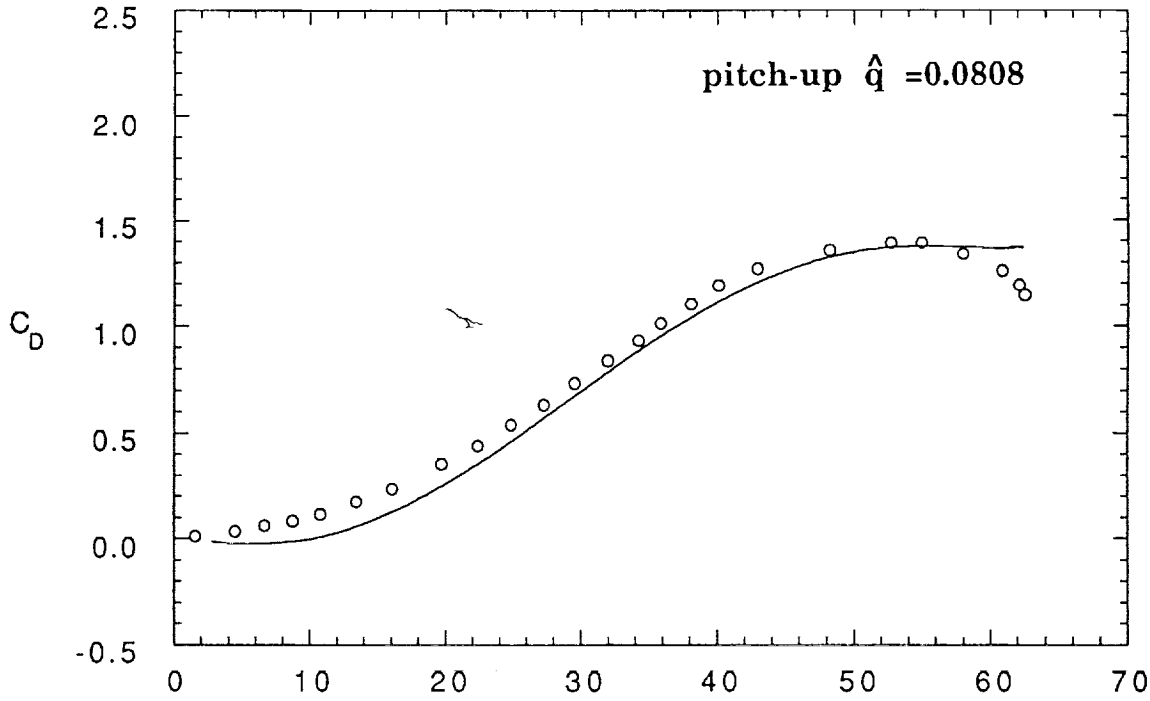

(b)Drag Data

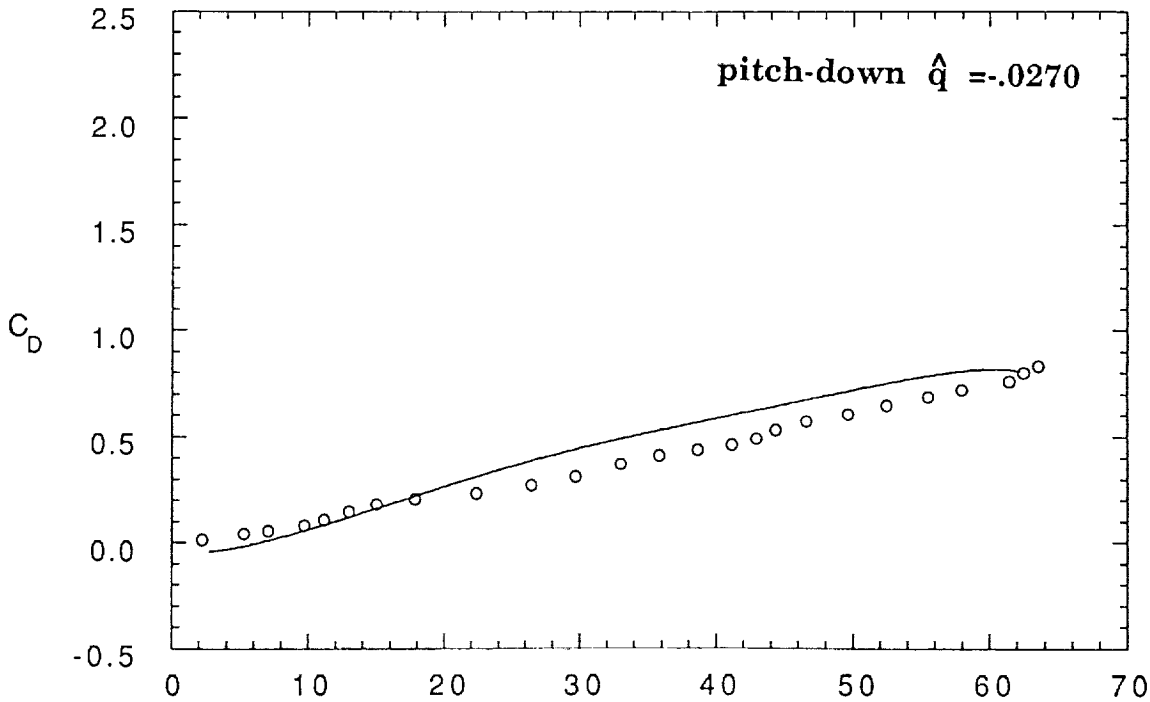

(b)Drag Data

Figure 11 Continued.

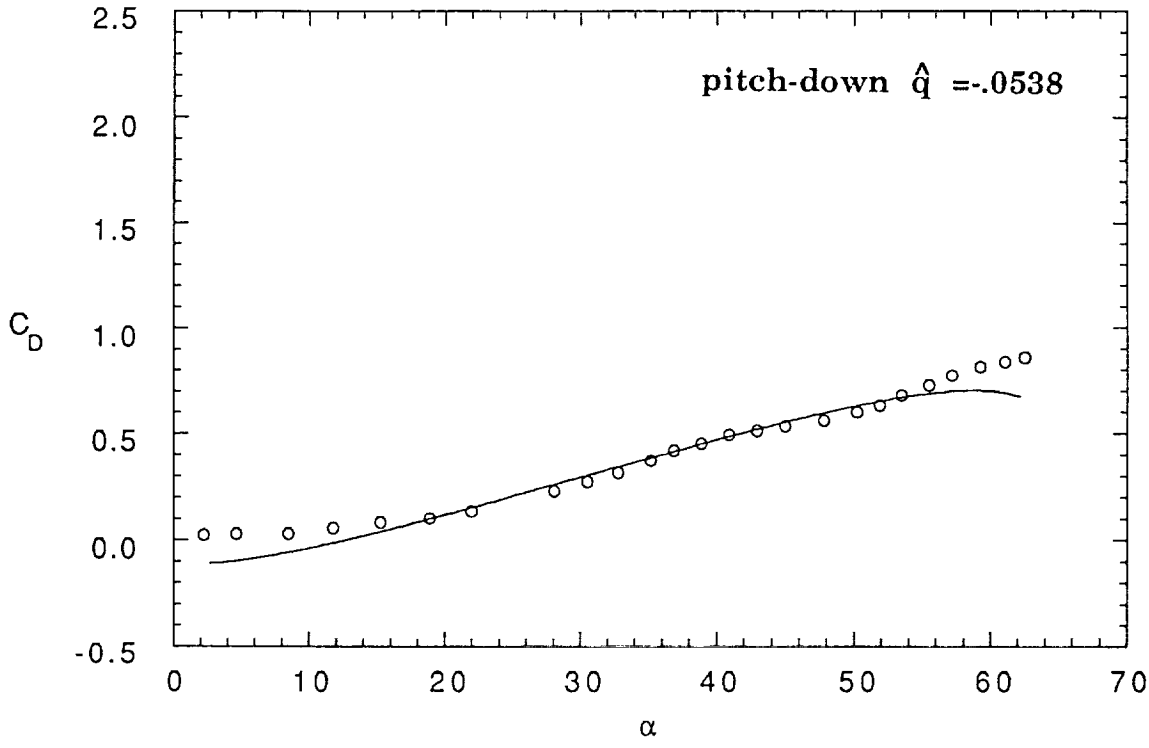

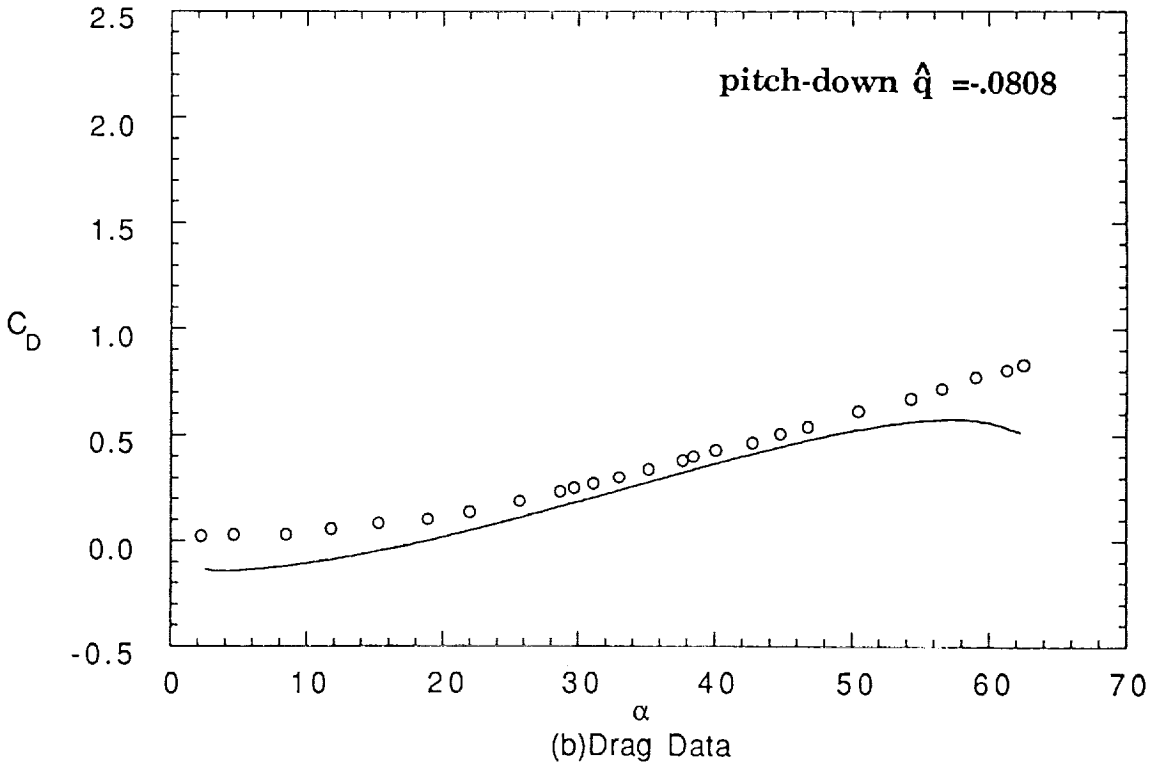

(b)Drag Data

Figure 11 Continued.

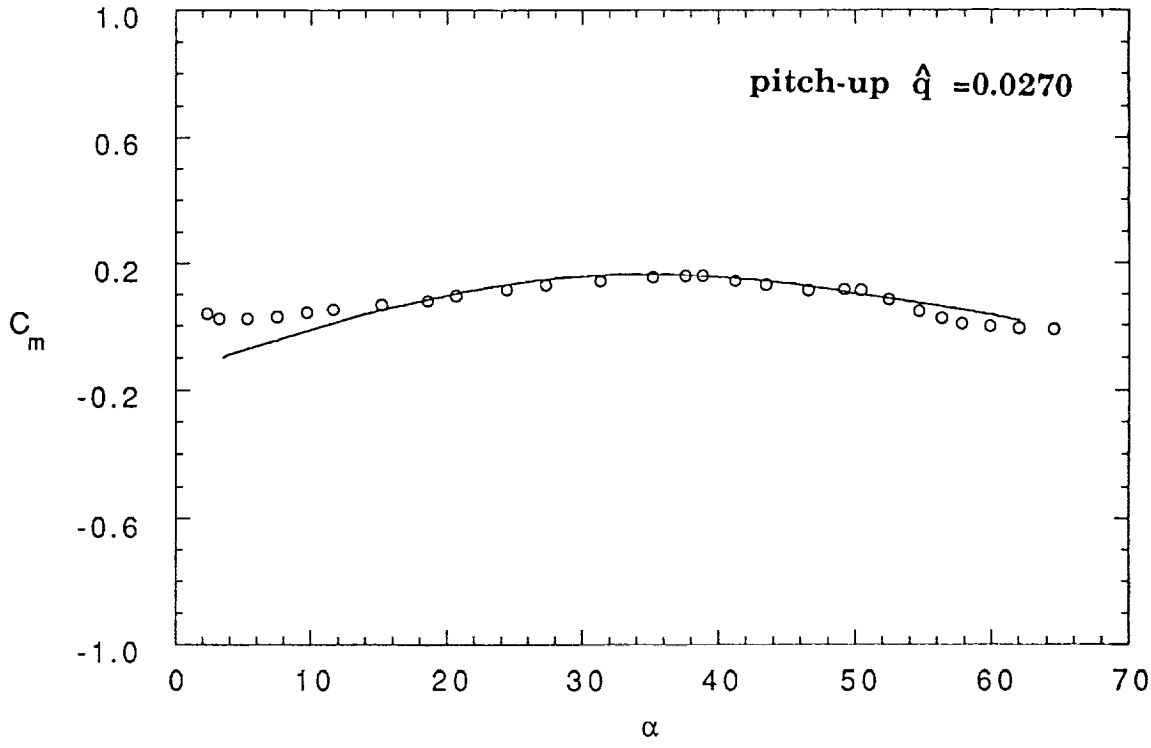

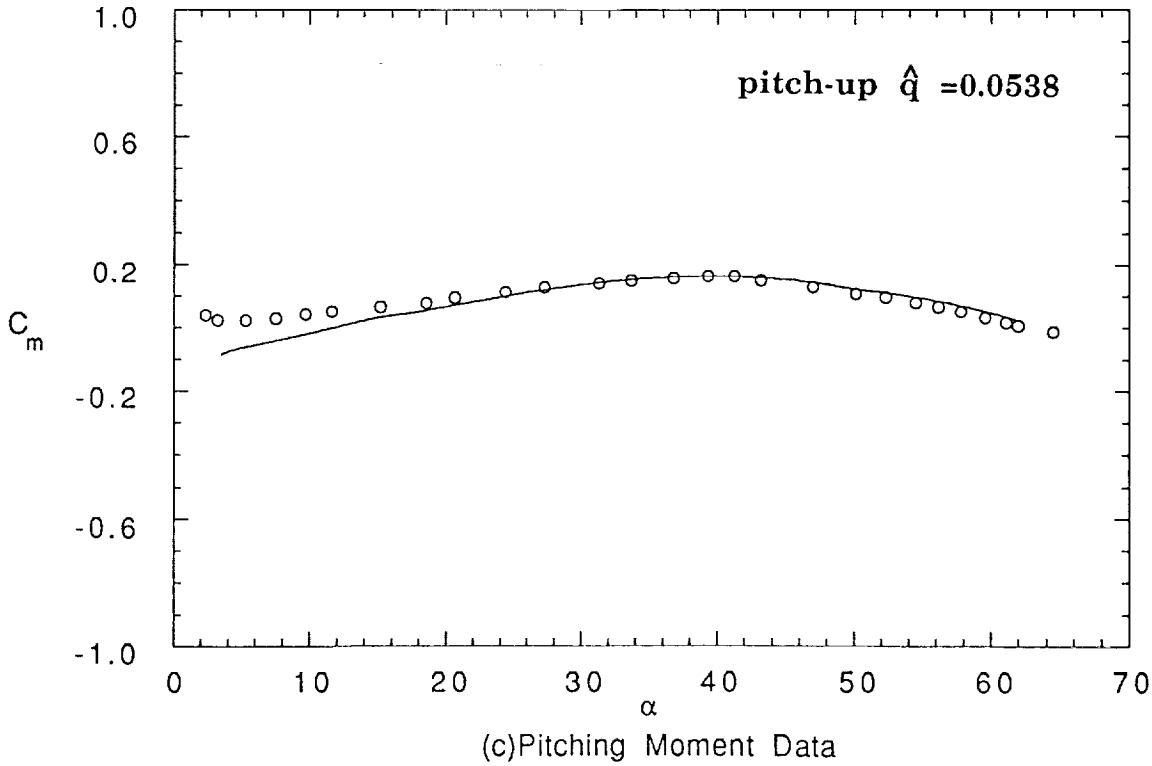

(c)Pitching Moment Data

Figure 11 Continued.

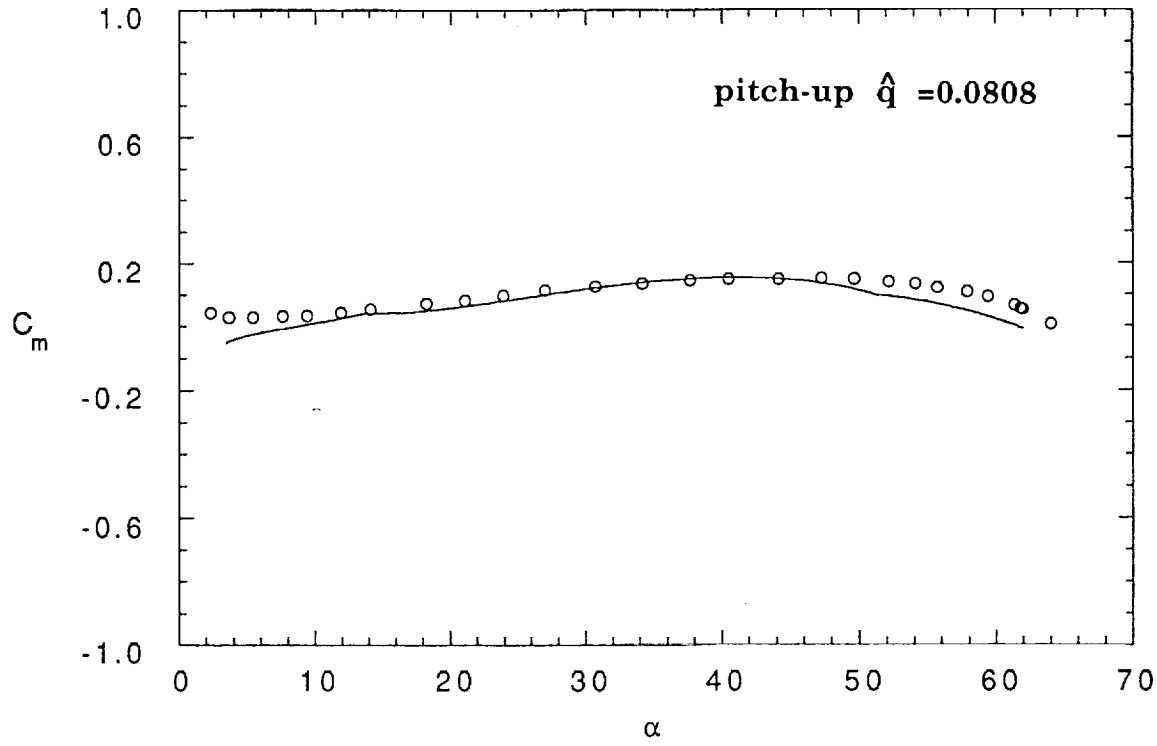

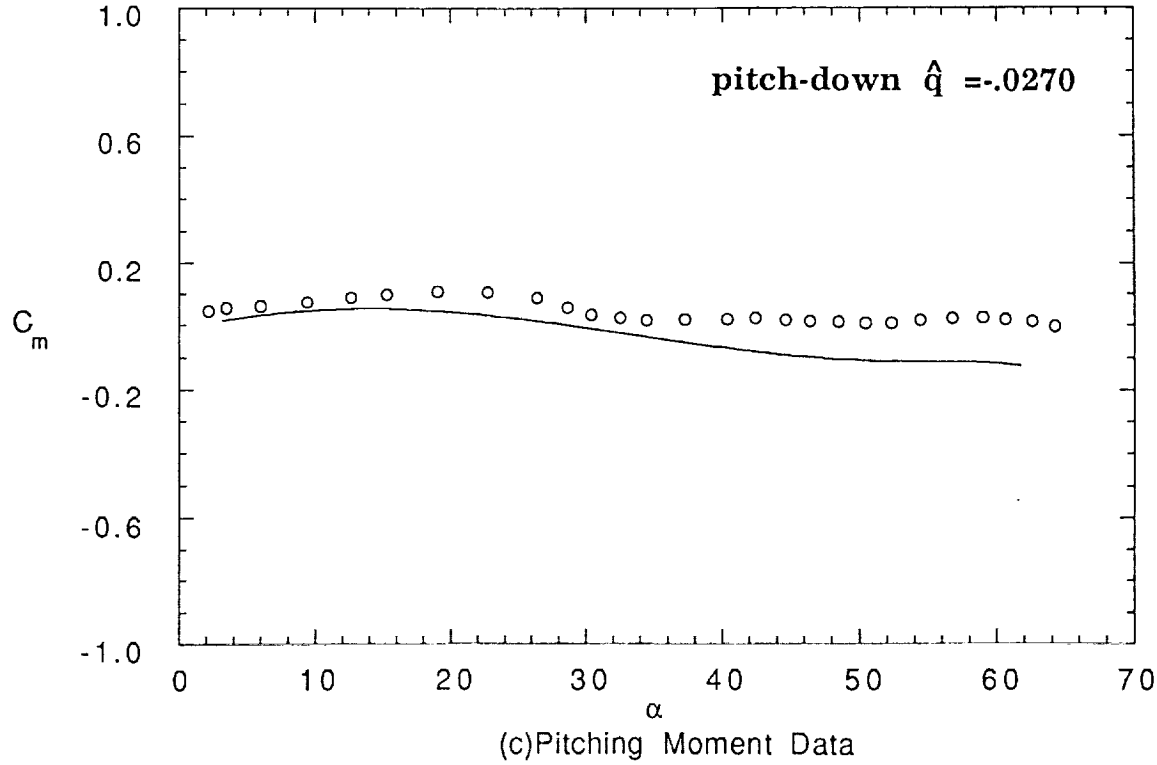

(c)Pitching Moment Data

Figure 11 Continued.

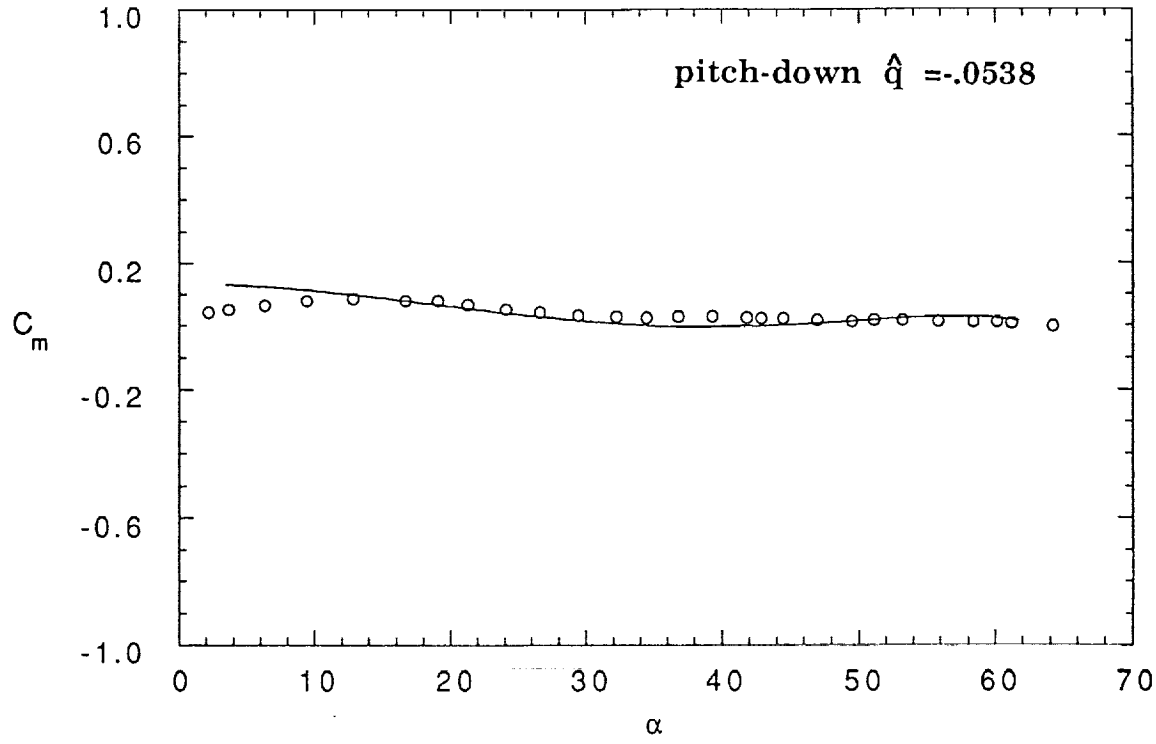

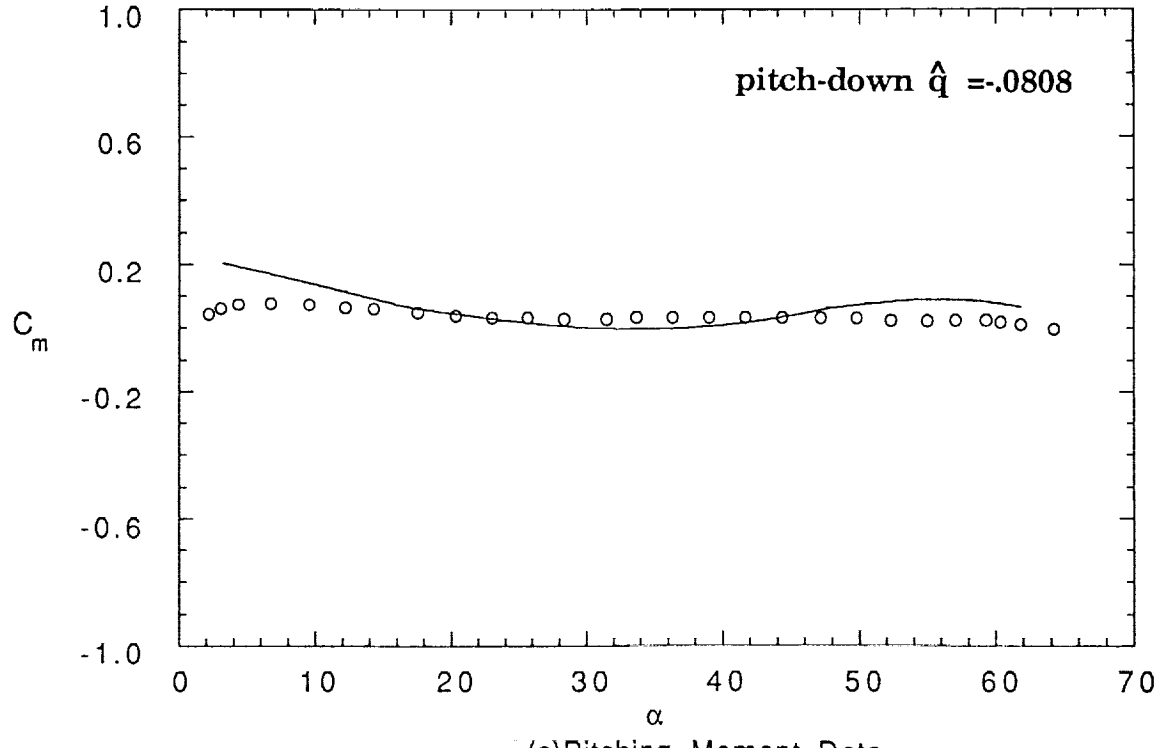

(c)Pitching Moment Data

Figure 11 Concluded.

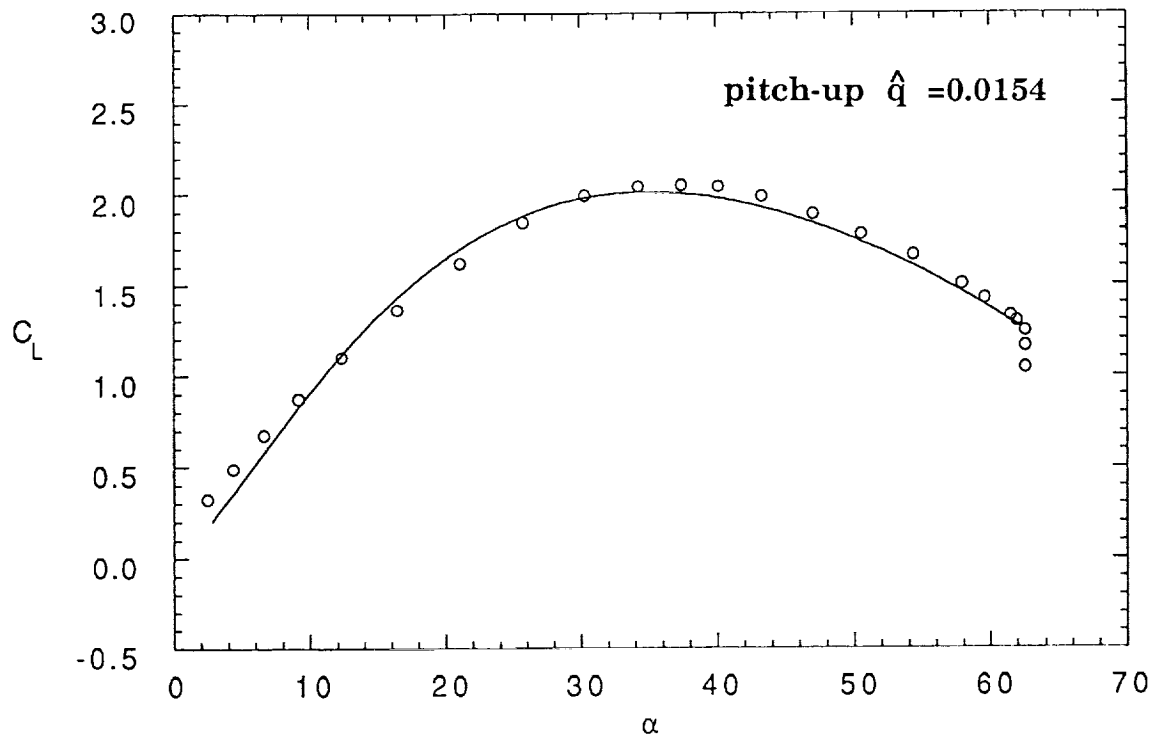

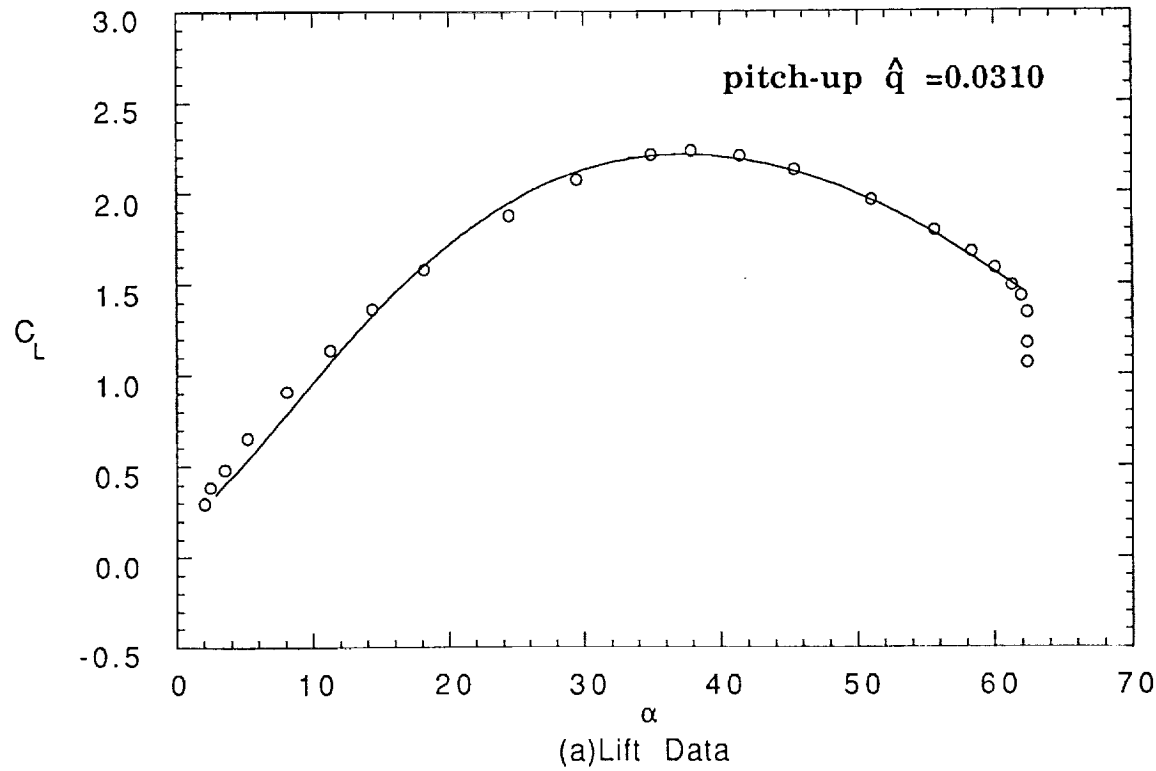

(a)Lift Data

Figure 12 Constant-Rate Pitching Motion Responses by Indicial Formulation for An F-18 Model.

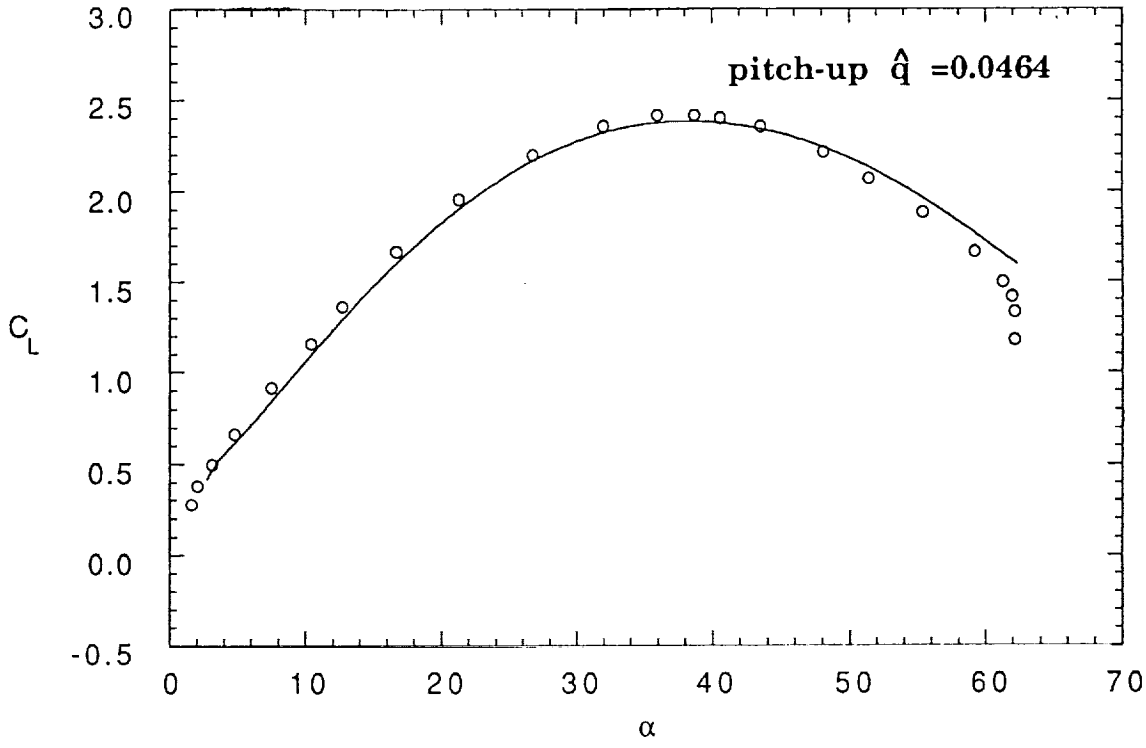

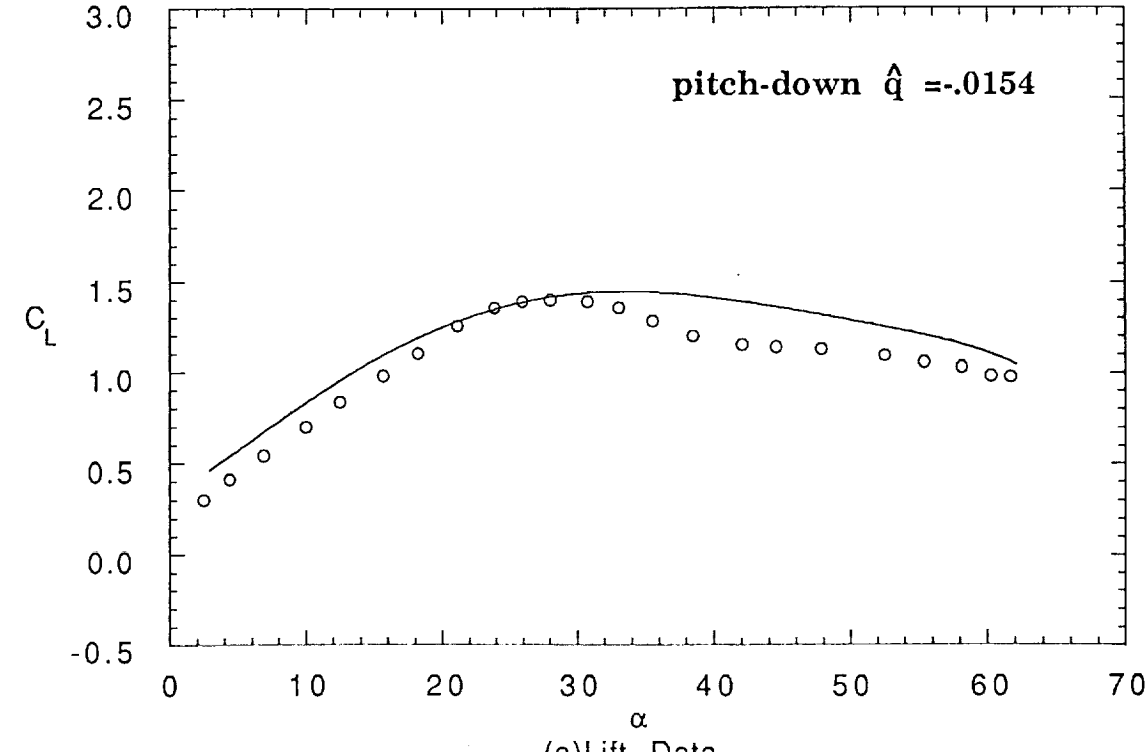

(a)Lift Data

Figure 12 Continued.

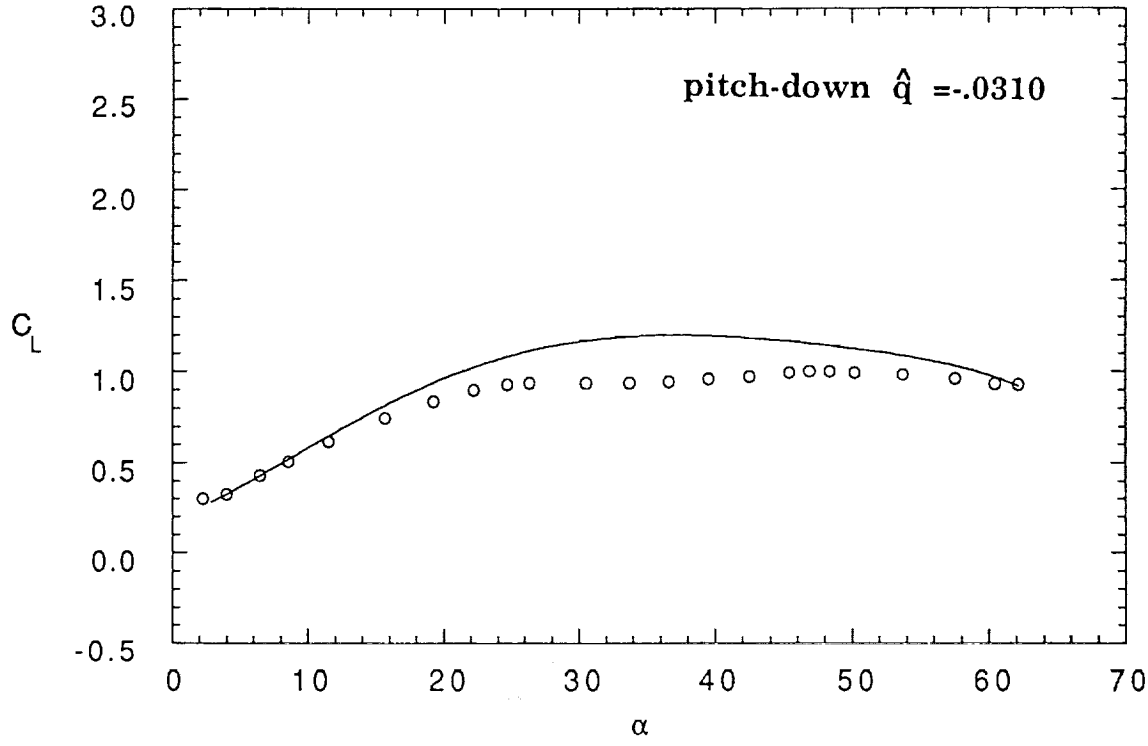

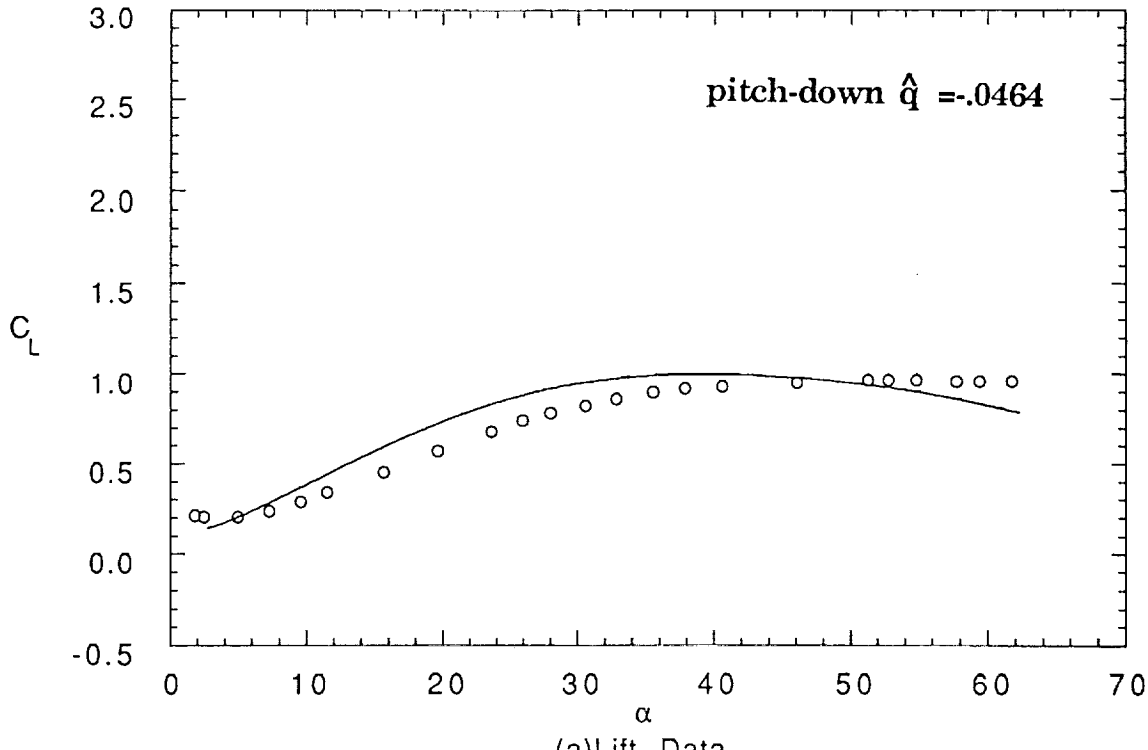

(a)Lift Data

Figure 12 Continued.

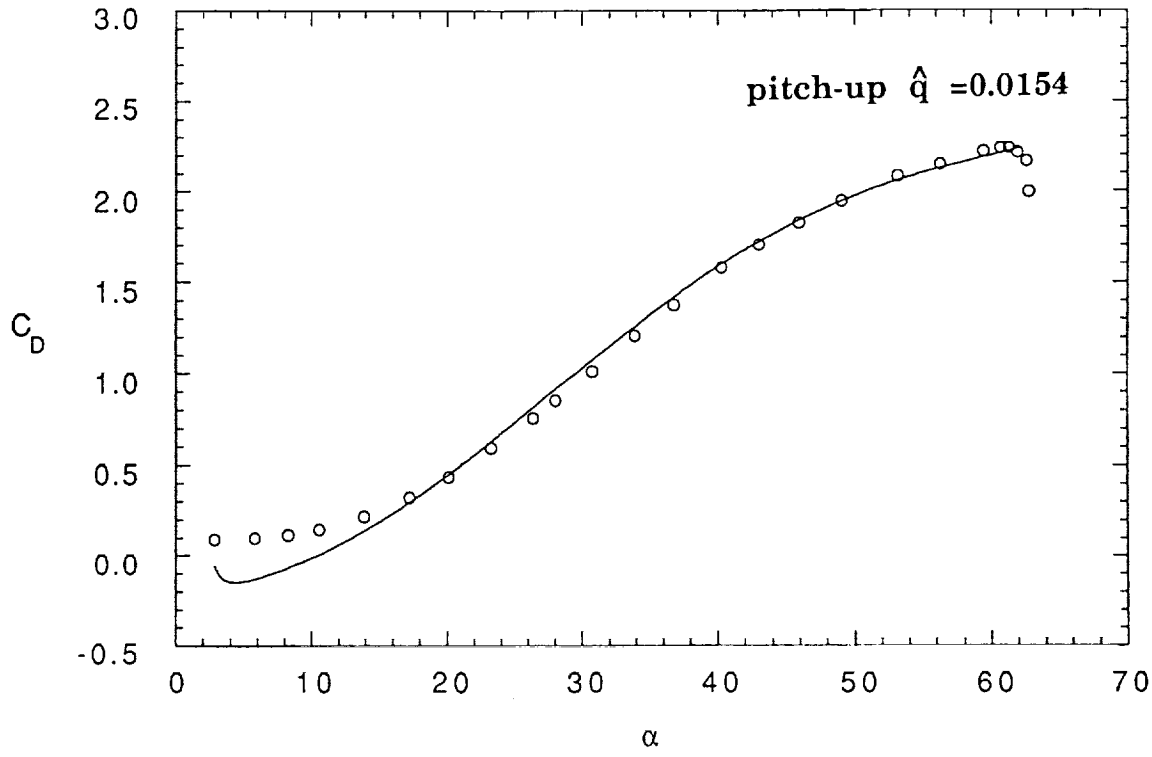

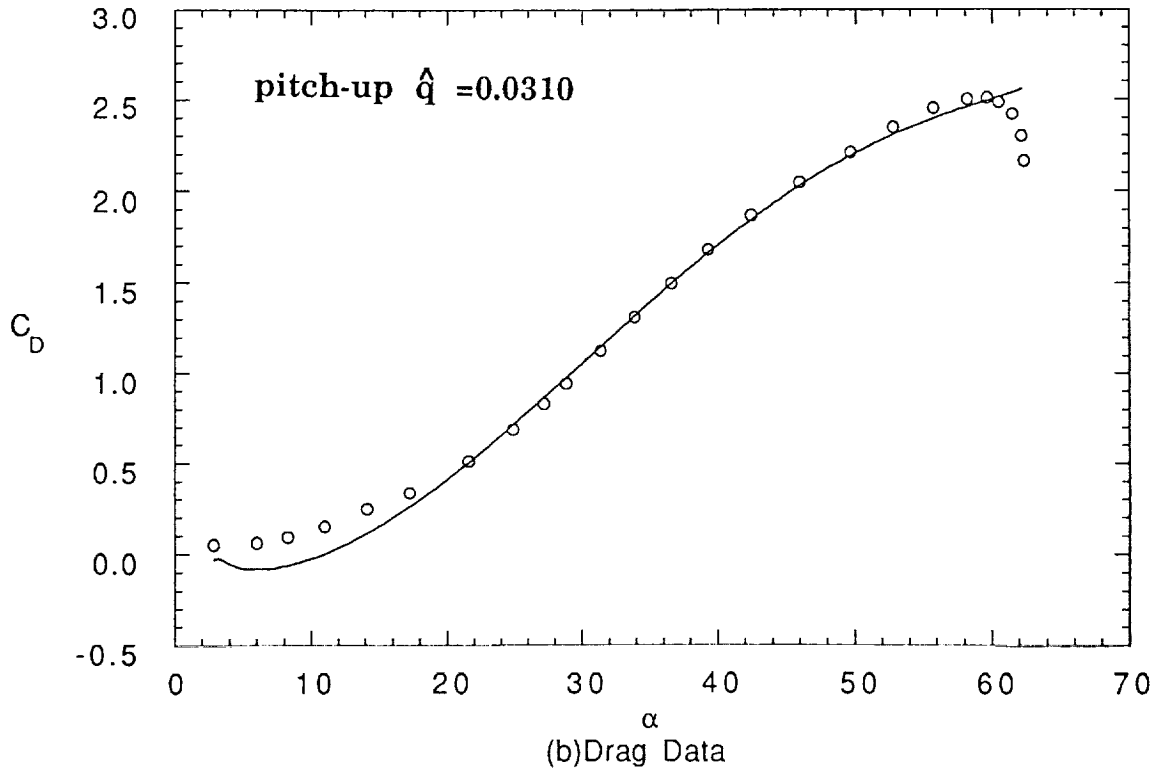

(b)Drag Data

Figure 12 Continued.

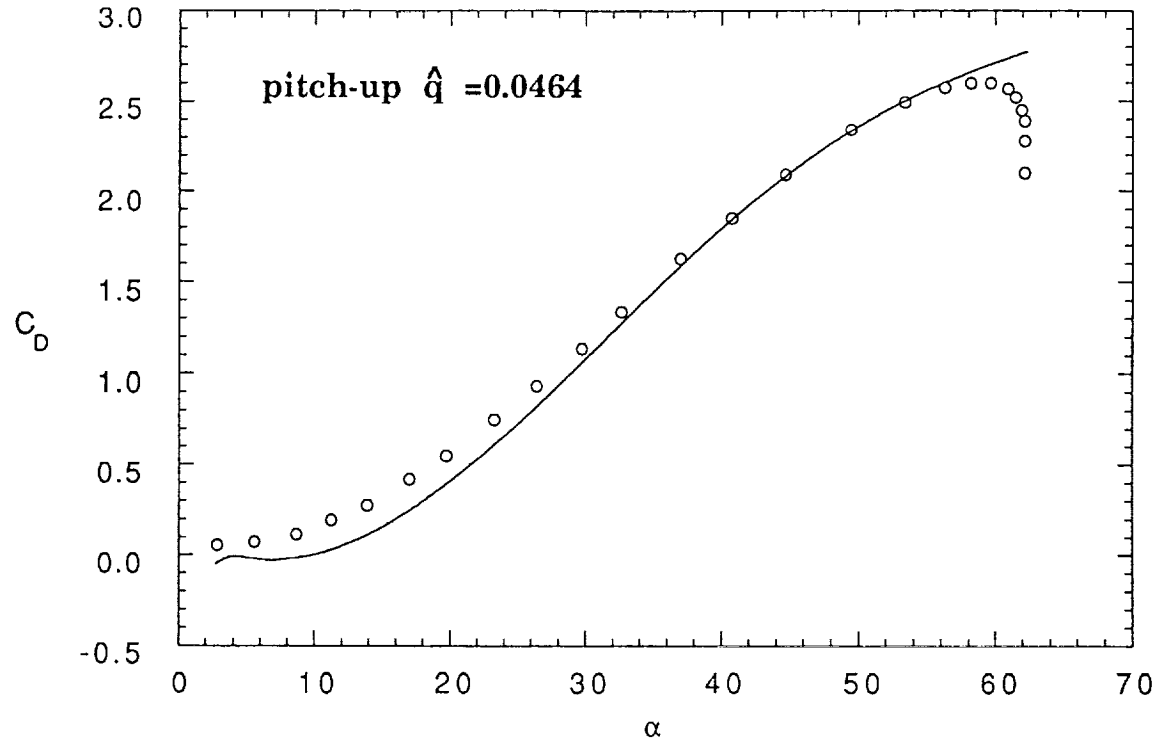

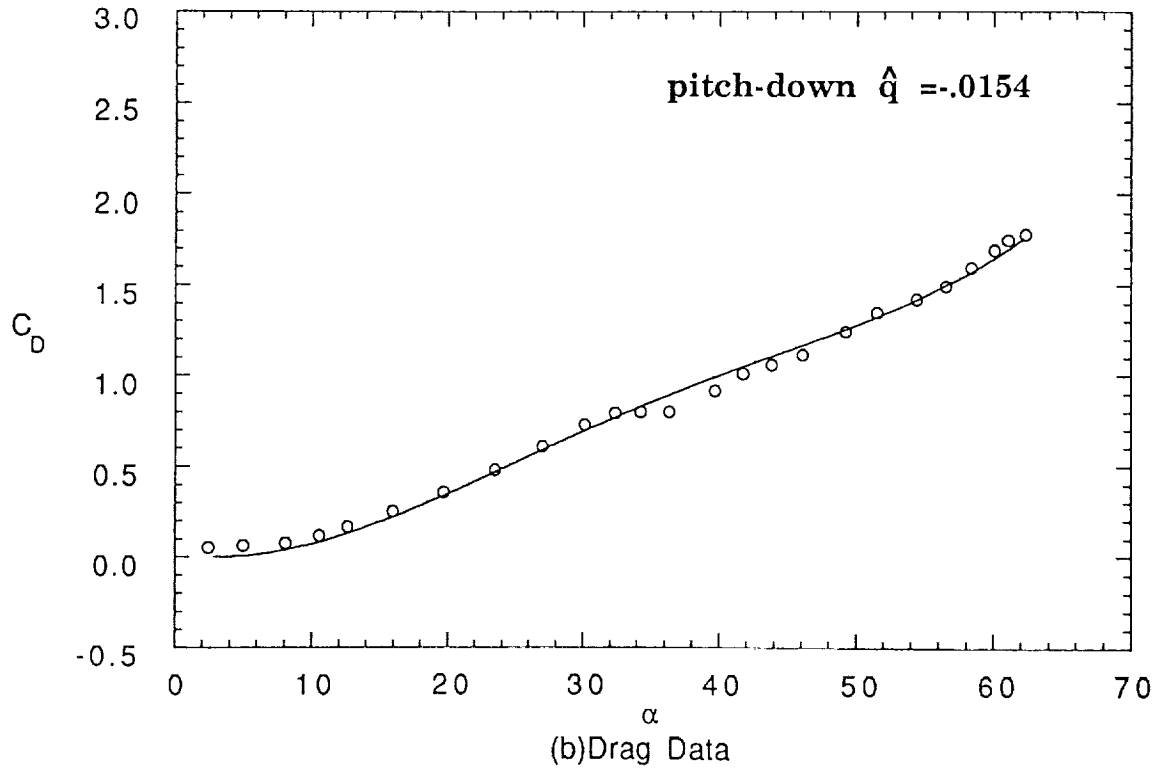

(b)Drag Data

Figure 12 Continued.

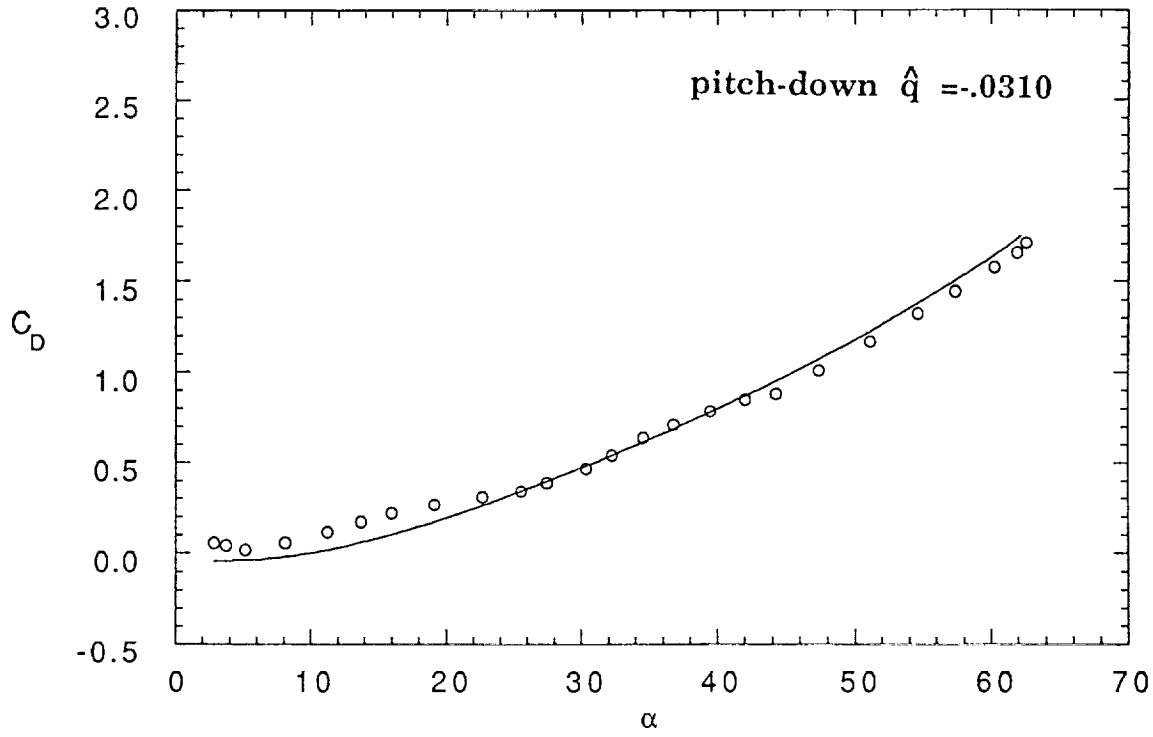

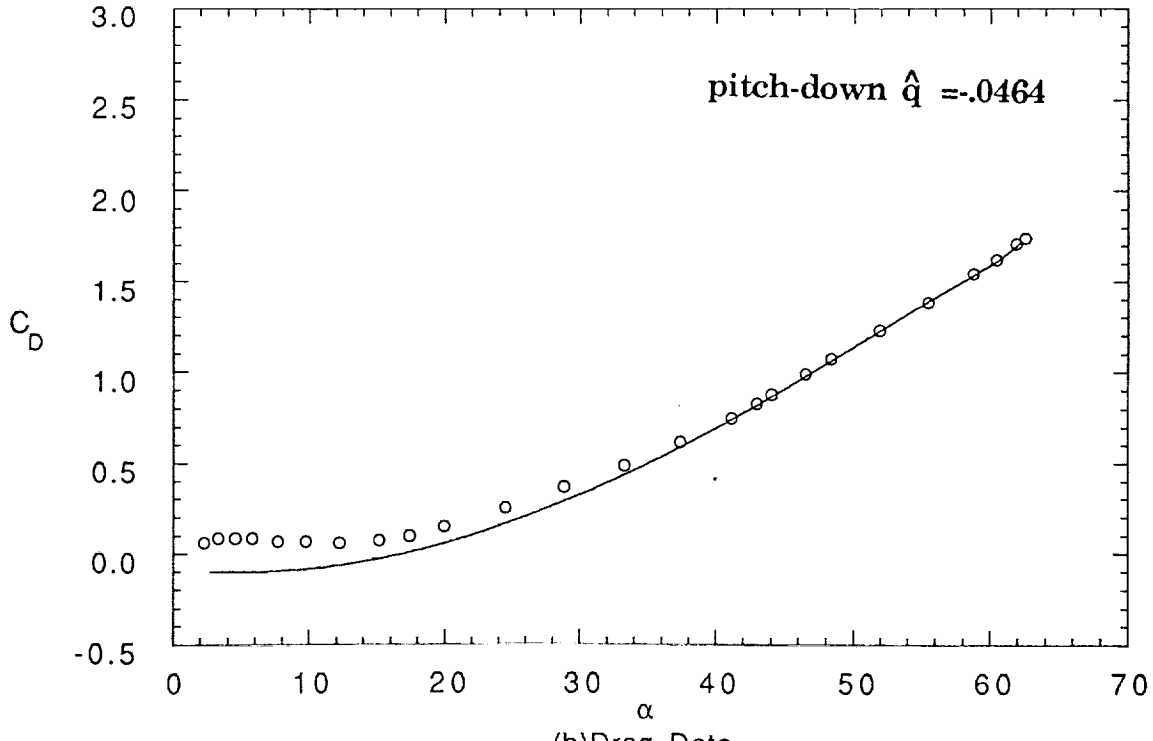

(b)Drag Data

Figure 12 Continued.

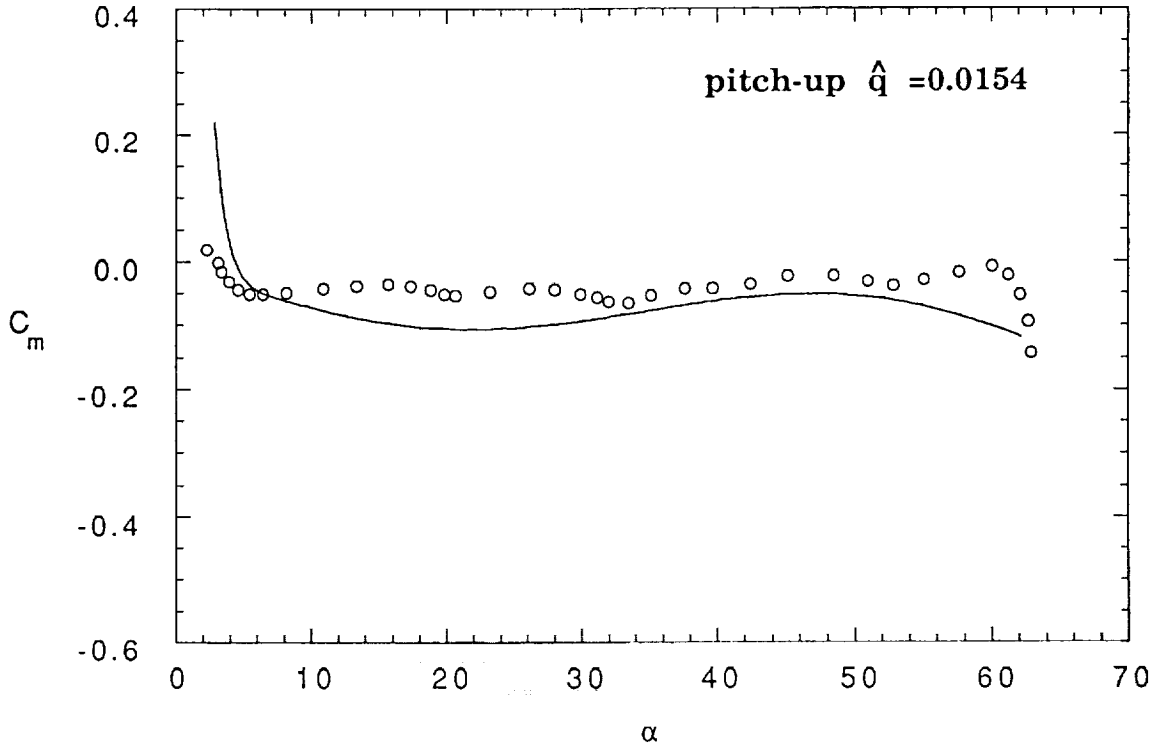

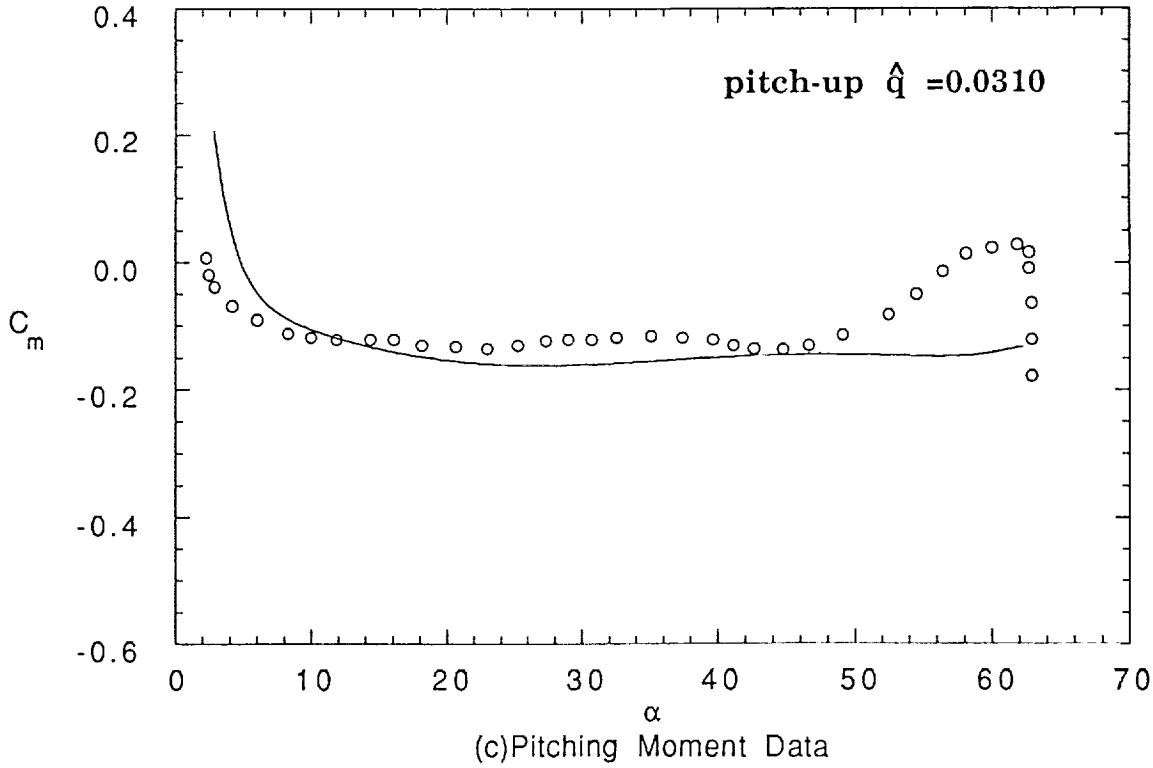

(c)Pitching Moment Data

Figure 12 Continued.

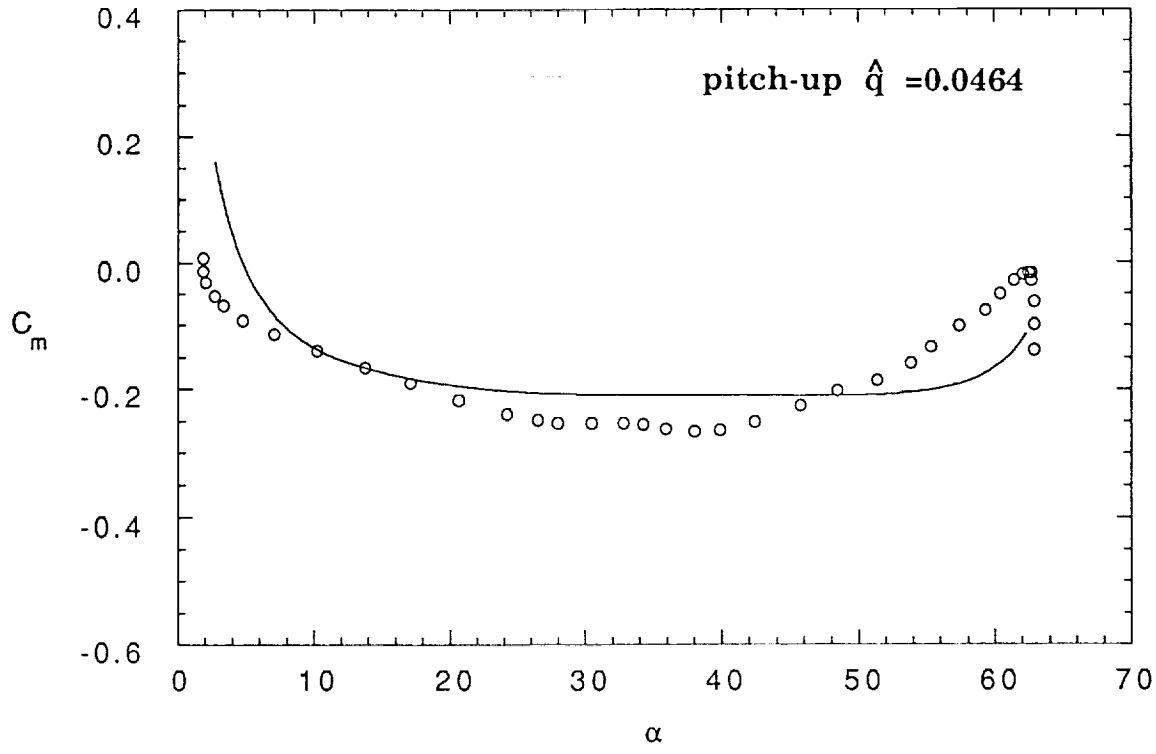

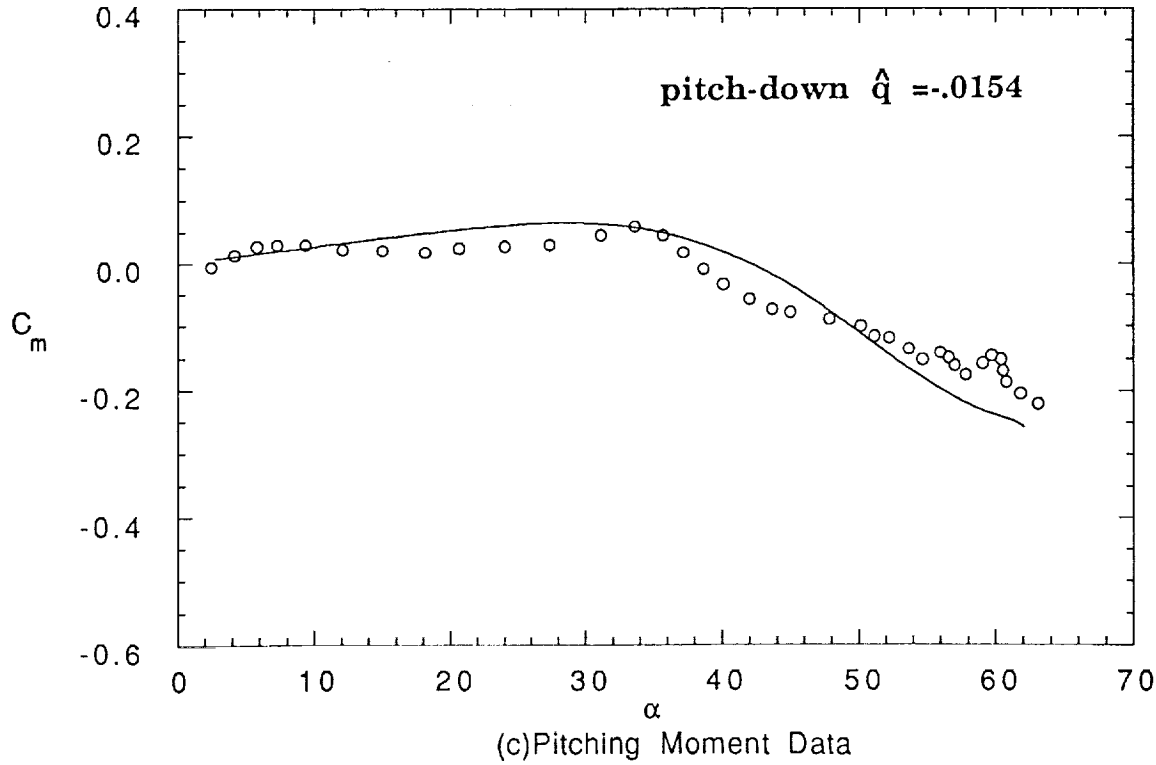

(c)Pitching Moment Data

Figure 12 Continued

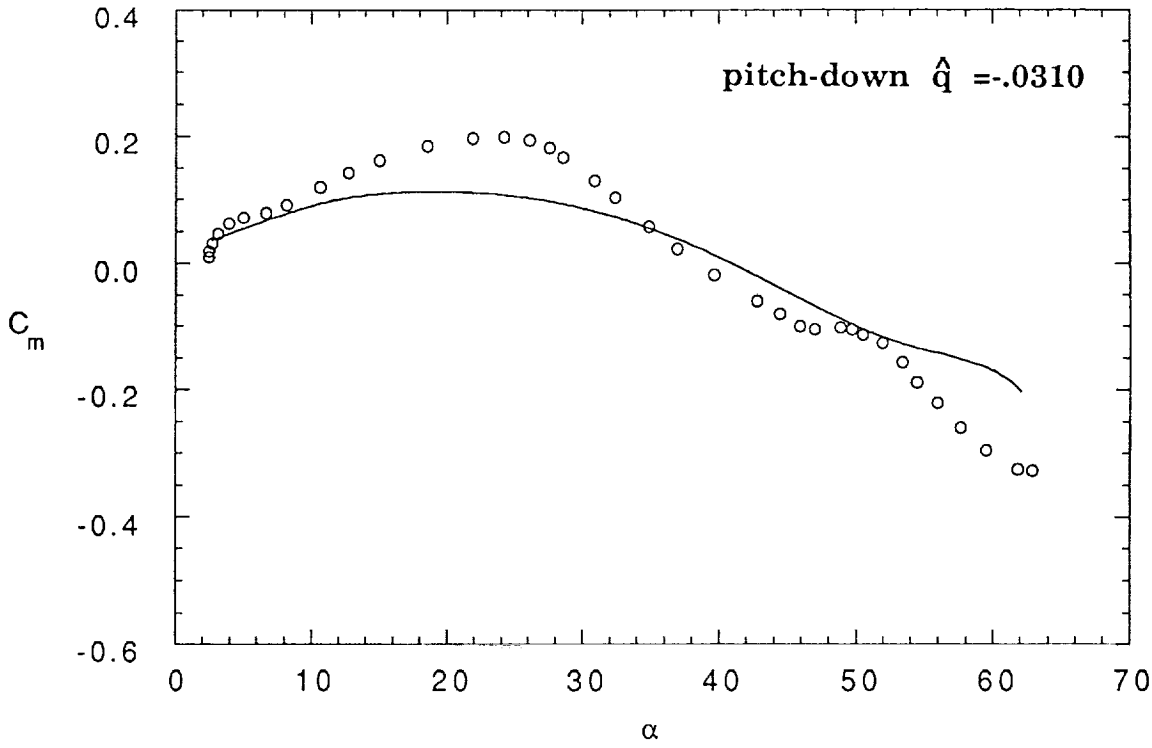

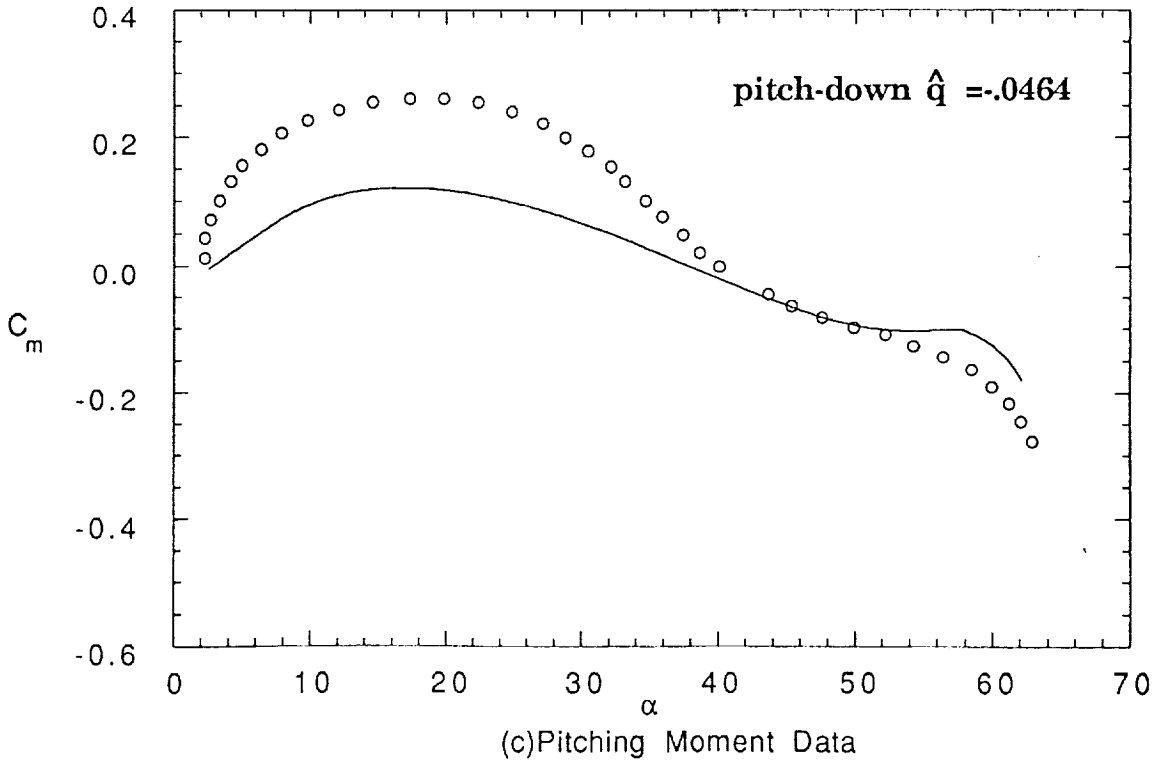

(c)Pitching Moment Data

Figure 12 Concluded.

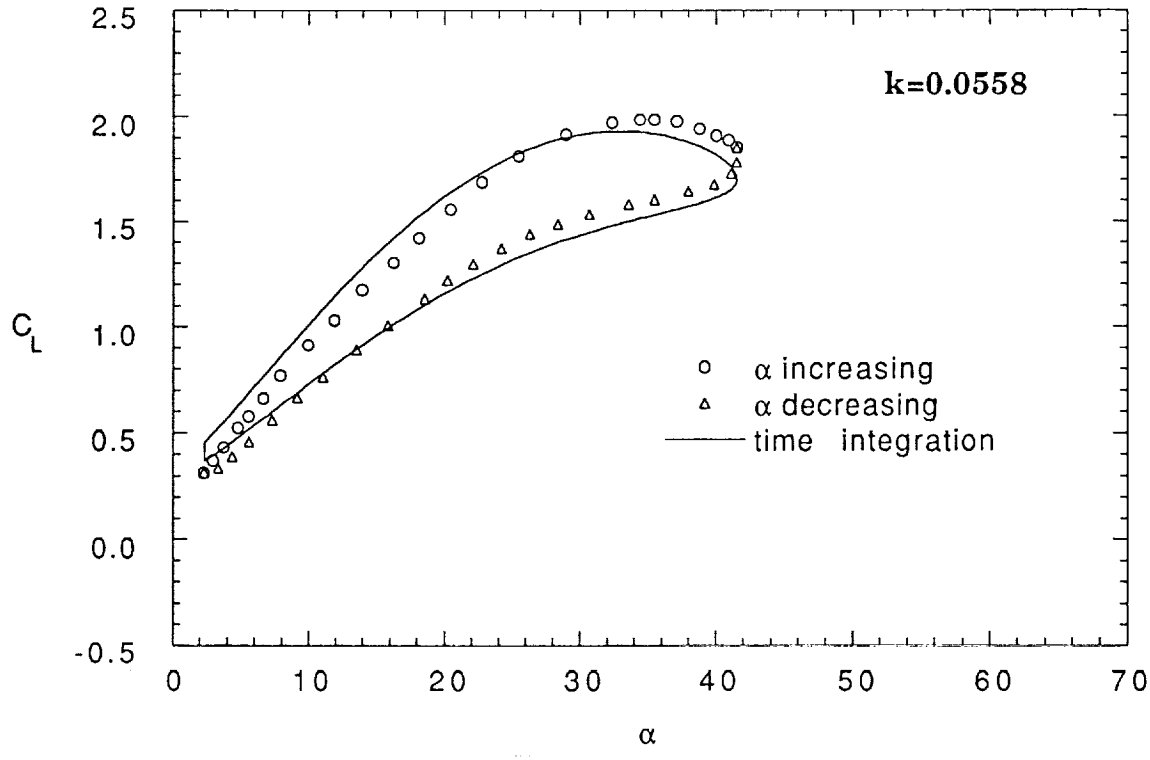

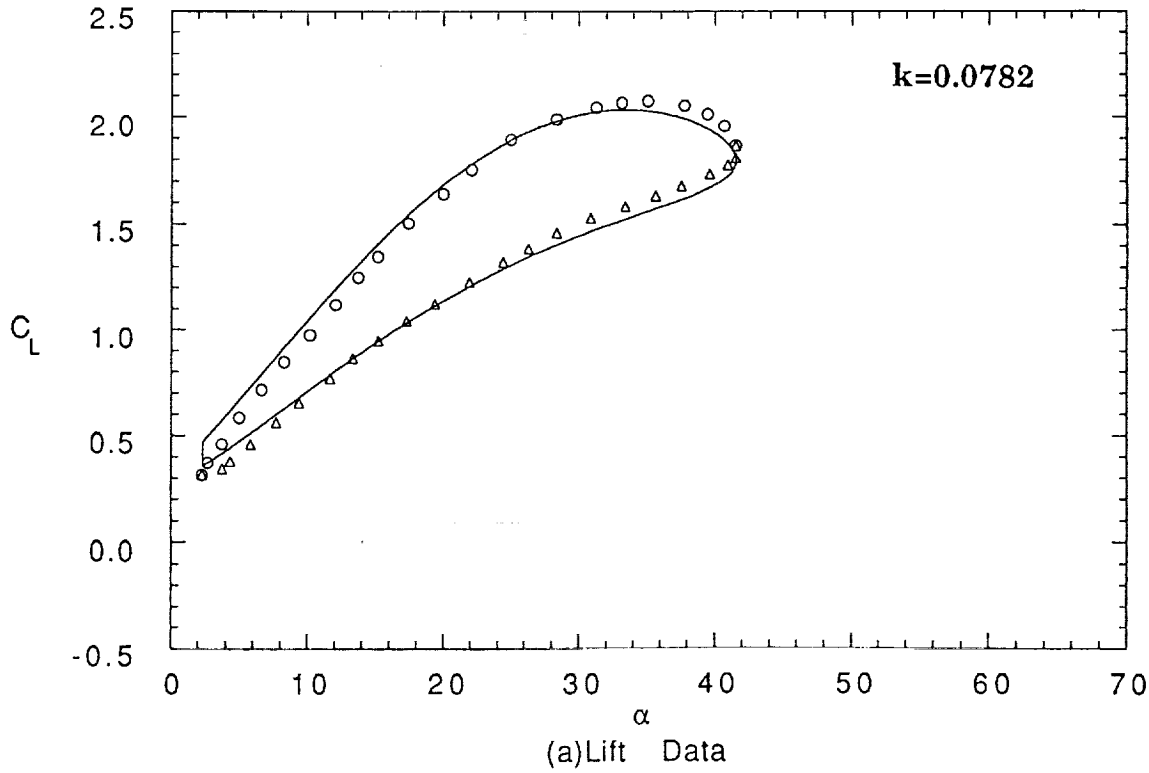

(a)Lift Data

Figure 13 Harmonic Responses with Medium Amplitude for An F-18 Model.

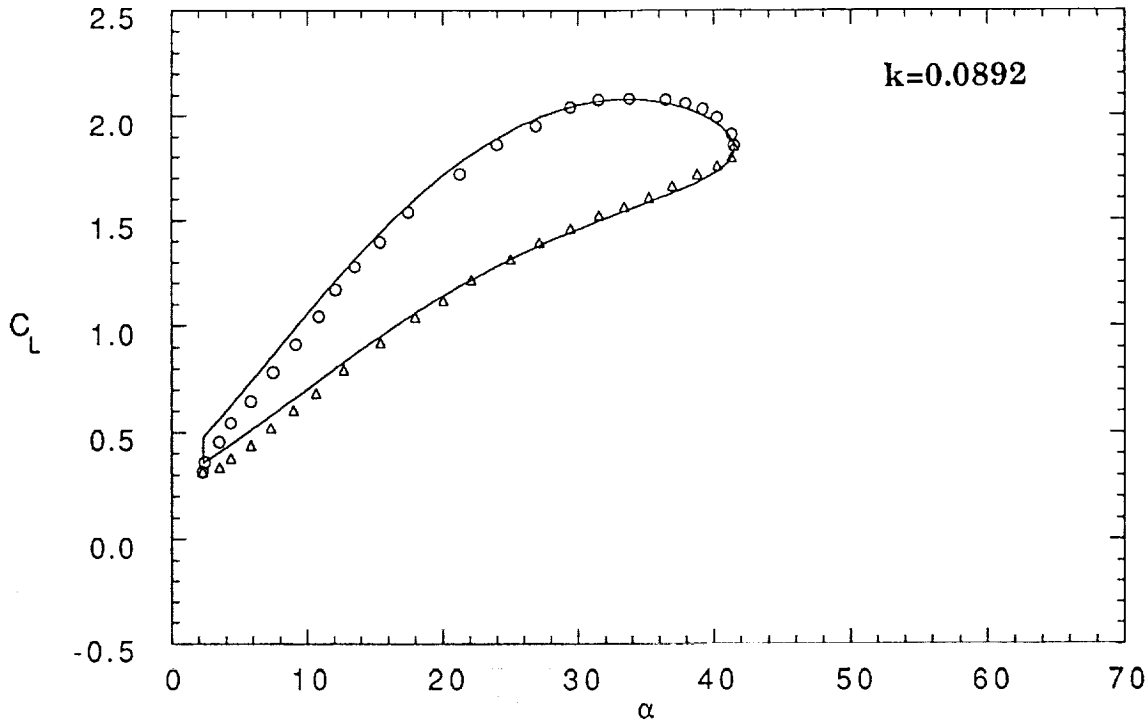

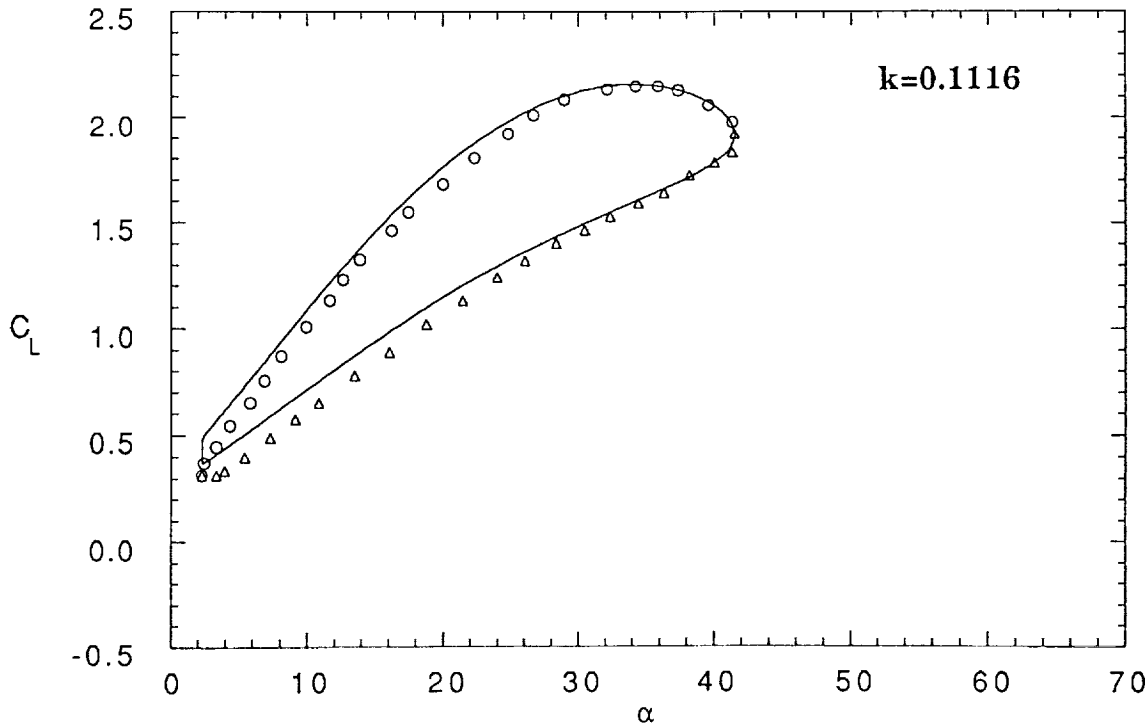

(a)Lift Data

Figure 13 Continued.

C-2

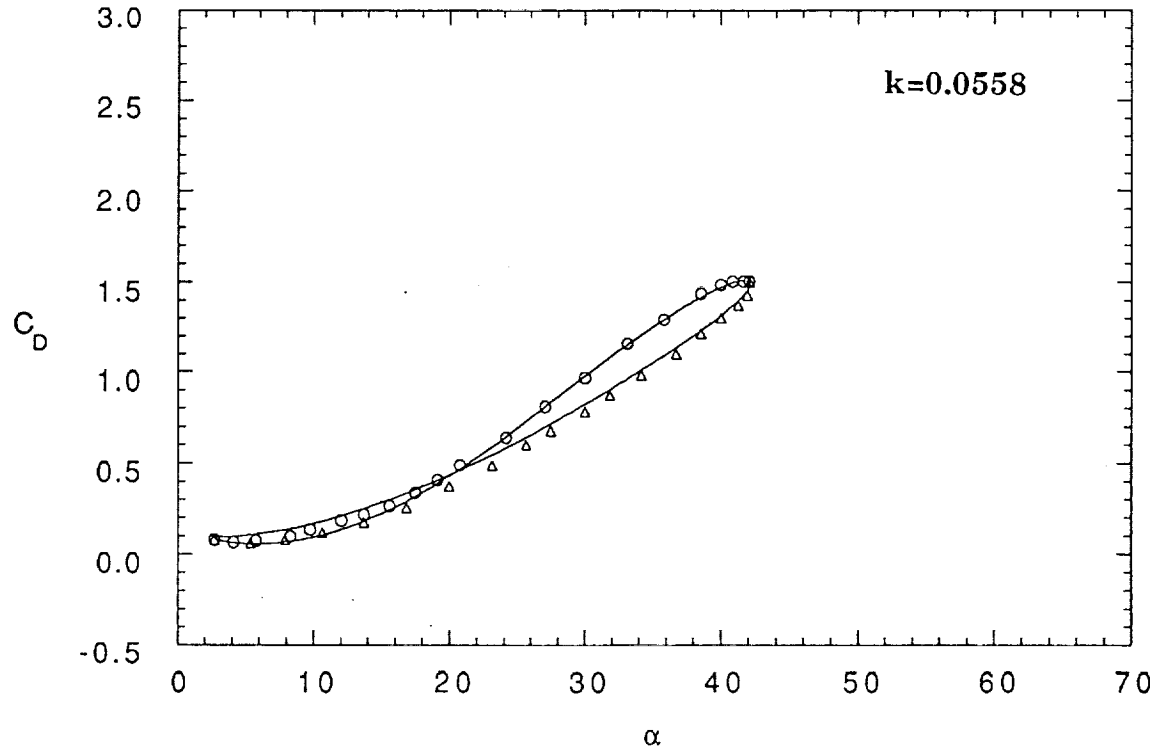

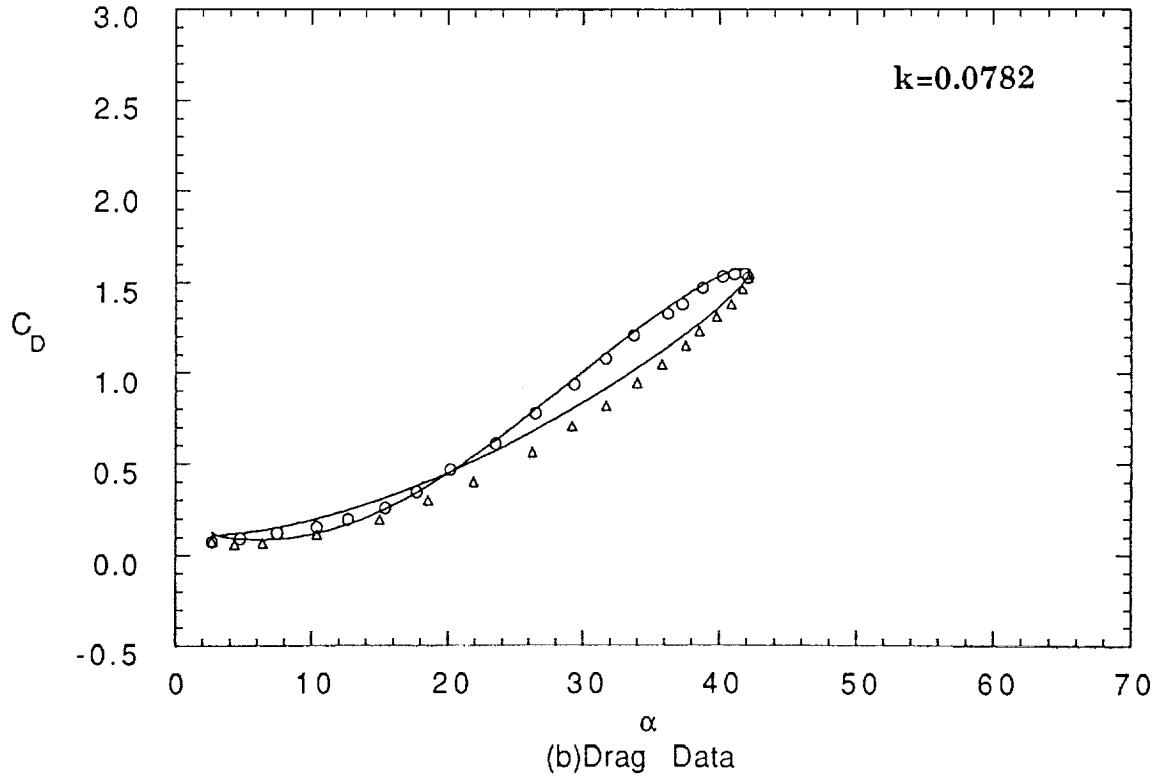

(b)Drag Data

Figure 13 Continued.

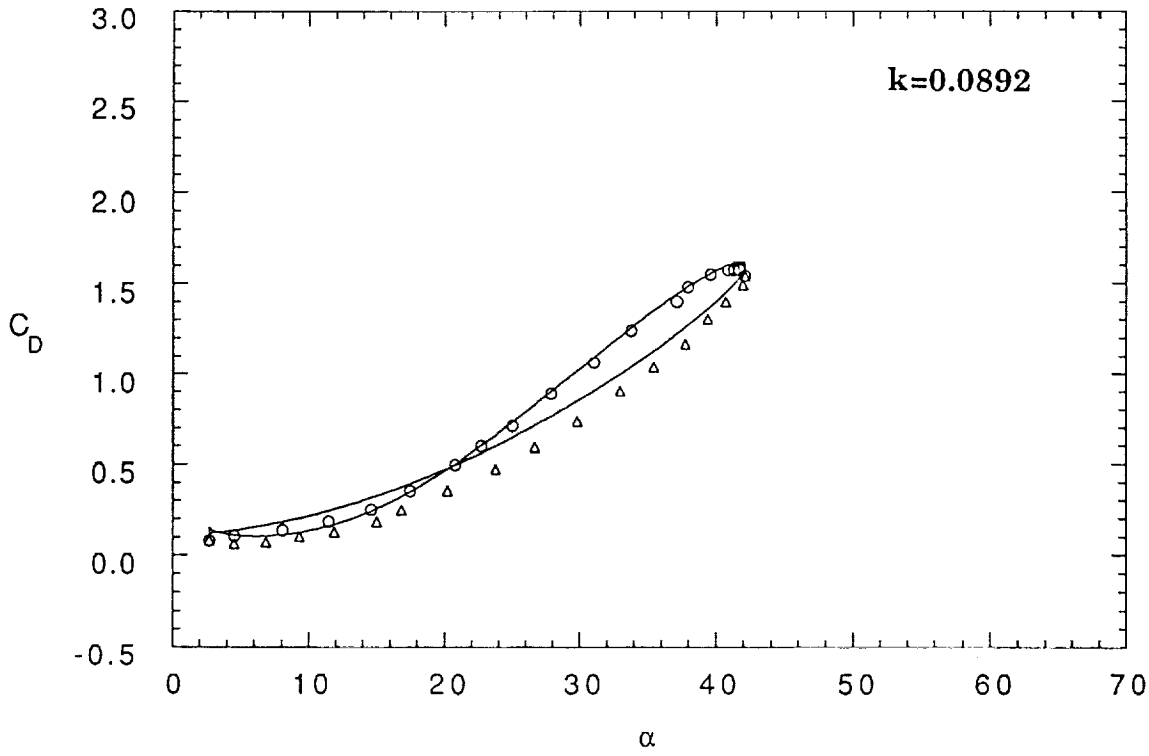

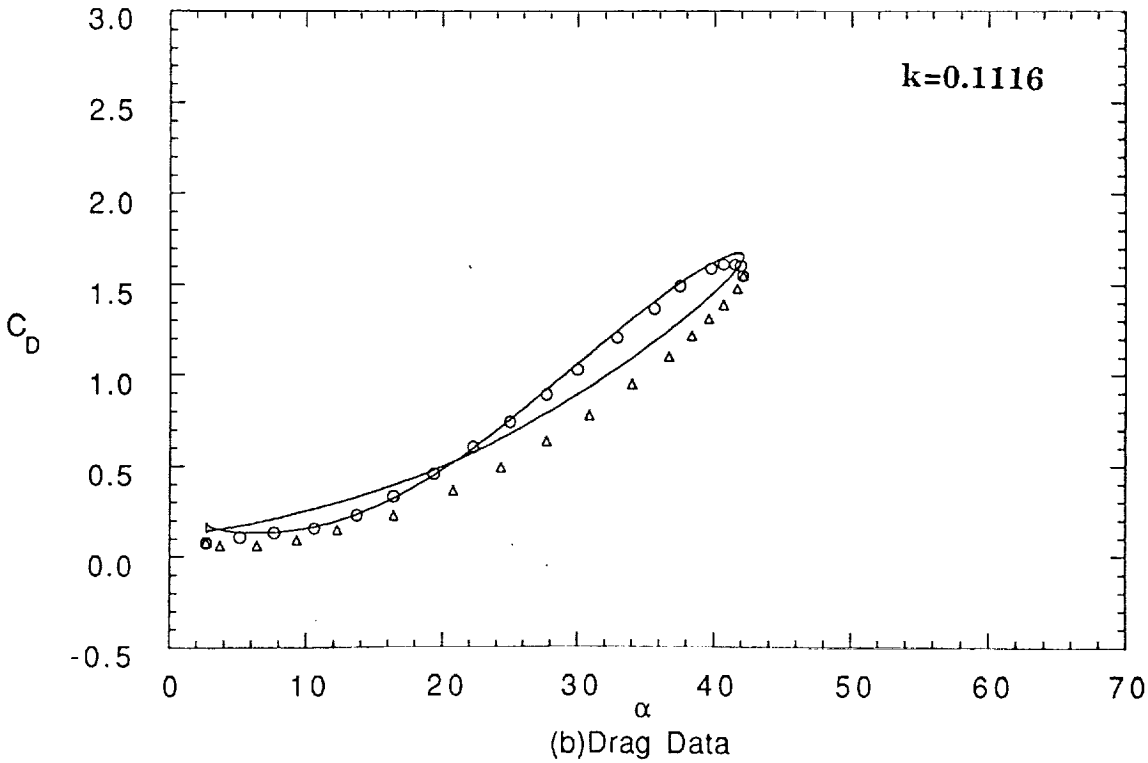

(b)Drag Data

Figure 13 Continued.

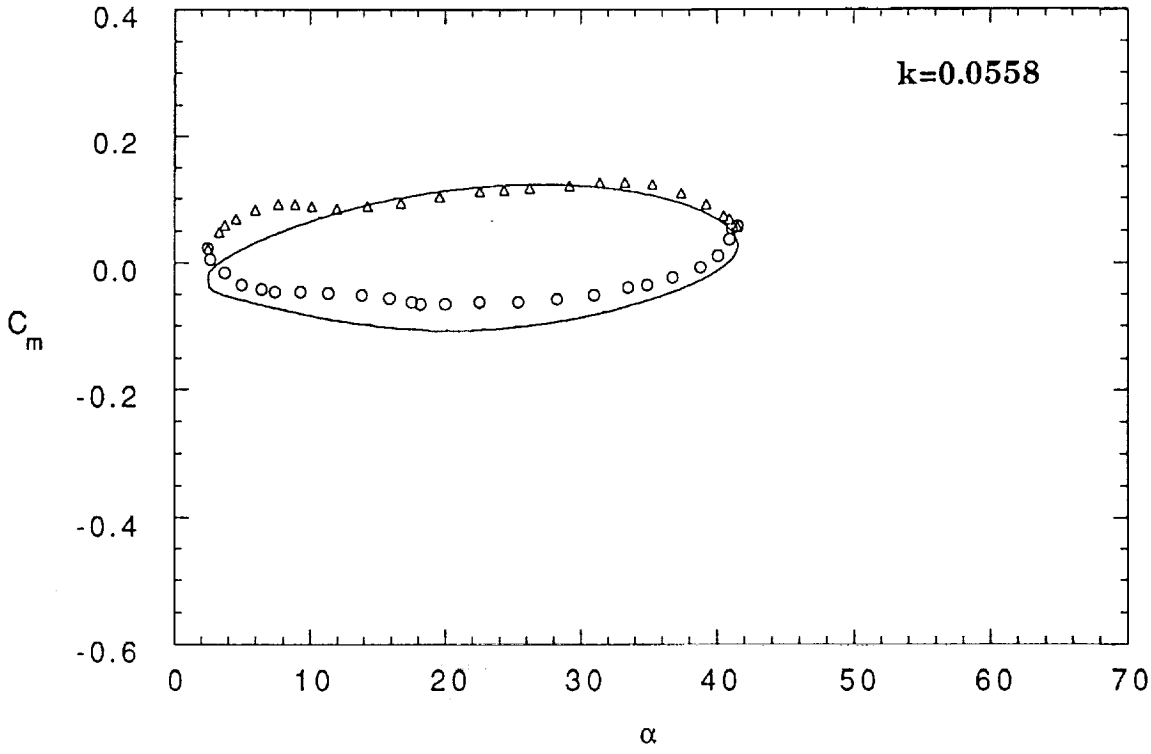

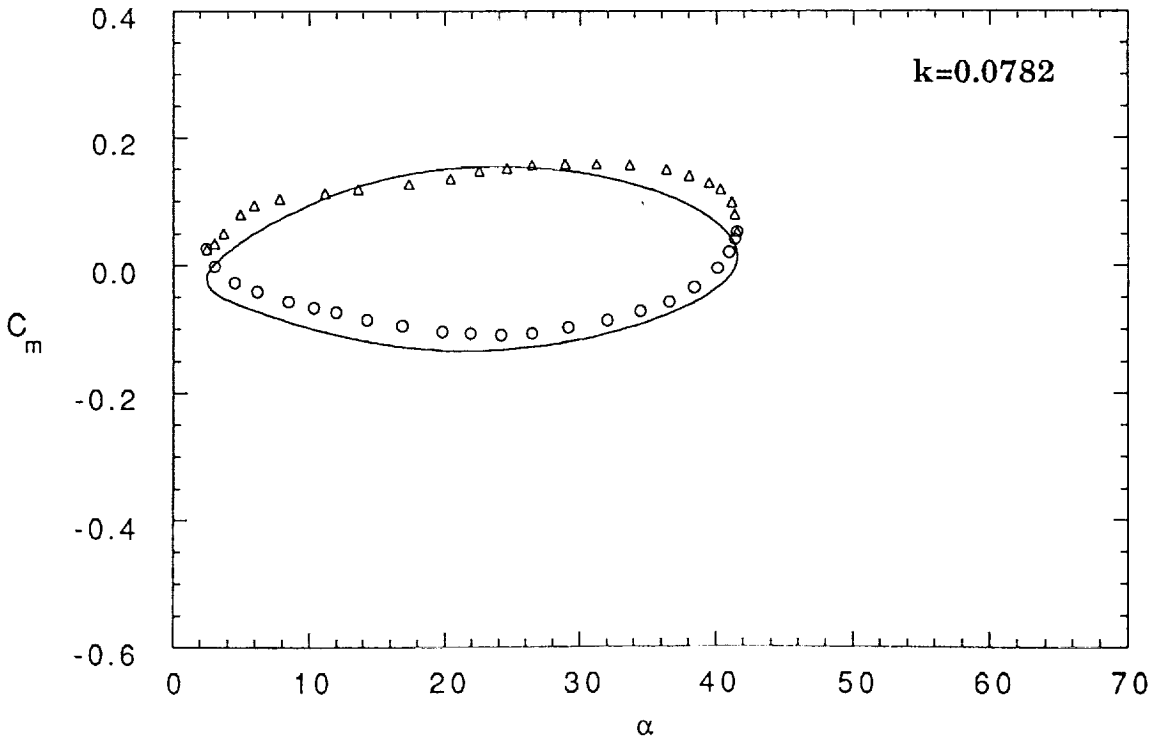

(c)Pitching Moment Data

Figure 13 Continued.

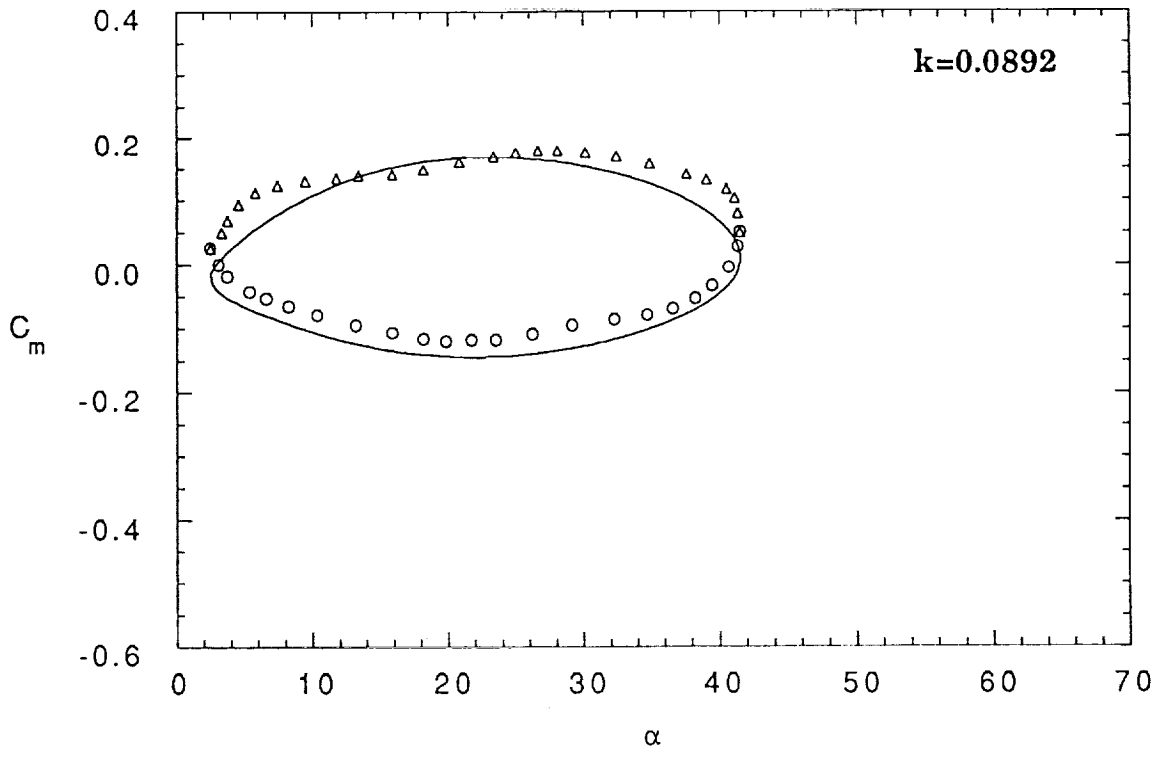

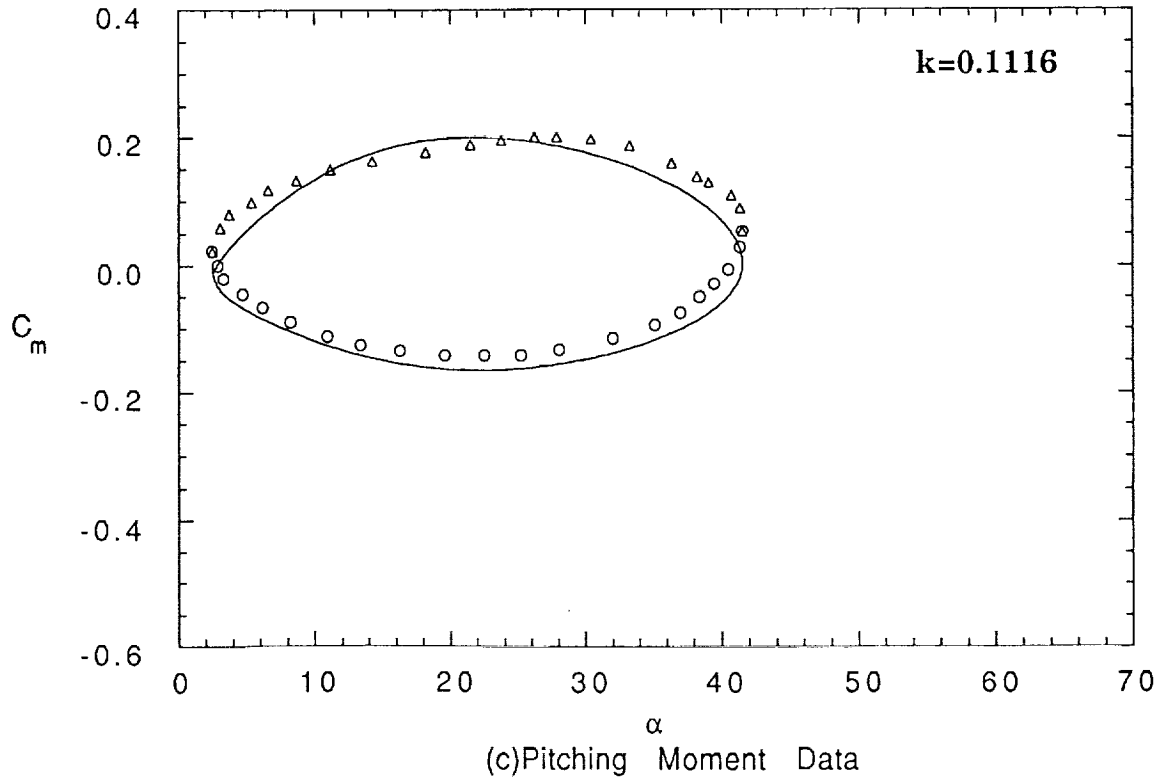

(c)Pitching Moment Data

Figure 13 Concluded.